

# **Florida State University Libraries**

---

Electronic Theses, Treatises and Dissertations

The Graduate School

---

2022

## **Combined Effects of Land Use Change and Climate Change on Soil Loss and Water Balance Variables**

Yashar Makhtoumi

FLORIDA STATE UNIVERSITY  
COLLEGE OF ENGINEERING

COMBINED EFFECTS OF LAND USE CHANGE AND CLIMATE CHANGE ON SOIL  
LOSS AND WATER BALANCE VARIABLES

By

YASHAR MAKHTOUMI

A Dissertation submitted to the  
Department of Civil and Environmental Engineering  
in partial fulfillment of the  
requirements for the degree of  
Doctor of Philosophy

2022

Yashar Makhtoumi defended this dissertation on November 09, 2022.

The members of the supervisory committee were:

Gang Chen  
Professor Directing Dissertation

Ming Ye  
University Representative

Wenrui Huang  
Committee Member

Ebrahim Ahmadisharaf  
Committee Member

Nasrin Alamdari  
Committee Member

The Graduate School has verified and approved the above-named committee members and certifies that the dissertation has been approved in accordance with university requirements.

## **ACKNOWLEDGMENTS**

I would like to express my genuine gratitude to my supervisor, Dr. Gang Chen, for his unconditional support and exceptional mentoring skills, and to my committee members, Dr. Ye, Dr. Ahmadisharaf, Dr. Huang, and Dr. Alamdari for their valued insights and support throughout this work. I learned a lot and I am honored to have them in my committee.

## TABLE OF CONTENTS

LIST OF TABLES.....	v
LIST OF FIGURES .....	vi
ABSTRACT.....	viii
1. CHAPTER ONE: INTRODUCTION .....	1
2. CHAPTER TWO: EVALUATING WATER BALANCE VARIABLES UNDER LAND USE AND CLIMATE PROJECTIONS .....	3
2.1 Introduction.....	3
2.2 Study Area .....	7
2.3 Materials and Methods.....	9
2.3.1 Spatial Data .....	9
2.3.2 Hydro-Meteorological Data .....	10
2.3.3 Future Climate Data .....	11
2.4 Scenario Development.....	15
2.5 Calibration and Validation.....	19
2.6 Results and Discussion .....	23
2.6.1 Future Climate and Hydrological Conditions .....	24
2.6.2 Annual and Seasonal Impacts of Future Climate and Water Regime .....	25
2.6.3 Implications of Future Water Regime .....	38
3. CHAPTER THREE: TOPSOIL LOSS UNDER EXTREME RAINFALL; FINDING SOIL LOSS HOTSPOTS USING WEATHER RADAR DATA.....	42
3.1 Introduction.....	42
3.2 Materials and Methods.....	45
3.2.1 Method and Data Collection .....	45
3.2.2 Study Area.....	48
3.2.3 Model Simulation and Performance Evaluation .....	49
3.3 Scenario Development.....	53
3.4 Results and Discussion .....	60
3. CHAPTER FOUR: CONCLUSION .....	75
APPENDIX A: SUPPORTING INFORMATION FOR CHAPTER 3 .....	78
REFERENCES .....	86
BIOGRAPHICAL SKETCH .....	113

## LIST OF TABLES

Table 1. NLCD land cover types and their coverage of the UCS area.....	7
Table 2 SWAT Input Data.....	11
Table 3 Selected models for Upper Choctawhatchee subbasin future climate projections.....	14
Table 4 CO <sub>2</sub> concentration for projections .....	14
Table 5 Model efficiency evaluation metrics .....	21
Table 6 Final Parameters used in SWAT simulation of Upper Choctawhatchee subbasin.....	22
Table 7 Percent changes of precipitation and temperature under different scenarios .....	26
Table 8 Percent changes to surface runoff, water yield, ET, and discharge based on the GCMs and under different scenarios .....	31
Table 9 basin-wide monthly average of hydrologic variables in UCS based on the three models under moderate and sever scenarios .....	34
Table 10 Model efficiency evaluation metrics .....	54
Table 11 Management Operation .....	56
Table 12 Rainfall statistics from 2016 to 2021 .....	59
Table 13 Scenario Development .....	59
Table 14 Percent change in annual soil loss under change in rainfall concentration ratio (CI) ...	66
Table 15 Change in flow (Q), Sediment Yield (SYLD), and Suspended Sediment Concentration (SSC) on the topmost .....	68
Table 16 Soil and Water Assessment Tool (SWAT) Input Data.....	78
Table 17 Sensitive Parameters (change based on your result) .....	82-83
Table 18 Water balance ratios .....	84
Table 19 Topsoil loss classification .....	85

## LIST OF FIGURES

Figure 1 (a) Location of Upper Choctawhatchee Subbasin (UCS) in Southeast, USA.....	8
Figure 2 Calibration and validation result for Bellwood station .....	22
Figure 3 Comparing GCMs results to the observed values .....	27
Figure 4 Comparing average, maximum, and minimum temperature between models and observed data .....	27
Figure 5 Comparing Monthly average of precipitation, ET, Water Yield, and Surface Runoff for models and observed data.....	28
Figure 6 Monthly average of average, maximum, and minimum temperature based on the models and emission scenarios, upper panel for the mid-century and lower panel for the late-century .....	29
Figure 7 Annual precipitation based on the models and under severe and moderate scenarios..	30
Figure 8 Average annual trend for hydrological components based on the three model under RCP4.5 and RCP6.0 .....	32
Figure 9 Monthly average of hydrological components in UCS based in the models and under RCP4.5 and RCP6.0 .....	35
Figure 10 Discharge monthly average at Bellwood station based in the models and under RCP4.5 and RCP6.0.....	36
Figure 11 Seasonal variation of hydrological components based on the model and under both emission scenarios for entire simulation period .....	40
Figure 12 (a) Location of the study area (HCW).....	50
Figure 13 Flow calibration and validation result for USGS 07277700 site.....	54
Figure 14 Sediment calibration and validation result for USGS 07277700 site.....	54
Figure 15 Left panel shows the rainfall distribution over the year for the scenarios .....	59
Figure 16 Left panel shows grazing practice distribution.....	61
Figure 17 (a) Annual rainfall distribution.....	66-67

Figure 18 (a) Daily flow discharge time series for all scenarios at the monitoring point (USGS 07277700).....	69
Figure 19 (a) Stage IV QPE radar rainfall over Mississippi on March 28 <sup>th</sup> , March 31 <sup>st</sup> , June 9 <sup>th</sup> , and August 20 <sup>th</sup> .....	72
Figure 20 Distribution of soil loss caused by extreme rainfalls on March 28 <sup>th</sup> , March 31 <sup>st</sup> , June 9 <sup>th</sup> , and August 20 <sup>th</sup> over HCW under all scenarios .....	73
Figure 21 Distribution of suspended sediment concentration in reaches caused by extreme rainfalls on March 28 <sup>th</sup> , March 31 <sup>st</sup> , June 9 <sup>th</sup> , and August 20 <sup>th</sup> under all scenarios. ....	74
Figure 22 (a) Land use map .....	79
Figure 23 Main soil types and associated horizons .....	80
Figure 24 Calibration and validation result for days no or less amount of rainfall .....	81
Figure 25 Annual sediment loss distribution .....	84
Figure 26 Annual rainfall distribution .....	85

## ABSTRACT

Changes in water balance variables such as runoff and evapotranspiration (ET) are essential in planning and management of land and water resources. Two major factors affecting these variables are climate and land use change. There is a need to investigate the combined effects of land use and climate change at local scales. Towards that end, the hydrological processes were modeled using the Soil and Water Assessment Tool (SWAT) to investigate the impacts of climate and land use change in Southeast US (Makhtoumi, Li, Ibeanusi, & Chen, 2020). We integrated land use based on the Shared Socioeconomic Pathways (SSPs) with future climate data (CMIP5) to study the combined effects on hydrological response of Upper Choctawhatchee Watershed (UCW.) Future rainfall and air temperature, for two time periods (2040-2069 and 2070-2099), were obtained using Global Climate Models to provide SWAT with the climatic forcing in order to project water balance variables. The simulation was carried out under two radiative forcing pathways of Representative Concentration Pathways (RCP4.5 and RCP6.0.) Our results indicate that increased imperviousness resulted from urbanization has more impact on runoff than that of projected changes in climate. Impacts on water balance variables (runoff, ET, discharge) differed seasonally. Results showed peak surface runoff experienced changes under both emission scenarios in June up to five times increase. Among the water balance variables, ET as the least dominant pathways for water loss, showed the modest changes with the largest decrease during fall and summer. Projections indicated more frequent extreme behavior regarding precipitation, peak surface runoff, water yield (WY) and ET, during midcentury. Discharge was estimated to increase through the year and the highest changes were expected during summer and fall with 186.3% increase in November under RCP6.0. Relying on rainfall for farming along with reduced agricultural land use (11.8%) and increased urban area (47%) and population growth, would likely make the water use efficiency critical.

In our second study, we focused on the combined impact of land use and climate change on soil erosion at local scales. Topsoil loss is a widespread environmental concern causing adverse impacts on natural and human systems. Severe weather accompanied with human activities can exacerbate this issue degrading soil health and consequently accelerating global and regional food insecurity and injustice. Erosion impairs soil physical and chemical properties such as infiltration rate, water holding capacity, loss of nutrients including soil carbon and nitrogen. Although,

temporal properties of a rainfall event have meaningful implications for soil erosion, spatial heterogeneity of a rainfall contributes substantially and cannot be overlooked. Therefore, in the third chapter we investigated soil loss using SWAT in Northern Mississippi. First, we built a hydrological model and calibrated it for both flow and sediment discharge. Then we developed land use and climate scenarios. The land use scenarios include farming (soybean and corn) and grazing practices. The climate scenarios comprise of four different precipitation time series, S0 which no concentration is forced, while S1, S2, and S3 have 3%, 6%, and 9% concentration in top four rainy days, respectively. We coupled the land use and climate scenarios and evaluated a small watershed (Hickahala Creek Watershed) in response. We classified the subbasins into different classes of soil loss severity and then determined the hotspots for soil loss at subbasin scale. Our result suggests that the resolution of rainfall data is crucial in studying the soil loss. We found that pasture management by itself can manifold soil loss, and if accompanied with extreme rainfalls, soil loss accelerates impacting different subbasins each time. We found that spatial heterogeneity of extreme rainfalls (ERs) can be more substantial than land use in individual extreme rainfalls; however, over a year, soil moisture and type of the management practices (grazing and farming) could contribute more to soil loss. Soil loss can go as high as 350 (ton/ha/yr) under the ERs. Adding only the management practices can increase erosion 3600%. Under S1 parts of watershed yield more than 150 ton/ha/yr (extremely severe). Under S2 and S3 more soil loss hotspots emerge yielding approximately 200 ton/ha/yr. We found that in the hotspots, up to 10% increase in CI can increase annual soil loss up to 75%. Single ER can generate up to 35% of annual soil loss. Under one ER event hotspot subbasins can lose up to 160 ton/ha/day (subbasin 15). The results reveal that adding grazing and farming (S0) under one ER event can increase soil loss by 95%. 32% and 80% increase in rainfall amount in one ER event can increase soil loss by 94% and 285% respectively. Our results suggested the importance of site-specific managements to mitigate soil loss and all the consequences. It is essential to consider the varying sensitivity of subbasins for the sustainability of the agricultural landscapes.

# **CHAPTER 1**

## **INTRODUCTION**

Land use change has transformed our world more than any other environmental change. On the other hand, from the literature and witnessed abnormalities around the world, climate change is unequivocal fact. Land use and climate change have been affecting the Earth's system, with many changes on the land and in the oceans. Hydrological cycle is one of many parts of the Earth's system that is directly affected by land use and climate change. Warming weather will bring different weather patterns which means different amount of water from the past for a given area. Extreme weathers have a positive trend starting from a century ago (NOAA/NCEI, Climate Extreme Index). Prolonged severe droughts, heat waves, cold fronts, destructive hurricanes, unexpected tornado, seasonal timing change, early snowmelt, flash floods are extreme weather hazards or consequence of it. These changes will affect the farming practices which consequently will affect the individual farmers decision. These changes in individual farmers decision will add up to make the land use change in national and global scale. These decisions can include changes in farming crops, in agricultural practices such as tillage, in type and amount of fertilizer and pesticide. These changes will bring changes in hydrological and bio-geochemical processes. On the other hand, land use change has been accelerating. Southeast and Northwest of US has been experiencing rapid land use change. Population growth and advancement in technology were the main reason for these changes (Alamdari, Claggett, Sample, Easton, & Yazdi, 2022; Pachauri et al., 2014). Climate change, however, can take the lead with substantial impact on the hydrological cycle(Karl, Melillo, Peterson, & Hassol, 2009). Agricultural industry is the first ranked in Non-Point Source (NPS) pollution (Ribaudo, Horan, & Smith, 1999). Thus, not only will these changes alter the quantity of the water in cycle, but also, they will alter quality of it. Changes in the surface of the Earth alters the evapotranspiration process and energy budget because of modified albedo. Therefore, the relation between land use change and climate change is a feedback loop which can be a complex issue to tackle. These feedback loop will pose new norms on communities; therefore, it is vital to understand land use and climate change effects on the environment. In this study, we studied the combined effects of land use and climate change on soil loss and water balance

variables as a small attempt towards better understanding the loop and as such improving community resilience.

Water balance variables such as runoff, ET, water yield, discharge, and precipitation are essential for many hydrological applications. Continuous measurement of these variables is not logistically possible (Zink, Kumar, Cuntz, & Samaniego, 2017). Hydrological extremes are expected in many parts of the planet and will manipulate the water balance variables. There is a need to better understand the hydrological cycles and this gap can be filled with investigating the water balance variables. In that regard, we investigated the water balance variables under land use and climate changes in the second chapter.

Topsoil loss is also a widespread environmental concern that has on-site and off-site costs causing numerous adverse impacts on natural and human systems. Off-site costs can include sediment contribution to water quality, reducing the water storage capacity of reservoirs rising flooding risk, and degrading aquatic ecosystem habitat by depleting the topsoil nutrients and sediment into streams and waterbodies. On-site costs can include depleting the fertile topsoil nutrients causing long-lasting impact in crop productivity and accelerating global and regional food insecurity and injustice. Erosion impairs soil physical and chemical properties such as infiltration rate, water holding capacity, loss of nutrients including soil carbon and nitrogen. Human activities and inclement weather can complicate the process but ultimately worsen the issue. Therefore, soil erosion cannot be overlooked. To address these issues, we modeled topsoil loss and evaluated the watershed response without management practices and with the practices and under three extreme rainfall series using weather radar data in the third chapter.

## CHAPTER 2

### EVALUATING WATER BALANCE VARIABLES UNDER LAND USE AND CLIMATE PROJECTIONS

#### 2.1 Introduction

From different studies and witnessed abnormalities around the globe, it is now clear that climate change has brought and will bring vulnerabilities. CO<sub>2</sub> in the atmosphere has set the record in 2018 since preindustrial era (1850-1900) (Poloczanska, Mintenbeck, Portner, Roberts, & Levin, 2018). Consequently, global mean temperature has been rising 1.5°C above preindustrial (1850-1900) era (Poloczanska et al., 2018). Other key indicators of the critical situation are Sea Level Rise (SLR) and Sea Ice Extent (SIC); both are the direct consequence of greenhouse gas (GHG) increase in the atmosphere. SLR has hit the record in 2019 of 3.2 mm/year during the 1993-2019 period and also Arctic extent has been decreasing (Poloczanska et al., 2018). On the local scale, the warming has been consistent with the weather and climate variabilities related to climate change; North America has been unusually cold due to the crisis (Poloczanska et al., 2018). Extreme precipitations, more frequent hurricanes, intense tropical cyclones, unexpected thunderstorms and tornados, sever cold breaks, prolonged droughts, and seasonal timing shifts are expected to be common (Diffenbaugh, Scherer, & Trapp, 2013; Diffenbaugh, Swain, & Touma, 2015; Emanuel, 2013; Y. Gao, Leung, Lu, & Masato, 2015; Groisman et al., 2005; Sobel et al., 2016). These threats not only target human communities but also do threaten ecosystems functionality.

Significant changes in hydrological regimes in most part of the land surface of the planet will be likely to occur by midcentury (2050) (Arnell & Gosling, 2013). The Fourth Assessment Report (AR4) (Field, Barros, Stocker, & Dahe, 2012) of Intergovernmental Panel for Climate Change (IPCC) regarding the anthropogenic impact on hydrological cycle like precipitation, snowmelt, and earlier spring peak flows, reported medium to high confidence where the latter was very likely (Field et al., 2012; Georgakakos et al., 2014). Climate change will have negative impacts on streamflow and water quality and consequently will jeopardize freshwater ecosystems (Cisneros et al., 2014).

In Southeast of the US, seasonal drying has been observed for spring, fall , and winter and in summer the soil moisture has increase during 1988-2010 (Georgakakos et al., 2014). Although potential evapotranspiration (PET) has projected to increase, evapotranspiration (ET) as the 2<sup>nd</sup> largest component of the hydrological cycle requires further studies to see possible implication (Georgakakos et al., 2014; Srivastava, Deb, & Kumari, 2020). Projections show 4.3°C and 7.72°C rise by mid-century (2036-2065) and late-century (2071-2100) under RCP 8.5 respectively (Vose, Easterling, Kunkel, & Wehner, 2017). Projections under RCP 8.5 by mid-century also reveal 40-50 days per year with temperature greater than 32°C as a key temperature threshold (Vose et al., 2017). For changes in numbers of nights below 0°C, show increase of 10-15 days for the Southeast (Katz, Parlange, & Tebaldi, 2003). Projected warm weather will increase ET, leading to reduced water availability and ground water recharge (Ingram, Dow, Carter, & Anderson, 2013; G. Sun, 2013; Walsh et al., 2014b). Uptake of soil water by forests is expected to increase, leading to decline in water yield under increased temperature and decreased precipitation in the Southeast region including Alabama (Ingram et al., 2013; G. Sun, 2013). Longer growing season and increased wildfire likelihood were also projected for southeast US forests (McNulty et al., 2013). Projected population growth and land use change will worsen the situation and pose threat on the economy and unique ecosystems; and land use change in Southeast which ultimately exacerbates the water scarcity, is faster than any other areas in US (Carter et al., 2014).

Southeast is categorized as the second vulnerable region to weather and climate disasters in the US for the past three decades (1980-2012); hurricanes can be considered as disasters for the coastal area; and tornados and storms are disasters for inland regions where they are close to the Gulf and Atlantic coasts (Carter et al., 2014). Many factors contribute to the climate of the Southeast region including closeness to the Atlantic Ocean and the Gulf of Mexico and El Nino-Southern Oscillation (ENSO), and land falling tropical weather systems (Katz et al., 2003). Projections for annual runoff and consequent stream flow in the Southeast indicate declines, which is consistent with long-term (multi-seasonal) droughts (Georgakakos et al., 2014). Also, historically, river floods have been decreasing in most part of the Southeast at least 6% percent per decade (Georgakakos et al., 2014; Villarini, Serinaldi, Smith, & Krajewski, 2009). River floods are more complex to be considered as the direct result of the heavy precipitation; and topography, soil moisture, channel condition, and anthropogenic influences such as land use change are thought

to play the key roles (Georgakakos et al., 2014). These highlight the importance of hydrological analysis with respect to non-stationary stressors in the region.

Few studies like Ge Sun et.al., (2013) have studied the impact of climate change in watershed scale in the Southeast. They demonstrated the importance of water supply stress and showed increase in runoff and sediment yield due to increase in erosivity and/or vegetation cover loss. They also stated that climate change and possible future stressors like population growth, land use change (LUC), energy security, and policy shift would jeopardize surface and groundwater availability (G. Sun, 2013).

There are LUC impact studies; but the land use scenarios are limited. Chen et al. (2017) have investigated only agricultural land use change and projected 12% to 20 % decline in crop ET by mid and end of 21<sup>st</sup> century respectively (Y. Chen, Ale, Rajan, & Srinivasan, 2017). Qihui Chen et al. (2019) have studied the effect of historical LUC within a watershed in China and found small impacts on hydrological extremes (runoff and drought) (Q. Chen et al., 2019). Villamizar et al. (2019) have studied LUC within a watershed in Colombia with 3 hypothetical LUC and identified strategic points for conservation practices (Villamizar, Pineda, & Carrillo, 2019). Marhaento et al. (2018) studied climate and LUC in a tropical watershed in Indonesia and they found intensified in annual stream flow and surface runoff if the drivers combined; the LUC scenarios used in the study were based on extrapolation of trends (Marhaento, Booij, & Hoekstra, 2018). Separate and combined effect of climate and LUC were investigated by Tamm et al. (2018) and they found strong linear correlation forest cover change and annual runoff. Their study area was heavily forested and afforestation and deforestation LUC scenarios were used (Tamm, Maasikamäe, Padari, & Tamm, 2018). Wang et al. (2013) have studied a coastal watershed in southwest Alabama using a spatially explicit LUC based on population growth. They found small effects in changes in streamflow but significant changes in partitioning streamflow causing higher surface runoff (Wang, Kalin, Kuang, & Tian, 2014). Impacts of afforestation and deforestation on hydrological response have also been studied (Cecílio, Pimentel, & Zanetti, 2019; McNulty et al., 2013; Sunde, He, Hubbart, & Urban, 2017); and consistent results have not been an outcome of the impact of forest on water yield (Cecílio et al., 2019). There are few LUC impact studies in the Southeast, US; and Southeast region in the US has been experiencing rapid LUC comparing to

other regions in the country (Trail et al., 2013), therefore, there is a need for LUC impact studies in this region.

Moreover, catchment specific characteristics like seasonality and storm frequencies have implications in the flood peaks (Villarini & Smith, 2010). Natural hazards like droughts, floods, and in general vulnerabilities produced by climate, are results of regional behavior not global (Hoyos et al., 2019; Mahmood et al., 2010). Also, it is essential to improve regional projections to determine the mechanisms of the regional forcings and related climate impacts clearly (NRC & CRC, 2005). Although, most studies on hydrological future projections have come to the conclusion that water balance components will be affected under climate scenarios, the hydrological response itself varies depending on region-specific characteristics, topography, geography, location, and precipitation regimes (Sunde et al., 2017). Previous studies have revealed the general impacts of the climate change for the entire Southeast of the US. On the other hand, since climate variables should be calculated to investigate the climate change impact on hydrology, it is necessary to couple an improved downscaled General Climate Models (GCMs) with SWAT (B. K. Pandey, Khare, Kawasaki, & Mishra, 2019). In past few years, researcher have used the predecessors of the GCMs (Y. Chen et al., 2019; Hoyos et al., 2019; B. K. Pandey et al., 2019; Sunde et al., 2017). Therefore, in this study we coupled an improved downscaled GCMs on the watershed scale, in Southeast, US.

The novelty of the work is that we used the Coupled Model Intercomparison Projects - Phase 5 (CMIP5) downscaled data with increased robustness and detailed outcome combined with new LUC projections based on the Shared Socioeconomic Pathways (SSP). These maps are consistent with four IPCC emissions scenarios with improved demographic and spatial allocation models. We carried out the investigation on the subbasin scale and with new developed techniques for data preparation. This study provides greater details on combined effects of the drivers for a better understanding of the hydrological processes in Southeast, US.

We used SWAT for hydrological modeling and coupled it with three representative GCM models in which the data are downscaled using a new developed method called Localized Constructed Analogs (LOCA).The goals of the study are i) to establish a robust hydrological model for the watershed, ii) to couple the detailed projections with a new downscaling method as well as new LUC scenarios and iii) to analyze the response of the watershed to the future stressors.

## 2.2 Study Area

The Upper Choctawhatchee Subbasin (UCS) is in Southeast Alabama. It is a Subbasin of the Hydrologic Unit Code (HUC) of 03140201 (Seaber, Kapinos, & Knapp, 1987). The area is in East Gulf Coast Plain physiographic section of Alabama. It is heavily forested, mainly Evergreen land cover type (FRSE), based on National Land Cover Database (NLCD) land cover classification derived from Multi-Resolution Land Characteristics (MRLC) Consortiums (MRLC-Consortium, 2019). The second large land cover is Agricultural Land with 15.4 percentage of the UCS area. The main crops are cotton and peanut. Other crop types are corn, soybean, pecans, and sorghum (Hinson, Rogers, & Cook, 2015). The percentage of all classes of urban land cover adds up to 8%. It comprises of different land cover classes. Table 1 illustrates the main land use and their coverage area. The total drainage area is 3940 km<sup>2</sup>. The UCS is located between longitudes -86 and -85.26 and latitudes 31 and 31.88. The topographic characteristic of the area can be described as alluvial flood plains, prairies, sharp ridges, and gently rolling hills. Geologic structures are originally made from sediment; these units underlie the Coastal Plain and consist of sand, gravel, porous limestone, chalk, marl, and clay (Hinson et al., 2015).

**Table 1.** NLCD land cover types and their coverage of the UCS area.

LANDUSE	Area [ha]	Percentage of UCS Area
<b>Water → WATR</b>	3168.86	0.80
<b>Residential-Low Density → URLD</b>	21349.28	5.42
<b>Residential-Medium Density → URMD</b>	7184.80	1.82
<b>Residential-High Density → URHD</b>	2496.96	0.63
<b>Industrial → UIDU</b>	1082.28	0.27
<b>Southwestern US (Arid) Range → SWRN</b>	539.32	0.14
<b>Forest-Deciduous → FRSD</b>	52912.48	13.43
<b>Forest-Evergreen → FRSE</b>	92582.48	23.50
<b>Forest-Mixed → FRST</b>	26035.75	6.61
<b>Range-Brush → RNGB</b>	59858.78	15.19
<b>Range-Grasses → RNGE</b>	5827.57	1.48
<b>Hay → HAY</b>	39285.90	9.97
<b>Agricultural Land-Row Crops → AGRR</b>	60659.59	15.40
<b>Wetlands-Forested → WETF</b>	20050.99	5.09
<b>Wetlands-Non-Forested → WETN</b>	946.69	0.24

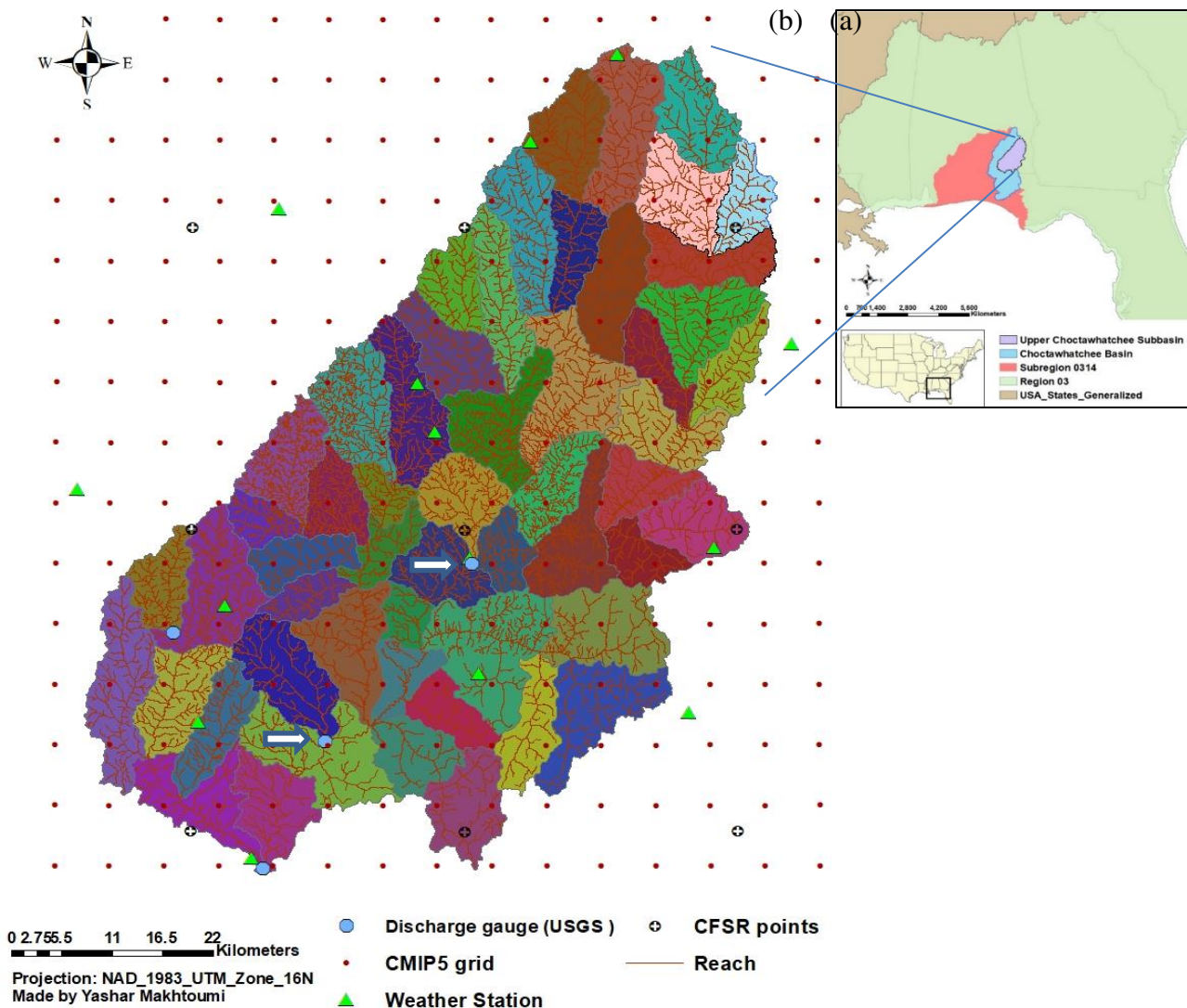


**Figure 1.** (a) Location of Upper Choctawhatchee Subbasin (UCS) in Southeast, USA. The legend represents the hydrologic division order from Region to Subbasin. (b) UCS delineation and 54 subwatersheds; Big blue dots represent the location of USGS discharge gages; Small black dots represent the CMIP5 grid; yellow rectangles indicate the weather station locations; plus marks indicate CFSR points; and reaches were shown in green lines. Monitoring points are also shown with white arrows where the upper station is Newton (NW) (USGS2361000) and the lower station is Bellwood (BL) (USGS2361500).

According to the Index of Biotic Integrity, the biological stream condition of the subbasin and the Pea River Subbasin (located at the west of the UCS) is as follows: 64% is rated very poor to fair, 30% is rated good and 6% is rated excellent (Hinson et al., 2015; O’Neil, Shepard, & Cook, 2006). Farmers have been using traditional ways of irrigation, thus undeveloped agricultural practices as a sign of lack water management could pose threats to the already-degraded ecosystem. Climate in the region is considered to be sub-tropical, consequently, it is humid with hot summers and mild winters. Annual mean temperature is around 18.5°C. Average daily temperature for cold time of the day is 18.5°C as opposed to 32°C as the hottest moment. Average annual precipitation ranges from 1295 mm to 1422 mm (USWeatherService, 2019). Figure 1 illustrates the area of study.

## 2.3 Materials and Methods

### 2.3.1 Spatial Data

We incorporated spatial analysis using Geological Information System (GIS) techniques and developed a code (SWATpy) in Python programming language to semi-automate and perform the analyses. The code is under development to fully automate the entire modeling process. Python 3 and ArcSWAT version 2012.10.19 (SWAT v2012, rev.667) were used. Soil, Land use, and elevation data (Digital Elevation Model (DEM)) are in a gridded format. US soil database includes two types of soil data: State Soil Geographic Database (STATSGO) and gridded Soil Survey Geographic Database (gSSURGO) (SoilSurvey, 2019b). The former is built in SWAT soil database and the latter were derived from United States Department of Agriculture (USDA) (Winchell, Srinivasan, Di Luzio, & Arnold, 2013). gSSURGO was selected for the modeling due to greater detail and better performance (SoilSurvey, 2019a). The UCS soil map has more than 250 soil classes. The elevation and land use data sets were derived from US Geological Survey (USGS) and Multi-Resolution Land Characteristics (MRLC) Consortiums, respectively. The Digital Elevation Model (DEM) of 1/3 arc-second (approximately 10m resolution for the study area) was used. It is a 3DEP (3D Elevation Program) map (U.S.GeologicalSurvey, 2017). The data extent is 1\*1 degree. The land use data set is NLCD2016 in 30 m resolution (L. Yang et al., 2018); and the corresponding 2001-2006 lookup table was used.

### 2.3.2 Hydro-Meteorological Data

SWAT uses 5 type of daily weather data as input: precipitation, temperature, solar radiation, wind speed, and humidity (Neitsch, Arnold, Kiniry, & Williams, 2011). For Precipitation and temperature, measured data from weather stations were used. For other climate variables, we used the model's Weather Generator (Neitsch et al., 2011). The generated variables are created using statistical data calculated from monthly average values for the climatic variables within the SWAT weather databases (JG Arnold et al., 2013; Neitsch et al., 2011). The data used in this study are daily and span from 1998 to 2013.

Big gaps between Land-based weather station (LBWS) can be problematic (Fuka et al., 2014). Since we had noticeable gaps between some of the LBWS, two weather data were tested: Climate Forecast System Reanalysis (CFSR) from the National Centers for Environmental Predictions (NCEP) and LBWS data. The preliminary result for latter was better. Therefore, the LBWS data were selected. We believe this is due to the courser resolution of the CFSR data comparing to the distances weather stations. The CFSR resolution is  $0.5^{\circ}$  latitude  $\times 0.5^{\circ}$  longitude (Saha et al., 2010). A few studies have done the same analysis and reached the same conclusion (Dile & Srinivasan, 2014; Roth & Lemann, 2016). Even though, the distribution of the LBWSs was irregular as opposed to gridded distribution of CFSR data, the land-based data performed better. SWAT assigns one weather station data to each subbasin (closest LBWS to the centroid of a subbasin) (Masih, Maskey, Uhlenbrook, & Smakhtin, 2011; Winchell et al., 2013). There are two methods to connect LBWS to the subbasins: the centroid method and time dynamic Voronoi tessellation (Andersson, Zehnder, Wehrli, & Yang, 2012; Neitsch et al., 2011; Tuo, Duan, Disse, & Chiogna, 2016; Winchell et al., 2013). The former was utilized which had advantages and disadvantages (Cho, Bosch, Lowrance, Strickland, & Vellidis, 2009; Galván, Olías, Izquierdo, Cerón, & de Villarán, 2014; Tuo et al., 2016). Considering the procedure for assigning gauge station in SWAT, we carried out a sensitivity analysis for our original LBWSs and then three LBWSs were removed due to false allocation of the weather data.

The observed streamflow data were derived from the National Water Information System (NWIS) of U.S Geological Survey (USGS). From four stream sites within the UCS, two of them that had representative location and long recorded data were selected. The selected sites (Newton (NW) (USGS2361000) and Bellwood (BL) (USGS2361500)) have mean daily discharge data

since 1921/12/01. The observed discharge data used for this study spans from 2000 to 2010 as the base line.

**Table 2.** SWAT Input Data.

Data Type	Description	Available Source	Spatial resolution
Soil Elevation	gSSURGO: US gridded soil map 3DEP-DEM 1/3 arcsecond	<a href="#">Geospatial Data Gate</a> <a href="#">The National Map</a> <a href="#">Multi-Resolution Land Characteristics (MRLC) Consortium</a>	10m*10m 10m*10m
Land Cover	NLCD2016	<a href="#">National Water Information System</a>	30m*30m
Observed discharge data	Discharge, cubic feet per second (Mean)		Daily
Observed climate data	Daily measured rainfall and temperature. Wind speed, humidity, and solar radiation was generated by SWAT	<a href="#">SWAT Model Website</a>	Daily
Future climate data	Downscaled bias-corrected daily precipitation and (min/max) temperature	<a href="http://loca.ucsd.edu/">http://loca.ucsd.edu/</a>	Daily

### 2.3.3 Future Climate Data

A set of benchmark emission scenarios referred to Representative Concentration Pathways or RCPs (R. Moss et al., 2008) are possible development trajectories for the main climate change drivers (Van Vuuren, Edmonds, et al., 2011). Research on the multi-gas emission scenarios were the base of the RCPs development (Clarke et al., 2007; Fujino, Nair, Kainuma, Masui, & Matsuoka, 2006; Riahi, Grübler, & Nakicenovic, 2007; Smith & Wigley, 2006; Van Vuuren et al., 2007; Wise et al., 2009). They collectively encompass (extending to year 2100) radiative forcing values from 2.6 to 8.5 W/m<sup>2</sup> relative to year 1750 (59, 27). These scenarios are as follows: RCP2.6, RCP4.5, RCP6, and RCP8.5. RCP 2.6 is a mitigation scenario, and its goal is to keep the global mean temperature rise under 2°C (R. Moss et al., 2008; R. H. Moss et al., 2010; Van Vuuren, Stehfest, et al., 2011). The radiative forcing for RCP2.6 increases up to around 3 Watts per square meter (W/m<sup>2</sup>) before 2100 and then declines (Meinshausen et al., 2011; Van Vuuren, Stehfest, et al., 2011). Under RCP4.5 and RCP6, concentration of GHGs are stabilized (without overshoot) after 2100 (R. H. Moss et al., 2010). RCP4.5 stops increasing radiative forcing at 4.5 W/m<sup>2</sup> by year 2100 and the forcing becomes constant afterward (Thomson et al., 2011). RCP6 pathway controls the increasing radiative forcing at 6 W/m<sup>2</sup> without exceeding the value afterward (Masui et al., 2011). GHGs emission increase by around 2060 and then decline till 2100 (64). RCP8.5

assumes high population and slow economic growth which leads to increasing GHGs emissions resulting in radiative forcing as high as  $8.5 \text{ W/m}^2$  by end the 21<sup>st</sup> century and it is assumed to rise afterward (Riahi et al., 2011). Additional actions are required to halt continuously rising level of GHG concentrations which are due to the growth of global population and economic activities (Pachauri et al., 2014). These actions are dependent upon the political and socio-economic conditions on the global scale (Van Vuuren et al., 2007; Van Vuuren, Stehfest, et al., 2011). With taking the current global political condition and its possible future pathway into account, we selected the RCP 4.5 and RCP6.0 as moderate and severe pathways, respectively.

The Global Climate Models (GCMs) use these RCPs to produce future climate data. The main source of climate projections is the modeling results of the Coupled Model Intercomparison Projects (CMIP3 & CMIP5) (Sunde et al., 2017). Since GCMs' horizontal resolution is low, it is difficult to derive regional scale climate information from them (Flato et al., 2014). In general, GCM results are not reliable for models with resolution less than 200 km (Gerard A Meehl et al., 2007). Hydrological processes occur on a scale (in order of 10km) at which GCMs (resolution of 1° to 2.5° latitude-longitude) cannot provide reliable results (Kundzewicz et al., 2007; D. Pierce & Cayan, 2016). Moreover, GCMs are not able to capture frequency and magnitude of extreme events (Christensen & Christensen, 2007; Fowler, Blenkinsop, & Tebaldi, 2007). Therefore, for important climate variables like precipitation and temperature it is necessary to use higher resolution. Downscaling techniques have been used rigorously to produce climate variables from GCMs on the desired scale for hydrological modeling of climate change impact studies (Fu et al., 2013; Maraun et al., 2010; Sunde et al., 2017). Between two types of the existing downscaling techniques which are dynamical and statistical, we used the statistical downscaling method due to availability of the algorithm. Statistical method downscales GCMs' output based on the historical relationship between large- and small-scale conditions (D. W. Pierce, Cayan, & Thrasher, 2014). In this study we used a statistical downscaling called Localized Constructed Analogs (LOCA). LOCA chooses analog days from observed data and applies a multiscale spatial matching scheme to estimate suitable downscaled climate variables (D. W. Pierce et al., 2014). More realistic regional patterns of precipitation, better estimates of extreme events, and reduced number of light-precipitation days are the advantages of LOCA (D. W. Pierce et al., 2014). More information on LOCA can be found here: <http://loca.ucsd.edu/>, (Ficklin & Barnhart, 2014).

Considering the complexity of the GCMs, CMIP5 outputs are inevitably biased (Taylor, Stouffer, & Meehl, 2012; Teutschbein & Seibert, 2010). Bias correction (BC) is the process of transforming GCM outputs using algorithms in order to adjust the outputs (Y. Chen et al., 2019; Teutschbein & Seibert, 2010). Basically, biases are detected by comparing the observation and simulation results and then they are used to correct baseline and projections (Y. Chen et al., 2019; Teutschbein & Seibert, 2010). Bias-corrected inputs for hydrological modeling improve the result, hence bias correction is needed for GCMs output (D. W. Pierce, Cayan, Maurer, Abatzoglou, & Hegewisch, 2015; Wilby et al., 2000). LOCA as a downscaling technique improved based on constructed analogs (CA) process contains a bias correction step (Hidalgo León, Dettinger, & Cayan, 2008; D. W. Pierce et al., 2014). The BC in LOCA includes 3 steps. First, a preconditioning technique is used to correct the annual cycle and then two different distribution techniques are used, one for temperature and one for precipitation , and finally a frequency-dependent bias correction (FDBC) is used to adjust the sequencing of variation for different time scales, since the sequencing for GCM outputs potentially differ from observed ones (H. Li, Sheffield, & Wood, 2010; D. W. Pierce et al., 2015). We obtained and analyzed CMIP5 output the LOCA dataset for three models, CCSM4, GISS-E2-R, and GFDL-CM3, under RCP4.5 and RCP6.0 from Downscaled CMIP5 Climate and Hydrology Projections (<https://gdo-dcp.ucar.edu/>) (Bureau of Reclamation, 2013; L. J. Donner et al., 2011; Gent et al., 2011; Schmidt et al., 2006; Taylor et al., 2012). These models were selected among 32 GCMs based on metrics such as spatial correlation, bias, and root mean square error (RMSE). These metrics were based on Sheffield et al. (2013) study and used to quantify the error relative to observed annual and seasonal precipitation and temperature in the Southeast US (Sheffield et al., 2013).

The downloaded data are bias-corrected 1/16<sup>th</sup> degree latitude-longitude (~6km ×6km) daily precipitation (mm/day), and maximum and minimum temperature (°C) projections. Hereafter the downloaded dataset, which is downscaled, and bias corrected by LOCA, is referred as “the CMIP5 multi-model ensemble LOCA”. The LOCA dataset contains future projections under RCP4.5 and RCP6.0 for 32 GCMs for the conterminous US from 1950 to 2099. For selected models, errors w.r.t. to observation from Livneh et al. (2015) in southeast US, are less than 5%, 0.5 °C and 0.5 °C for daily precipitation, daily maximum temperature, and daily minimum temperature, respectively (Livneh et al., 2015; D. W. Pierce et al., 2014). From the evaluation and

verification results, it can be concluded that the LOCA performance is better for Southeast region comparing to other regions across the US (<http://loca.ucsd.edu/>.)

In hydrological projection process using GCMs, their initial condition, future scenarios, and hydrological model, all incorporate uncertainties to the result (J. Chen, Brissette, Poulin, & Leconte, 2011). Ouyang et al. (2015) have concluded that different result of the future projections are partially due to the different climate models (Ouyang et al., 2015). Considering the numerous numbers of the GCMs and the variability they could cover based on the model skill and independency, we selected the three models to be able to analyze broad extents of changing climate variables within the UCS; in this way we were able to address the uncertainty (Sanderson, Knutti, & Caldwell, 2015a, 2015b; Sunde et al., 2017). Locating and Selecting Scenarios Online (LASSO) tool from Environmental Protection Agency (EPA) (<https://lasso.epa.gov/>) was used to filter out the selected model from 32 GCMs. Through the different steps of the tool, we have examined climate parameters variabilities with two time periods (annual and seasonal) and selection strategies to reach the goal of three representative models. Models' name, their associated institution, type of experiment, and ensemble member are shown in Table 3 (Taylor et al., 2011).

**Table 3.** Selected models for Upper Choctawhatchee subbasin future climate projections.

Model identifier	Institution	Experiment	Ensemble Member
CCSM4	National Center for Atmospheric Research	RCP4.5, RCP6.0, historical	r6i1p1
GISS-E2-R	NASA Goddard Institute for Space Studies	RCP4.5, RCP6.0, historical	r6i1p1, r2i1p1
GFDL-CM3	National Oceanic and Atmospheric Administration (NOAA)- Geophysical Fluid Dynamics Laboratory	RCP4.5, RCP6.0, historical	r1i1p1

**Table 4.** CO<sub>2</sub> concentration for projections.

Time period	Emission scenarios	CO <sub>2</sub> concentration (ppm*)
2000-2010	Historical	369
2039-2069	RCP4.5	487
2039-2069	RCP6.0	478
2070-2099	RCP4.5	541
2070-2099	RCP6.0	670

\* ppm: parts-per-million.

## 2.4 Scenario Development

Two projection periods, both under RCP4.5 (moderate) and RCP6.0 (severe) were presented, mid-century (2040-2069) and late-century (2070-2099). The results of hydrological simulation were shown in monthly, seasonal, and annual time scales. The seasons were defined as DJF (winter: December, January, February), JJA (summer: June, July, August), MAM (spring: March, April, May), and SON (fall: September, October, November). It would be more appropriate to refine these general scenarios to the study area by getting inputs from regional stakeholders. This is a limitation of this study and a potential area for future research.

SWAT incorporates CO<sub>2</sub> to account for its impact on plant water requirements and on level of the potential evapotranspiration (PET) (Neitsch et al., 2011). It takes the CO<sub>2</sub> concentration amount as a single input value for each subbasin. The CO<sub>2</sub> concentration values for the historical and future projections are shown in Table 4. The values are derived from Meinshausen, Smith et al. (2011).

Projected population for the conterminous US indicates significant increase in demand for food, energy, and urban development (Sohl et al., 2014). From 2001 to 2011, the Southeast region (AL, AR, FL, GA, KY, LA, MS, NC, SC, TN, and VA) has lost more than 100 and 1400 mi<sup>2</sup> agricultural land and forest, respectively, and gained 600 mi<sup>2</sup> developed land cover (Sleeter et al., 2018). For UCS and Pea and Yellow River Subbasin, farming land decreased 27.21% and urban area increased 42.55% from 1992 to 2011 (Hinson et al., 2015). Regarding land use condition in the future, there have been few studies (national US and global scale) based on different scenarios including Special Report on Emission Scenarios (SRES) (96) , RCP, and Shared Socioeconomic Pathways (SSP) (95) of Intergovernmental Panel for Climate Change (IPCC) (Nakicenovic et al., 2000; Riahi et al., 2017; Sleeter et al., 2018; Sohl et al., 2014; Sohl, Wimberly, Radeloff, Theobald, & Sleeter, 2016; Wear, 2011). Sohl et al. (2014) using different land use forecasting model, has predicted 22.9% to 61% increase in urban land cover for conterminous US by the year 2050. They projected noticeable loss of natural covers which was due to expansion of anthropogenic land uses. The fourth National Climate Assessment reported 50% and 80% increase in urban land use allocation by 2100 under SSP2 and SSP5 respectively with 2010 land use condition as the baseline (Sleeter et al., 2018). To account for these changes, we obtained and analyzed projected land covers for each decade till 2100 from Fourth National Climate Assessment dataset through Global

Change Explorer (GCX) (GCX, 2020). The land use scenarios (land-use change scenarios for the conterminous United States forecast decadally from 2000 to 2100) used in this study, are the results of the Integrated Climate Land Use Scenario ICLUSv.2 model. ICLUS couples demographic growth model with a spatial allocation model (Spatially-Explicit Regional Growth Model (SERGoM) (Theobald, 2005); and produces land use scenarios consistent with IPCC (Sohl et al., 2016). Bierwagen et al. (2010) has studied the model and related components. The maps were verified by developing a regression tree model and with values from three “ground-truth” datasets generated from high-resolution aerial photography, which showed good fit of  $R^2=0.96$  ( $y=0.624x+5.730$ ). They also compared conditions in 1989 for 56 watershed (14-digit Hydrologic Unit Code) and found good fit with  $R^2=0.96$   $y=0.823x-1.060$ ) (Bierwagen et al., 2010). These maps are based on SSP scenarios with 19 land cover classes (Agency, 2017; Bierwagen et al., 2010). One possible caveat though, is that there is not much agreement between different forecasting models and they appear to be at the beginning stage of development (Sohl et al., 2016). Future projection results for all models in this study were presented in monthly, seasonal, and annual average and compared to the historical result to analyze the future hydrological condition within the UCS. Then we did the same comparison for SWAT simulation, mainly discharge. Corresponding land use projections to projection periods (mid-century and end-century) were used in SWAT modeling to simulate the discharge and evapotranspiration (ET). Finally, we demonstrated seasonal changes of the climate and hydrological variables.

SWAT: For this study we used Soil & Water Assessment Tool (SWAT)(Jeff Arnold, 1994). SWAT is assemblages of mathematical equations representing different parts of hydrological cycle including movement, fate, and transport of water, sediments and nutrients in and on soil, through groundwater, and in river streams and reservoirs (J. G. Arnold, Srinivasan, Muttiah, & Williams, 1998; ASABE, Jun. 2017). The development of the model started in early 1990s and it has been evolving by United States Department of Agriculture (USDA) Agricultural Research Service (ARS) (J. G. Arnold et al., 2012; Gassman, Reyes, Green, & Arnold, 2007). It is a process based and semi-distributed continuous-time river basin scale model (JG Arnold et al., 2011; J. G. Arnold et al., 2012). It has been written in Fortran language including more than 310 subroutines representing different parts of the hydrological and bio-geochemical processes (JG Arnold et al., 2011; J. G. Arnold & Fohrer, 2005). It was originally developed to evaluate water resources

management and Nonpoint Source (NPS) pollution in large river basin (J. G. Arnold et al., 2012). It has proven to be effective for its purposes and computationally efficient and can be used for long term continuous simulation including climate change impact studies (J. G. Arnold et al., 2012; Gassman et al., 2007). It operates on a daily time step and outputs daily, monthly, and yearly results (J. G. Arnold et al., 2012; Gassman et al., 2007). SWAT splits a watershed into subwatersheds that are further split into hydrologic response units (HRUs) (J. G. Arnold et al., 2012; Gassman et al., 2007). HRUs are nonspatial units and unique combination of homogeneous land use, soil, slope and management characteristics (J. G. Arnold et al., 2012; Gassman et al., 2007). This gives SWAT the capability to model surface runoff, infiltration, soil water movement, ET, in-stream transformations, sediment movement, canopy interception, plant uptake, and nutrients circulation including biogeochemical processes at HRU level (Neitsch et al., 2011). Main components of a SWAT model for a given watershed are weather, hydrology, erosion/sedimentation, plant growth, nutrients, pesticides, agricultural management, stream routing and pond/reservoir routing (J. G. Arnold & Fohrer, 2005). Simulation in SWAT has two parts, land phase and routing phase; in land phase, the amount of water, sediment, nutrient, and pesticide loadings are regulated into the main channel in each subbasin, and in the routing phase, in- stream processes including water movement, sediment transport and the nutrients loading are simulated (J. G. Arnold et al., 2012; Neitsch et al., 2011). In SWAT, water balance is the base of all the processes and the hydrological cycle is climate driven, thus, SWAT requires precipitation, minimum and maximum temperature, solar radiation, relative humidity, and wind speed at a daily time scale (J. G. Arnold et al., 2012; Deb & Kiem, 2020).

SWAT uses equation (1) to simulate water balance (J. G. Arnold et al., 1998; Neitsch et al., 2011):

$$SW = SW_0 + \sum_{i=1}^t (R_{day} - Q_{surf} - E_a - w_{seep} - Q_{gw}) \quad (1)$$

where  $SW$  and  $SW_0$  are soil water content for beginning and end of the model, respectively.  $t$  (day) is time.  $R_{day}$  is rainfall;  $Q_{surf}$  is surface runoff;  $E_a$  is evapotranspiration;  $w_{seep}$  is percolation to vadose zone, and  $Q_{gw}$  is return flow amount, and all variables are in mm (J. G. Arnold et al., 1998; Neitsch et al., 2011).

Water yield as part of subbasins blue water is the amount of water after leaving HRUs and entering the main channel is calculated with equation (2) (JG Arnold et al., 2013; Neitsch et al., 2011; Veettil & Mishra, 2016):

$$WYLD = Q_{surf} + Q_{lat} + Q_{gw} - tloss - \text{Pond abstractions} \quad (2)$$

where WYLD is the amount of water yield,  $Q_{surf}$  is surface runoff,  $Q_{gw}$  is return flow amount,  $Q_{lat}$  is the amount of lateral flow,  $tloss$  is transmission losses, and the abstracted water from the pond; all variables are in mm (JG Arnold et al., 2013; Chanapathi, Thatikonda, & Raghavan, 2018; B. K. Pandey et al., 2019).

In SWAT surface runoff can be estimated in two ways: SCS (Soil Conservation Service) runoff curve number method (USDA-SCS, 1972) and the Green & Ampt infiltration method (1911) (Neitsch et al., 2011)(45). We used the former. Equation (3) is SCS runoff curve number method (J. G. Arnold et al., 1998; Neitsch et al., 2011):

$$Q_{surf} = \begin{cases} \frac{(R_{day} - 0.2S)^2}{(R_{day} + 0.8S)} & R_{day} > 0.2S \\ 0 & R_{day} \leq 0.2S \end{cases} \quad (3)$$

where  $Q_{surf}$  is surface runoff;  $R_{day}$  is rainfall; and  $S$  is retention parameter.  $0.2S$  is estimated as the initial abstraction including surface storage (Neitsch et al., 2011). Retention parameter varies through the watershed and time owing to changes in soil, land use and management (Neitsch et al., 2011).  $S$  is estimated as follows:

$$S = 254 \left( \frac{100}{CN} - 10 \right) \quad (4)$$

where CN is the curve number which is adjusted for different soil moisture level and slope (Neitsch et al., 2011).

For surface runoff equation 3 was used. For flow routing the variable storage coefficient method were used (Neitsch et al., 2011; J. R. Williams, 1969). Since our modeling required simulation of CO<sub>2</sub> climate change effects, the Penman-Monteith method was used for calculation of potential evapotranspiration(Allen, 1986; Allen, Jensen, Wright, & Burman, 1989; Monteith, 1965). Actual evapotranspiration (AET) was calculated by procedure established by Ritchie (1972) (J. T. Ritchie, 1972). The UCS was delineated into 54 subbasin and 1821 HRUs. ‘SWAT2012 rev64’ version was used to perform the modeling.

## 2.5 Calibration and Validation

Calibration can be manually done or through a combination of manual and auto calibration procedures (D. Moriasi, Wilson, Douglas-Mankin, Arnold, & Gowda, 2012). Our approach to calibrate and validate was the later through a split-sample strategy (D. Moriasi et al., 2012). To evaluate the performance of the model we have first carried out a sensitivity analysis (SA) manually and then using SWAT Calibration and Uncertainty Procedures (SWAT-CUP) to filter out insensitive parameters to reduce the computational workload of the calibration (K. C. Abbaspour, Vejdani, Haghhighat, & Yang, 2007; Ghoraba, 2015; Gupta, Sorooshian, & Yapo, 1999; Saltelli, Tarantola, Campolongo, & Ratto, 2004). Sensitivity analysis is to estimate how much model outputs change with respect to each model parameter (input) change (J. G. Arnold et al., 2012; Saltelli et al., 2004). First a set the parameters were selected according to UCS hydrologic characteristics and the literature (K. C. Abbaspour et al., 2015; K. C. Abbaspour, Yang, et al., 2007; J. G. Arnold et al., 2012; Joh et al., 2011; Osei et al., 2019; Qiu, Shen, Chen, & Hou, 2019; Sudheer, Lakshmi, & Chaubey, 2011). Then using one-factor-at-a time sensitivity analysis initial parametrization was carried out and parameters were optimized, and their initial ranges were predicted (K. C. Abbaspour et al., 2015; Green & Van Griensven, 2008; Morris, 1991). After a set of manual calibration using first set of the parameters, we used SWAT-CUP to modify the selected parameters and perform sensitivity and uncertainty analysis (J. G. Arnold et al., 2012). We used the Sequential Uncertainty Fitting version algorithm (SUF12) within SWAT-CUP (K. C. Abbaspour, Johnson, & Van Genuchten, 2004; K. C. Abbaspour, Yang, et al., 2007). The SUFI2 is based on the invers modeling and is to estimate parameters using observed data (K. C. Abbaspour et al., 2004; K. C. Abbaspour, Yang, et al., 2007). In other words, it uses initial large parameter uncertainty and through steps, decrease the uncertainty until the uncertainty range falls within a range/band called 95% Prediction Uncertainty (95PPU) (K. Abbaspour, 2015; K. C. Abbaspour et al., 2004). SUFI2 uses a global search approach to carry out optimization and uncertainty analysis and it can handle many parameters (K. Abbaspour, 2015; K. C. Abbaspour et al., 2004). For accuracy quantification of the model, our objective function includes Nash–Sutcliffe Efficiency (NSE), Coefficient of Determination ( $R^2$ ), Percent Bias (PBAIS), RMSE–observations standard deviation ratio (RSR) (Gupta et al., 1999; Legates & McCabe Jr, 1999; D.

N. Moriasi et al., 2007; Nash & Sutcliffe, 1970). The metrics for satisfactory thresholds were selected based on the literature (K. C. Abbaspour et al., 2015; D. N. Moriasi et al., 2007; Santhi et al., 2001). Table 5 shows the objective function and the thresholds of the metrics and final results for calibration and validation period. Following are the formulas used for these metrics.

$$NSE = 1 - \left[ \frac{\sum_{i=1}^n (Y_i^{obs} - Y_i^{sim})^2}{\sum_{i=1}^n (Y_i^{obs} - Y^{mean})^2} \right] , \quad -\infty < NSE \leq 1 \quad (5)$$

$$R^2 = \left[ \frac{\sum_{i=1}^n (Y_i^{obs} - Y^{mean})(Y_i^{sim} - Y^{simmean})}{\left[ \sum_{i=1}^n (Y_i^{obs} - Y^{mean})^2 \right]^{0.5} \left[ \sum_{i=1}^n (Y_i^{sim} - Y^{simmean})^2 \right]^{0.5}} \right]^2 , \quad 0 \leq R^2 \leq 1 \quad (6)$$

$$PBAIS = \left[ \frac{\sum_{i=1}^n (Y_i^{obs} - Y_i^{sim}) \times (100)}{\sum_{i=1}^n (Y_i^{obs})} \right] , \quad -\infty < PBAIS < +\infty \quad (7)$$

$$RSR = \frac{\sqrt{\sum_{i=1}^n (Y_i^{obs} - Y_i^{sim})^2}}{\sqrt{\sum_{i=1}^n (Y_i^{obs} - Y^{mean})^2}} , \quad 0 \leq RSR < +\infty \quad (8)$$

where  $Y_i^{obs}$  is the  $i$ th measured stream flow;  $Y_i^{sim}$  is  $i$ th simulated stream flow;  $Y^{mean}$  is the mean of observed stream flow data;  $Y^{simmean}$  is the mean of simulated data,  $n$  the total number of observations.

NSE value between 0.0 and 1 is considered acceptable with 1 being the optimal value indicating the plot of observed versus simulated fits perfectly (D. N. Moriasi et al., 2007; Nash & Sutcliffe, 1970). For  $R^2$ , the higher the value the lesser the error variance and values greater than 0.5 are considered to be acceptable (D. N. Moriasi et al., 2007; Santhi et al., 2001). Negative PBIAS means overestimation and positive PBIAS means underestimation, with 0 being the optimal value. RSR ranges from 0.0 to a positive large number, with 0.0 being the optimal condition meaning the RMSE is zero. The lower RSR, the lower residual variation, indicating better model performance (D. N. Moriasi et al., 2007). NSE,  $R^2$ , and RSR are unitless and PBAIS has the unit of the constituent being evaluated which for our case is cms ( $m^3/s$ ). The global sensitivity analysis (where all parameters are allowed to change through analysis) were carried out through SWAT\_CUP to prioritize the most responsive parameters and remove parameters with smaller sensitivity from further sampling (K. C. Abbaspour, Yang, et al., 2007). Through the SA, a multiple regression analysis was used to determine the parameter sensitivity statistics (t-stat and

p-value) (K. Abbaspour, 2015). t-stat and p-value were used to describe the relative significance and significance of sensitivity, respectively (Chanapathi et al., 2018). Sensitive parameters correspond to larger absolute t-stat values among the parameters and to smaller p-values (close to 0; commonly accepted threshold is 0.05) (K. Abbaspour, 2015). Based on the SA, the following parameters were identified as responsive: SOL\_AWC (Available water capacity of the soil layer), RCHRG\_DP (Deep aquifer percolation fraction), CH\_K2 (Effective hydraulic conductivity in main channel alluvium), SLSUBBSN (Average Slope Length), ESCO (Soil evaporation compensation coefficient), GWQMN (Threshold water level in the shallow aquifer for the base flow), and ALPHA\_BF (Baseflow alpha factor). Table 6 shows final parameters and their fitted values. It is worth mentioning that the SA result is the prediction of the average changes of the objective function being produced by changes in a given parameter as other parameters are also changing (Khalid et al., 2016). p-factor and r-factor were also considered for SUFI2 performance evaluation as well as measuring the goodness of calibration (K. C. Abbaspour et al., 2004; K. C. Abbaspour, Yang, et al., 2007). p-factor is the percentage of observations covered by the 95PPU and r-factor is the ratio of the 95PPU average thickness and the standard deviation of the observations (K. Abbaspour, 2015; K. C. Abbaspour et al., 2015). The extent from 2.5% to 97.5% of the cumulative distribution of the simulated variable resulting from the Latin hypercube sampling is 95PPU (K. C. Abbaspour et al., 2004; K. C. Abbaspour et al., 2015; K. C. Abbaspour, Yang, et al., 2007). p-factor ranges from 0 to 1; p-factor greater than 0.7 means acceptable goodness of fit; r-factor varies between 0 and infinity; here r-factor less than 1.5 was considered satisfactory (K. Abbaspour, 2015; K. C. Abbaspour et al., 2004; K. C. Abbaspour et al., 2015; K. C. Abbaspour, Yang, et al., 2007).

**Table 5.** model efficiency evaluation metrics.

Metrics	Satisfactory threshold	Calibration period	Validation period
NSE	> 0.5	0.88	0.86
R <sup>2</sup>	> 0.6	0.89	0.87
PBIAS	± 25%	3.9%	6.4%
RSR	≤ 0.7	0.34	0.38
p-factor	> 0.7	0.68	0.50
r-factor	≤ 1.5	0.69	0.42

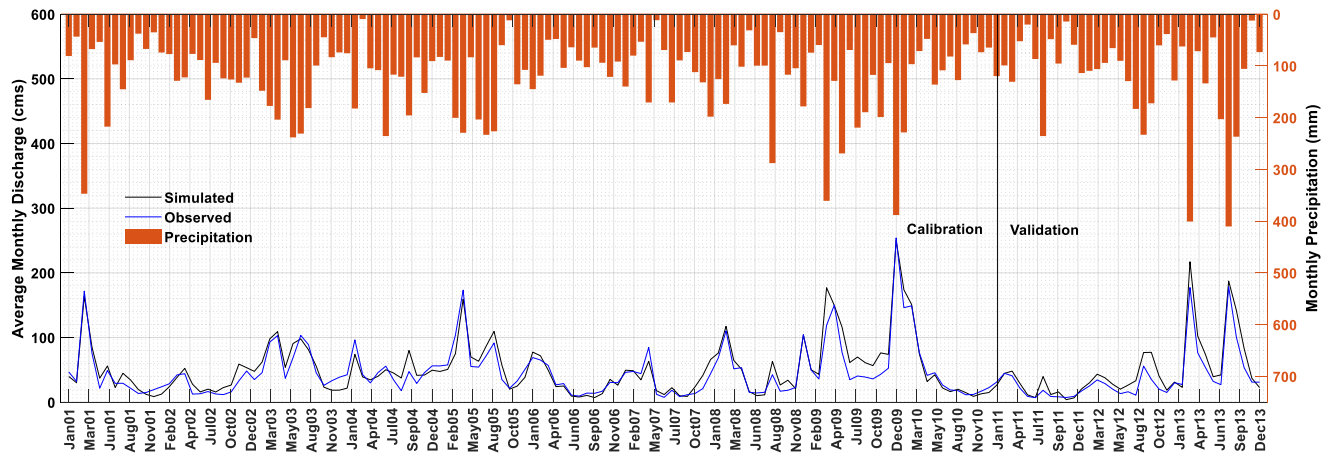


**Figure 2.** Calibration and validation result for Bellwood station.

**Table 6.** Final parameters used in SWAT simulation of Upper Choctawhatchee subbasin.

parameters	Description	Fitted value	Min_value	Max_value	File Ext
CN2	SCS* moisture condition II curve number for pervious areas	0.91	0.56	1.12	.mg t
GW_REVAP	Groundwater revap coefficient	0.20	0.11	0.25	.gw
ESCO	Soil evaporation compensation coefficient	-0.19	-0.37	-0.17	.hru
CH_K2	Effective hydraulic conductivity in main channel alluvium (mm/hr)	-0.72	-1.05	-0.52	.rte
CH_K1	Effective hydraulic conductivity in tributary channel alluvium (mm/hr)	0.70	0.48	0.95	.sub
GWQMN	Threshold water level in the shallow aquifer for the base flow (mm H <sub>2</sub> O)	-0.21	-0.35	-0.07	.gw
SOL_AWC	Available water capacity of the soil layer	-0.35	-0.62	-0.31	.sol
SLSUBBSN	Average Slope Length (m)	-0.03	-0.07	0.03	.hru
CANMX	Maximum canopy storage	0.23	0.16	0.37	.hru
ALPHA_BF	Baseflow recession constant	-0.15	-0.29	-0.14	.gw
ALPHA_BF_D	Base Flow Alpha Factor for Deep Aquifer	0.31	0.19	0.34	.gw
REVAPMN	Threshold depth of water in the shallow aquifer for "revap" to occur (mm H <sub>2</sub> O)	-0.85	-1.03	-0.50	.gw
RCHRG_DP	Deep aquifer percolation fraction	0.26	0.14	0.40	.gw

\*SCS: Soil Conservation Service.

Table 5 shows the goodness of fit metrics. The selected parameters were used to calibrate SWAT at two USGS site (Newton (USGS2361000) and Bellwood (USGS2361500)) for subbasins 29 and 52, respectively. Observed data from the later site is used for SA and uncertainty analysis. The

number of simulations was 450 with 4 iterations. SWAT was performed for period from 1998 to 2013. From 1998 to 2000 was considered as warm up; from 2001 to 2010 was the calibration period and from 2010 to 2013 was the validation period. Given the final values for the model performance metrics (Table 5) and the accepted thresholds, it was determined SWAT stream flow estimation for the UCS was efficient. Figure 2 shows the calibration results for both calibration (2001-2010) and validation periods (2011-2013).

## 2.6 Result and Discussion

The CMIP5 multi-model ensemble LOCA results for precipitation and temperature during baseline period show consistency with the observed values (Figure 3). Between the 3 models, GFDL-CM3 has the closest distribution to the observed precipitation with the 6.8% median difference and the closest number of outliers. The 25<sup>th</sup> percentile for the observation and GFDL-CM3 are 71.4°C and 74.68°C respectively. 75<sup>th</sup> percentiles are the same (148.3°C). Therefore, it indicates similar distribution. Figure 3b illustrates the temperature distribution for the observed and baseline period. It represents quiet similarity, especially for model GFDL-CM3, where the distance is between 25<sup>th</sup> and 75<sup>th</sup> percentile and the whiskers' length are the same. The median difference of models (CCSM4, GFDL-CM3, GISS-E2-R) from the observed ones are 4.2%, 2.6%, and 4.7% respectively. We also compared the baseline ET from the climate data with the observation period (Figure 3c). Figure 3c also demonstrates similar distribution from 25<sup>th</sup> to 75<sup>th</sup> percentile from all datasets. However, upper whiskers for the observation is longer. This difference has no implication on the study, since here, we are not focused on extreme weather situation.

Average maximum and minimum temperature have important repercussions on hydrological implications. Figure 4 represents monthly average of basin-wide daily maximum temperature (Figure 4b), monthly average of basin-wide daily minimum temperature (Figure 4c) and monthly average of basin-wide daily temperature (Figure 4a). For average temperature (Figure 4a) models match the observed average temperature, from mid-March to June (Spring) and from mid-September to mid-November (Fall). For Winter (DJF) and Summer (JJA), however, there are differences up to 1°C. This trend is the same of maximum temperature (Figure 4b) and minimum temperature (Figure 4c). However, the discrepancies for maximum temperature during Summer (the peak of the graph) and for minimum temperature during Winter (the legs of the graph) are

more noticeable. This behavior indicates the more extreme the temperature, the more the difference between the models and the observed data.

Figure 5 shows the monthly average of precipitation, ET, water yield, and surface runoff for 10 year for both the baseline and observed period. From mid-March to mid-June, and September and November, the average observed rainfall is the same as the models prediction with negligible differences. During Summer and Winter, however, there exist some discrepancies. These discrepancies could be attributed to the model biases. As SWAT model uses these model results as climate data, the biases can be projected to the simulated hydrological results such as ET, water yield, and surface runoff. Model predictions for ET (Figure 5b) match with the observed data except during summer with small differences up to 8% in July. Highest level of water yield occurs during the month March (Figure 5c) where the differences with the model predictions is around 13%. During Spring, Summer, and Fall models predict the amount of average water yield close to the observed data. Since surface runoff amount and water yield are linked, the yearly pattern of surface runoff follows the water yield pattern. Surface runoff is underestimated. For example in March when the highest amount of surface runoff happens through the year, the models predictions is 17% low for CCSM4 and GISS-E2-R and 11% low for GFDL-CM3. This difference is due to land use changes through the time period. Therefore, it indicates the biases of the land use map. In this study, we have not looked for extreme events that partially account for these biases. Thus, considering the different source of inevitable biases it can be concluded that the results based on the models are reliable

### **2.6.1 Future Climate and Hydrological Conditions**

Observed annual average precipitation in UCS for observation period is 1440 mm. For the omission scenarios (moderate and severe) and projected future time period (mid-century and late-century) considered in this study, annual average rainfalls vary from 1486 mm to 1569 mm. Average annual maximum and minimum temperature for baseline period are 13°C and 26°C respectively. The projected average annual maximum and minimum has increases ranging 0.98 - 2.4 °C and 1.55-2.55 °C, respectively (Georgakakos et al., 2014; Villarini et al., 2009).

Figure 6 demonstrates the monthly behavior of the projected temperature (average, maximum, and minimum) through a year for the entire simulation period (2040-2099). The

projected maximum and minimum temperature shift above with increases up 3°C in June, July, and August during mid-century. There are not noticeable changes between moderate and sever emission scenarios for mid-century, except in summer, where changes are up 1°C. For the late-century period, however, changes are significant (Figure 6 lower panel). Projected increase for RCP6.0 is doubled compared to the projected increase in temperature under RCP4.5 during late century. For both mid and late century temperature increases for Spring and Fall is not as high as increases in Summer and Winter (Gerald A Meehl, Arblaster, & Branstator, 2012). This indicates a general warming weather with hotter Summer and Winters that could potentially lead to seasonal time shifting and early snow melts and consequently changes in hydrological cycle in UCS (G. Sun, 2013; Vose et al., 2017). The annual trend of average, maximum, and minimum temperature behavior supports these changes towards the end of the century (not shown). These changes have been quantified in Table 7. Maximum and minimum temperature is projected up to 10% increase by 90s under moderate scenario and 30% increase under sever scenarios compared to baseline period (Vose et al., 2017; Walsh et al., 2014b). Table 7 also reflects decadal percent change of rainfall. Based on the models and under moderate scenarios, annual rainfall is projected to increase slightly (Figure 7). However, under sever scenarios no pattern was found. For instance, average precipitation for 40s under RCP4.5 is projected to decrease 6.33% and 1% increase during 90s compared to baseline period. Under RCP6.0, however, for 40s, precipitation change is projected to be 6.8% decrease and for 90s is 8.45% increase. This pattern implicates the wiggling behavior of the precipitation which can implicate extreme precipitation (McNulty et al., 2013; G. Sun, 2013; Sunde et al., 2017).

## **2.6.2 Annual and Seasonal Impacts of Future Climate and Water Regime**

To obtain data required for future water regime, the CMIP5 multi-model ensemble LOCA was integrated with SWAT model. We then derived precipitation, surface runoff, water yield, ET, and discharge for Bellwood (USGS2361500) monitoring point. We analyzed the data at monthly, seasonal, and annual scales. Table 8 represents the projected mean annual changes to hydrological components for the entire simulation period and each decade. Mean annual change to the discharge at Bellwood station has an increase of 30.45% under moderate scenario and 29.67% increase under the severe scenarios during the entire simulation period.

Similarly, mean annual surface runoff during the period has significantly increased with 337.4% and 325.66% under moderate and severe scenarios, respectively (McNulty et al., 2013; G. Sun, 2013). Water yield also has shown increase of 18.34% and 18.08% under moderate and severe scenarios through the entire period. Slight decreases of 0.8% under moderate scenario and 2.46% under severe scenario were observed to mean annual ET during the entire simulation(Marhaento et al., 2018; Villarini et al., 2009; Walsh et al., 2014b). Table 8 presents the simulated mean annual changes to water balance components for mid-century and late-century period. During mid-century mean annual discharge at Bellwood station was estimated to increase by 24.2% under RCP4.5 and 32.93% under RCP6.0. for late century. However, the mean annual discharge at the station shows 36.72% increase under RCP4.5 and 26.4% increase under RCP6.0 (Georgakakos et al., 2014; Ingram et al., 2013). Under the severe scenario, despite the increased urbanization, the discharge amount at the station is projected to decrease towards the end of the century (Marhaento et al., 2018; Wang et al., 2014). It can be suggested that the last decade of water balance variables has been affected dramatically (Table 8). Average annual surface runoff during the mid-century is estimated to increase by 286.3% under RCP4.5 and 315.5% under RCP6.0. Mean annual surface runoff continues to increase during the late-century by an average increase of 388.5% under moderate scenario and 335.9% under the severe emission scenarios (Wang et al., 2014). These changes indicate the significant impact of the land use change on water balance variables (Q. Chen et al., 2019). Increases to mean annual water yield were observed under both scenarios of moderate and severe emissions by 12.55% and 21.42% during mid-century.

**Table 7.** percent changes of precipitation and temperature under different scenarios.

Time period	RCP4.5			RCP6.0				
	Precipitation % change	Temperature % change			Precipitation % change	Temperature % change		
		Ave TMP	Max TMP	Min TMP		Ave TMP	Max TMP	Min TMP
41-50	3.08	4.48	4.15	5.12	8.18	5.93	4.70	8.43
51-60	4.19	5.20	4.32	6.95	10.77	8.12	6.26	11.84
61-70	8.39	5.62	5.21	6.44	10.70	10.16	8.11	14.26
71-80	8.78	6.50	5.69	8.18	4.62	12.73	10.26	17.64
81-90	11.08	6.87	6.32	7.45	7.93	16.89	13.08	24.44
91-99	8.31	8.11	9.70	9.96	0.50	21.00	16.35	30.21

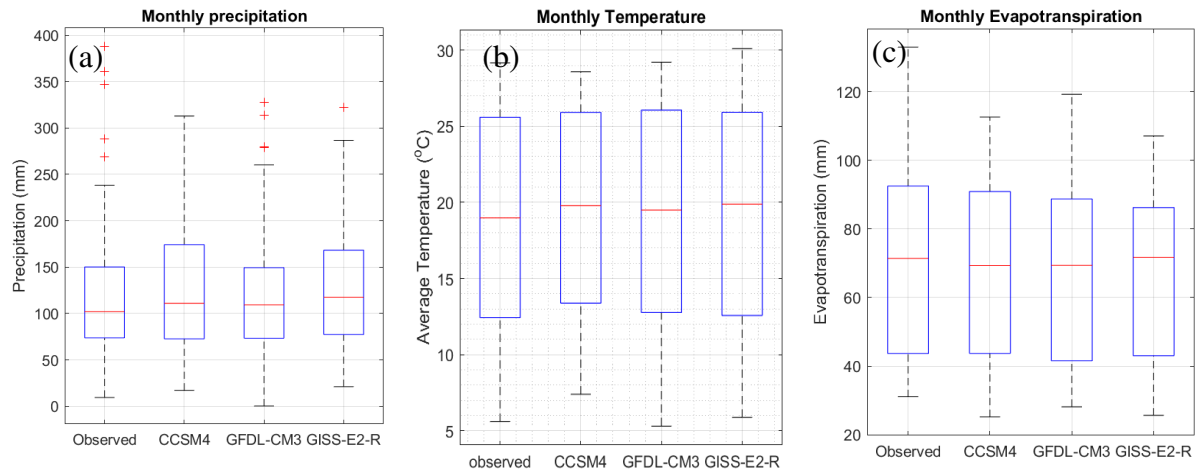


**Figure 3.** comparing GCMs results to the observed values.

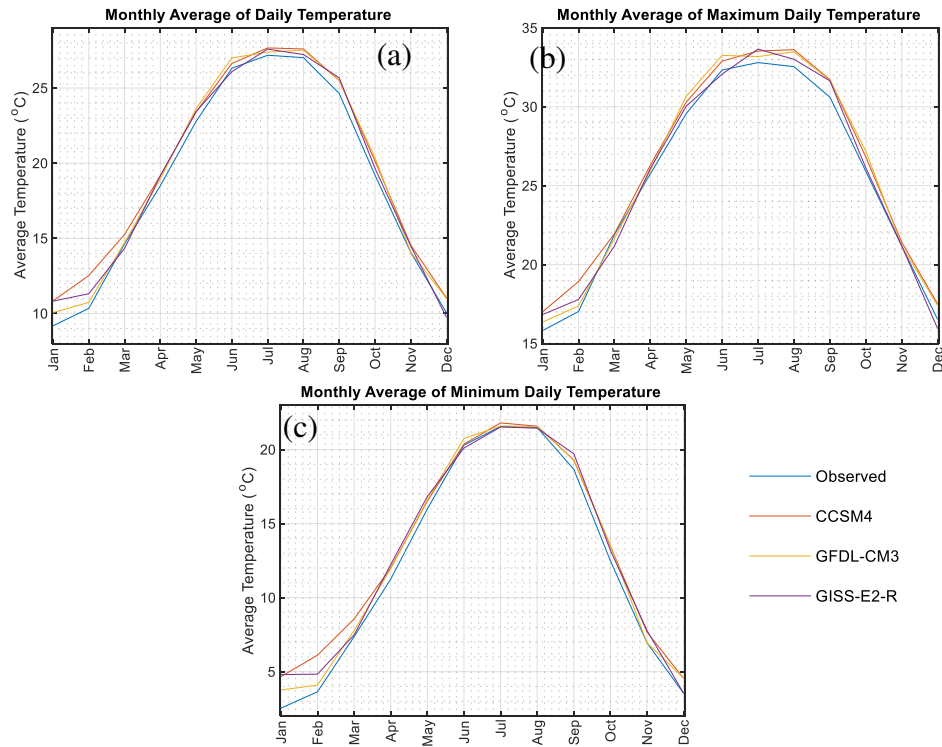


**Figure 4.** Comparing average, maximum, and minimum temperature between models and observed data.

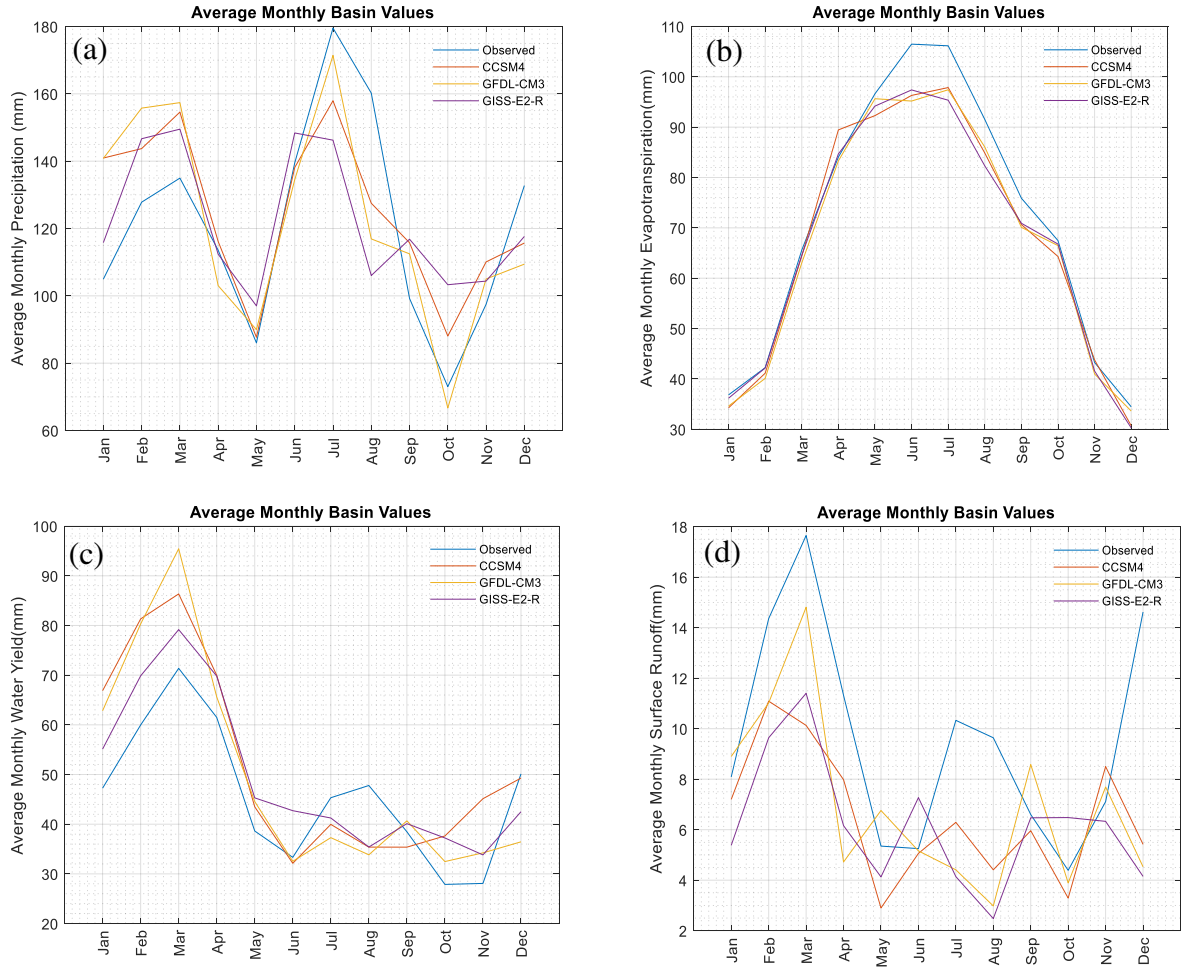


**Figure 5.** Comparing Monthly average of precipitation, ET, Water Yield, and Surface Runoff for models and observed data.

During late-century, average annual water yield is expected to increase by 24.14% under RCP4.5. For RCP6.0, however, average annual water yield is estimated to increase by 14.73% compared to baseline period. Increase in mean annual water yield under RCP6.0 compared to the increase under RCP4.5 is much smaller during the late century. This is partially due to the dramatic drop of the hydrologic components during the 90s (19). Unlike the other variables, slight decreases occur to mean annual ET during the mid and late century. For mid-century, a decrease of 0.63% and 0.01% respectively under the moderate and severe scenarios, is estimated. During late-century, average annual ET decreases further with 0.95% and 4.92% under RCP4.5 and RCP6.0, respectively (11). Figure 8 shows the mean annual trend of water balance variables (surface runoff, water

yield, and ET) during the simulation period based on the models and under the scenarios. The regression line for the surface under both scenarios indicate the increase during the entire simulation period. For water yield under moderate scenario the regression lines for all models are slightly steep. The regression slope, however, increases under the severe scenario. Annual trend towards end of the century, shows obvious decrease for ET under sever emission scenarios (Georgakakos et al., 2014; Srivastava et al., 2020).

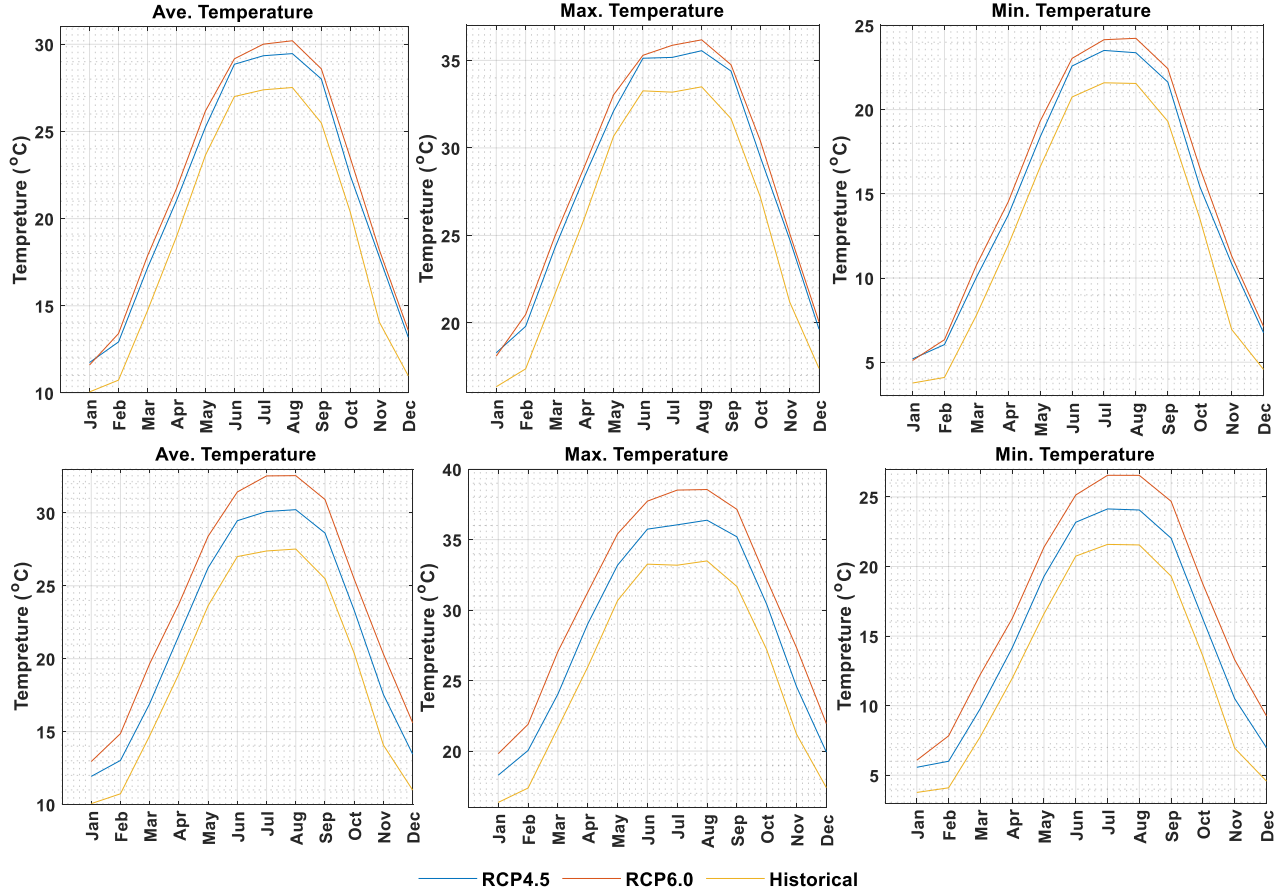


**Figure 6.** monthly average of average, maximum, and minimum temperature based on the models and emission scenarios, upper panel for the mid-century and lower panel for the late-century.

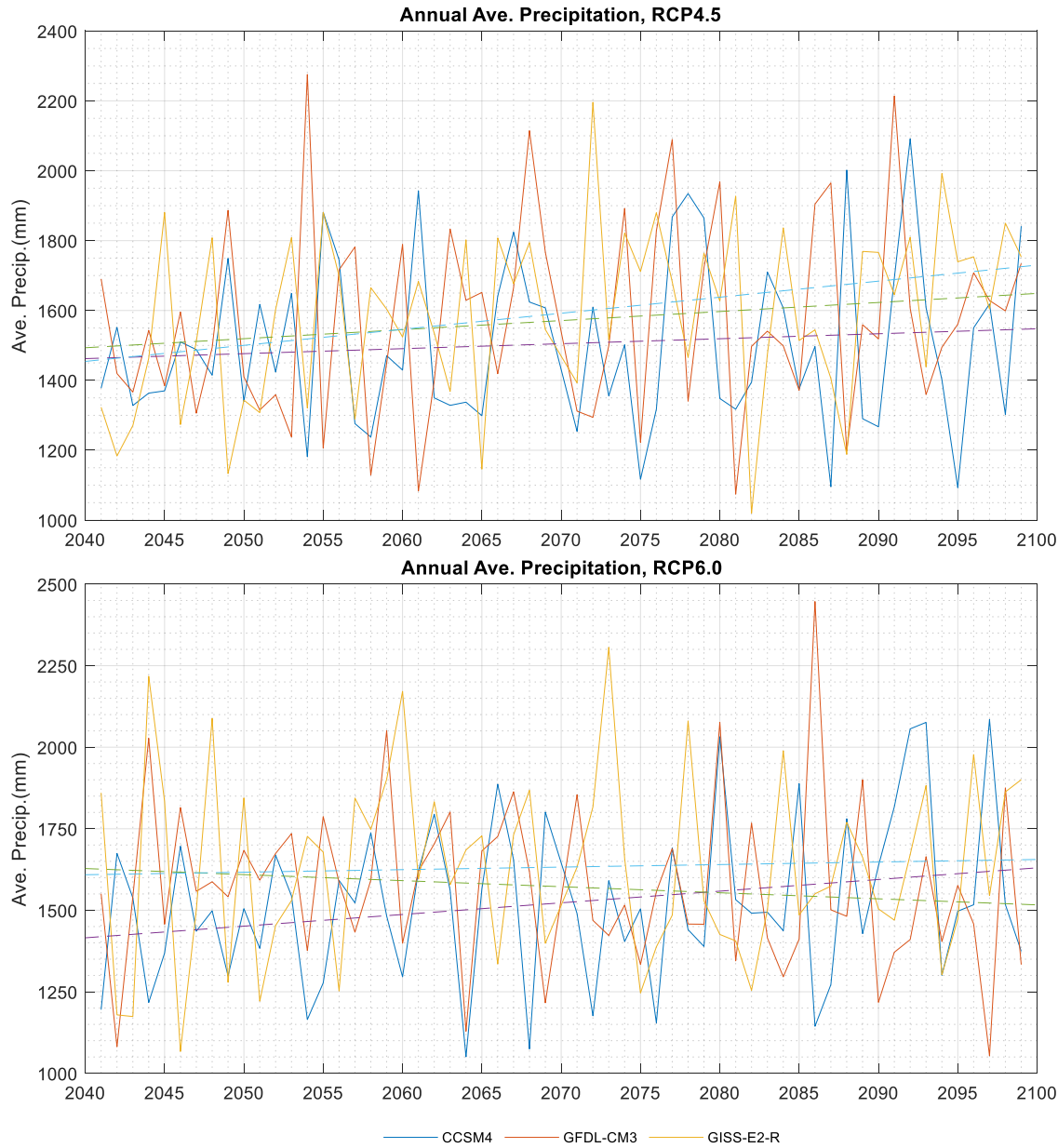


**Figure 7.** annual precipitation based on the models and under severe and moderate scenarios.

Basin-wide monthly average of the hydrological components is informative in investigating the water balance behavior of the watershed. The hydrological response to projected climate data in UCS changed for each month. Table 9 and Figure 9 illustrate these changes based on the models under both scenarios. During mid-century, under moderate GHG emission the largest changes to precipitation is projected in May (during flooding season) with increase of

48.5% compared to mean rainfall in the same month during the baseline period. For January, February, and March, it increases 18.9%, 22.6%, and 27.4%, respectively (Georgakakos et al., 2014).

The largest decrease in rainfall, however, is estimated in August and October with 23% and 26.7% respectively (RCP4.5, Mid-century). During the late-century under RCP4.5, the largest increase and decrease are projected in March with 36.1% and in August with 26.1%, respectively. For the severe emission scenario, the largest rainfall increase and decrease during mid-century are in January (41.8%) and December (21.1%), respectively. For the late century, however, precipitation decreases overall. The largest increase is expected to happen in September (29.9%) and the largest decrease in October (39.2%). Overall, August, October, and December are expected to be drier and January, March, and May are expected to be significantly wetter through the entire simulation period under both scenarios (Ingram et al., 2013; Srivastava et al., 2020; Walsh et al., 2014b). Similar to mean annual behavior of surface runoff, monthly estimates are also projected to increase dramatically (Wang et al., 2014). Under both scenarios, June has the highest increase of up to 5 times baseline period in monthly basin-wide surface runoff. The second highest increase is expected to happen in January with up to 4 times of the baseline period. The smallest increases in monthly mean surface runoff is projected in December with the lowest increase under RCP6.0 during late-century (36.2%) (Table 9 and Figure 9).

**Table 8.** percent changes to surface runoff, water yield, ET, and discharge based on the GCMs and under different scenarios.

Time period	Discharge	RCP4.5			RCP6.0			Water Yield	ET
		Surface Runoff	Water Yield	ET	Discharge	Surface Runoff			
mid-century	40s	22.43	282.93	10.72	- 2.77	30.75	303.68	19.10	- 1.48
	50s	21.54	293.57	10.39	- 0.66	33.96	307.91	22.81	1.48
	60s	28.59	282.36	16.54	1.50	34.10	334.81	22.35	- 0.01
Late-century	70s	32.95	376.46	20.77	- 1.59	28.93	329.52	17.86	- 6.65
	80s	36.42	391.33	24.03	- 0.72	33.99	367.69	21.87	- 3.22
	90s	30.87	397.60	27.61	- 0.56	18.37	310.35	4.47	- 4.88
	Entire period	30.45	337.38	18.34	- 0.80	29.67	325.66	18.08	- 2.46

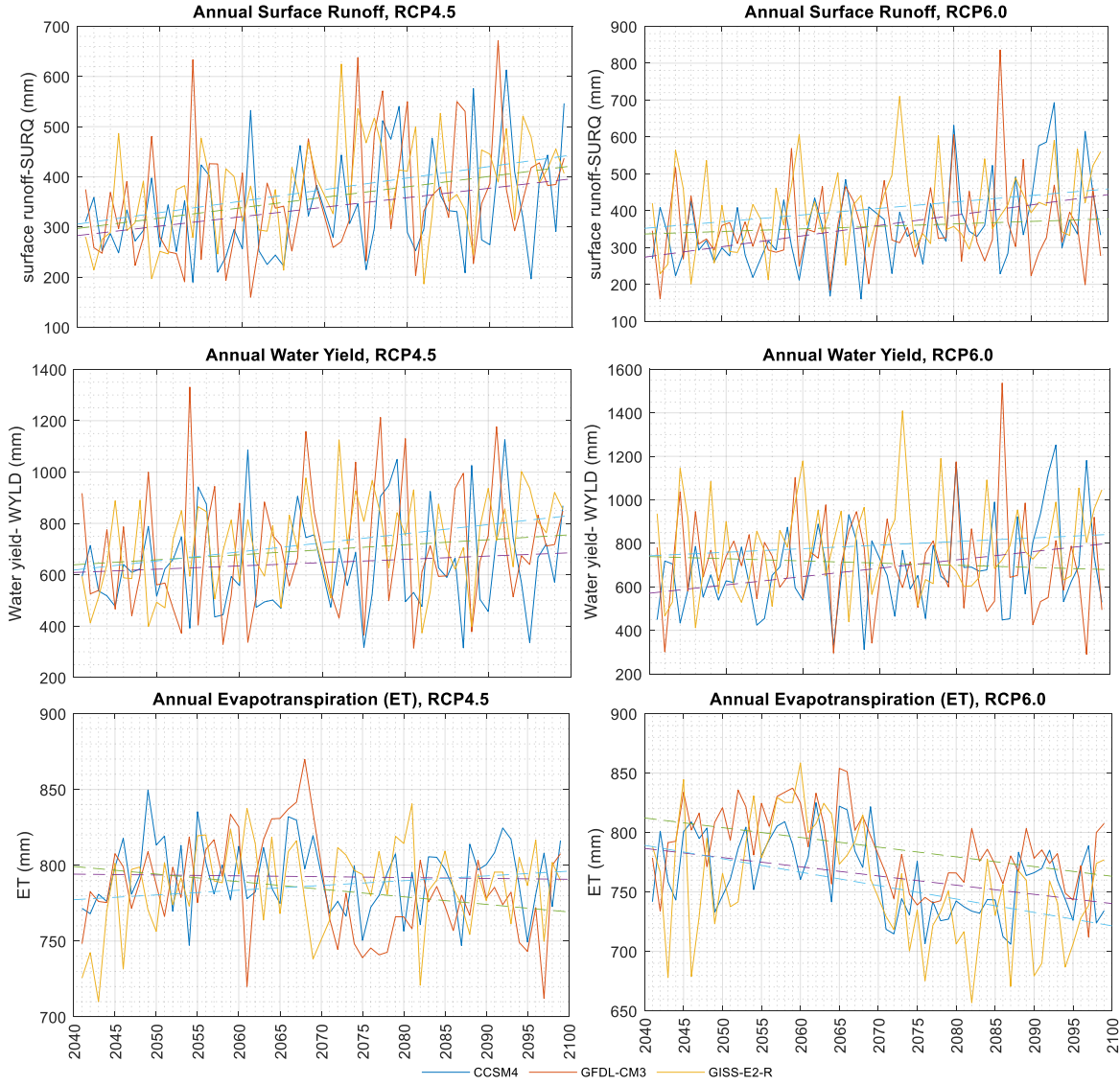


**Figure 8.** average annual trend for hydrological components based on the three model under RCP4.5 and RCP6.0.

Monthly behavior of water yield amount differs from rainfall and surface runoff (Tamm et al., 2018). Under RCP4.5, overall water yield is projected to be higher than that of mid-century. The largest changes under the moderate scenario is estimated in February (+58.6%) and March (+62.1%) during late century and in June (+42.9%) and July (+44.4%) during mid-century (RCP4.5). Under the moderate scenario water yield is estimated to decrease during mid-century in December by 12.4% and in August by 6.3%. Mean water yield for each month indicates different behavior under the sever emission scenario than expected. Under RCP6.0 and during mid-century,

January and June, and October have the increase of 58.4%, 62.7%, and 53.7%, respectively. Through the late-century, however, November has the largest increase of 99.4% in water yield amount. Under RCP6.0, water yield decreases only in December though the entire simulation period (Table 9 and Figure 9). Overall ET is expected to decrease slightly (Georgakakos et al., 2014). For all months mean ET drops except for April and May. Under both scenarios the largest decrease is estimated in November with close to 20% drop. From the Figure, one can notice the level of decrease in ET during Summer and Fall. Monthly discharge projection is shown in Figure 10 and Table 9. Under both scenarios discharge is estimated to decrease in April and December at Bellwood station with the largest drop of 31.2% in December during the mid-century under severe emissions (Cisneros et al., 2014; Field et al., 2012; Villarini & Smith, 2010). In other months, discharge is expected to increase. During the mid-century, the largest increase is observed in July (106.7%) and September (115.7%) under RCP4.5 and RCP6.0, respectively. During the late-century, February, July, and November have almost the same discharge under the moderate emissions. For the severe emission conditions, however, September and November have the highest increase of 133.7% and 186.3%, respectively. The discharge projections indicate increases in the months in which rainfall is expected to decrease. This can be attributed to the land use change (Carter et al., 2014).

Seasonal variations are also expected in hydrological response to future climate data. Interquartile range (IQR) can be used to express this variability (Figure 11). Outliers can be attributed to extreme weather (Y. Chen et al., 2019). Also, larger IQRs indicate more frequent severe weather (Sunde et al., 2017). The most frequent extreme rainfall in Spring is expected during 60s under moderate emissions. These extreme behaviors, however, is expected 2 decades earlier (40s) under the severe emissions. Under moderate emissions 50s has the wettest Spring and 80s has the driest. Under severe emissions, 60s and 70s have the wettest and driest Spring, respectively (compared to the baseline period) (Osei et al., 2019; Sunde et al., 2017).

IQR ranges for summer rainfall are noticeably smaller than that of spring, meaning smaller changes for summer rainfalls. Overall IQR under RCP6.0 is longer indicating more under severe emissions. Moderate emissions, however, reflects more outliers indicating greater likelihood for heavy rainfalls during summer. Under RCP4.5, 70s and 40s has the wettest and driest summer.

Under RCP6.0, however, 60s and 80s are expected to experience wettest and driest summer (Joh et al., 2011; Osei et al., 2019).

**Table 9.** basin-wide monthly average of hydrologic variables in UCS based on the three models under moderate and sever scenarios.

Hydrologic variable	Emission scenario	Simulation period	January	February	March	April	May	June	July	August	September	November	October	December
Precipitation	RCP4.5	Mid	18.9	22.6	27.4	-1.4	48.5	14.4	9.1	-	23.0	12.6	0.0	-
		Late	32.7	35.8	36.1	-0.9	31.1	19.3	3.0	-	26.1	10.0	1.7	-
	RCP6.0	Mid	41.8	6.0	37.7	6.2	37.3	26.7	6.4	-	12.3	20.0	-	-1.2
		Late	14.7	0.1	27.6	-4.4	28.1	19.8	6.3	-9.2	29.9	26.4	-	39.2
Surface runoff	RCP4.5	Mid	258.6	171. 6	182. 0	135. 2	289. 2	409. 0	241. 2	87.7	234. 2	290. 4	116. 9	68.7
		Late	386.9	282. 4	250. 9	159. 1	243. 4	527. 8	247. 0	121. 1	219. 5	349. 4	228. 1	138. 7
	RCP6.0	Mid	384.4	135. 4	208. 8	154. 4	229. 5	486. 7	228. 1	157. 6	209. 1	198. 2	256. 0	36.2
		Late	286.2	150. 6	217. 6	157. 5	225. 2	516. 8	332. 2	185. 4	322. 3	483. 6	118. 7	91.0
Water Yield	RCP4.5	Mid	26.8	42.3	42.5	11.0	19.8	42.9	44.4	-6.3	17.3	33.9	8.1	-
		Late	48.0	58.6	62.1	16.2	14.1	52.8	26.3	-9.8	2.3	31.9	32.5	12.2
	RCP6.0	Mid	58.4	30.1	53.2	13.8	14.0	62.7	37.0	14.6	27.2	29.0	53.7	-
		Late	26.9	18.4	38.6	8.3	0.5	50.1	51.5	16.3	36.4	99.4	22.0	-5.2
ET	RCP4.5	Mid	-0.4	-2.8	-0.4	8.5	4.1	-3.2	-	10.8	14.8	-	19.9	-9.4
		Late	-2.0	-3.4	1.6	10.1	3.8	-5.0	-	13.0	15.0	-	19.9	-10.8
	RCP6.0	Mid	-1.0	-0.7	2.8	9.4	4.2	-6.4	-	10.9	12.4	11.0	16.1	-8.8
		Late	-7.7	-8.4	-0.9	6.4	-2.0	-	13.3	19.1	11.2	14.6	19.0	-
Discharge	RCP4.5	Mid	14.7	65.4	40.9	-1.8	37.5	62.1	106. 7	-	29.8	94.0	82.4	7.8
		Late	32.6	81.0	61.5	1.8	28.8	70.8	80.0	-	27.1	70.7	80.3	32.3
	RCP6.0	Mid	42.7	49.1	52.1	-1.7	28.7	81.7	91.7	59.1	115. 7	77.3	54.8	-
		Late	13.3	36.6	36.8	-2.8	13.9	68.5	115. 4	67.2	133. 7	186. 3	20.4	22.5

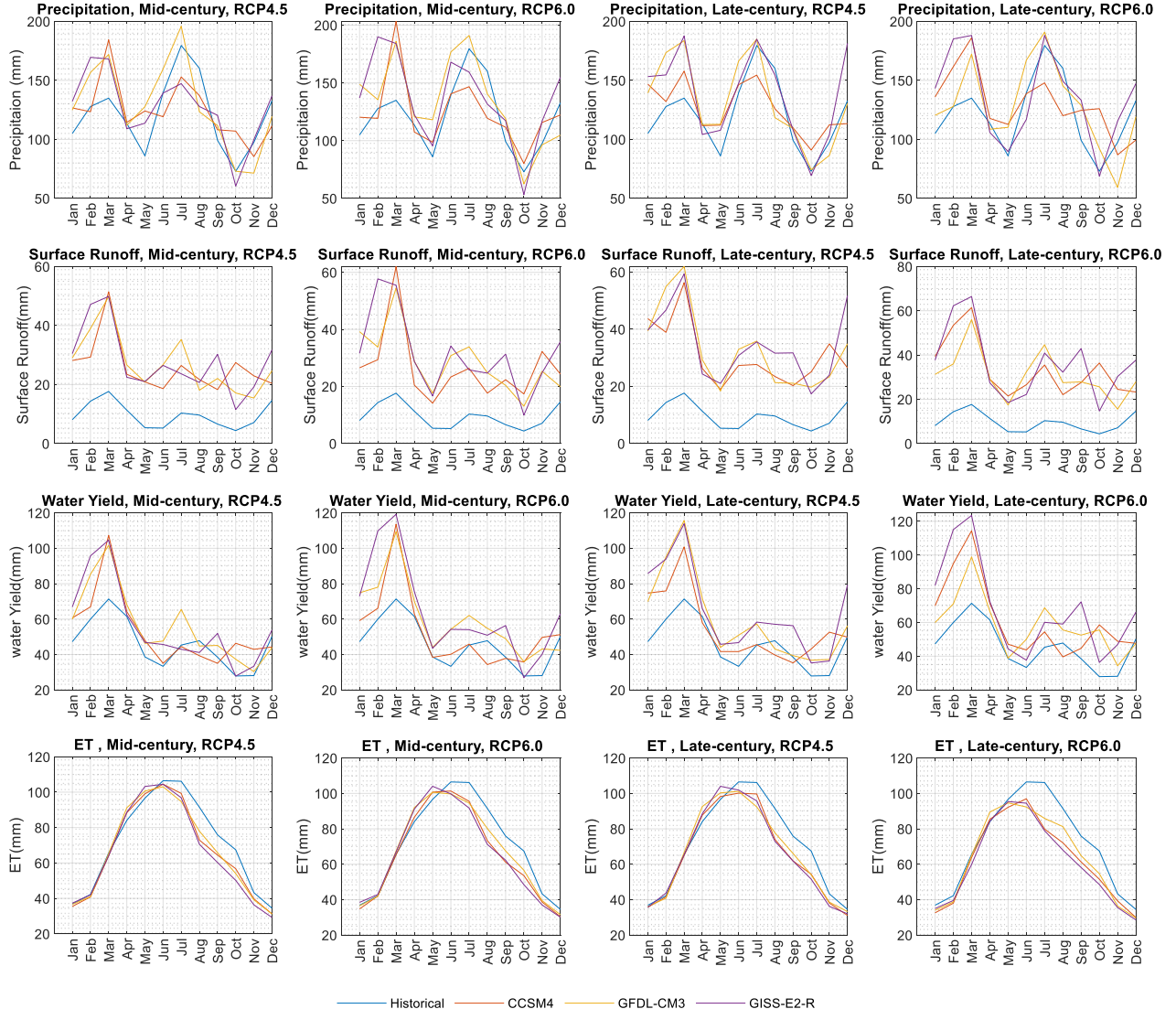


**Figure 9.** Monthly average of hydrological components in UCS based in the models and under RCP4.5 and RCP6.0.

Similar to summer rainfall, fall rainfall also has larger overall IQR under RCP6.0 than RCP4.5, indicating more changes under sever emissions. The smallest IQR ranging from -19.5% to -5.1% (under RCP4.5) is estimated during 60s where change variations indicate noticeable number of outliers meaning, strong fall precipitations compared to baseline period. Big portion of the 90s' IQR indicates increase, but for 50s a decrease is observed. This makes the end of the late century to have wettest fall and middle of the mid-century to have the driest fall (under RCP6.0)(Joh et al., 2011; Sunde et al., 2017).

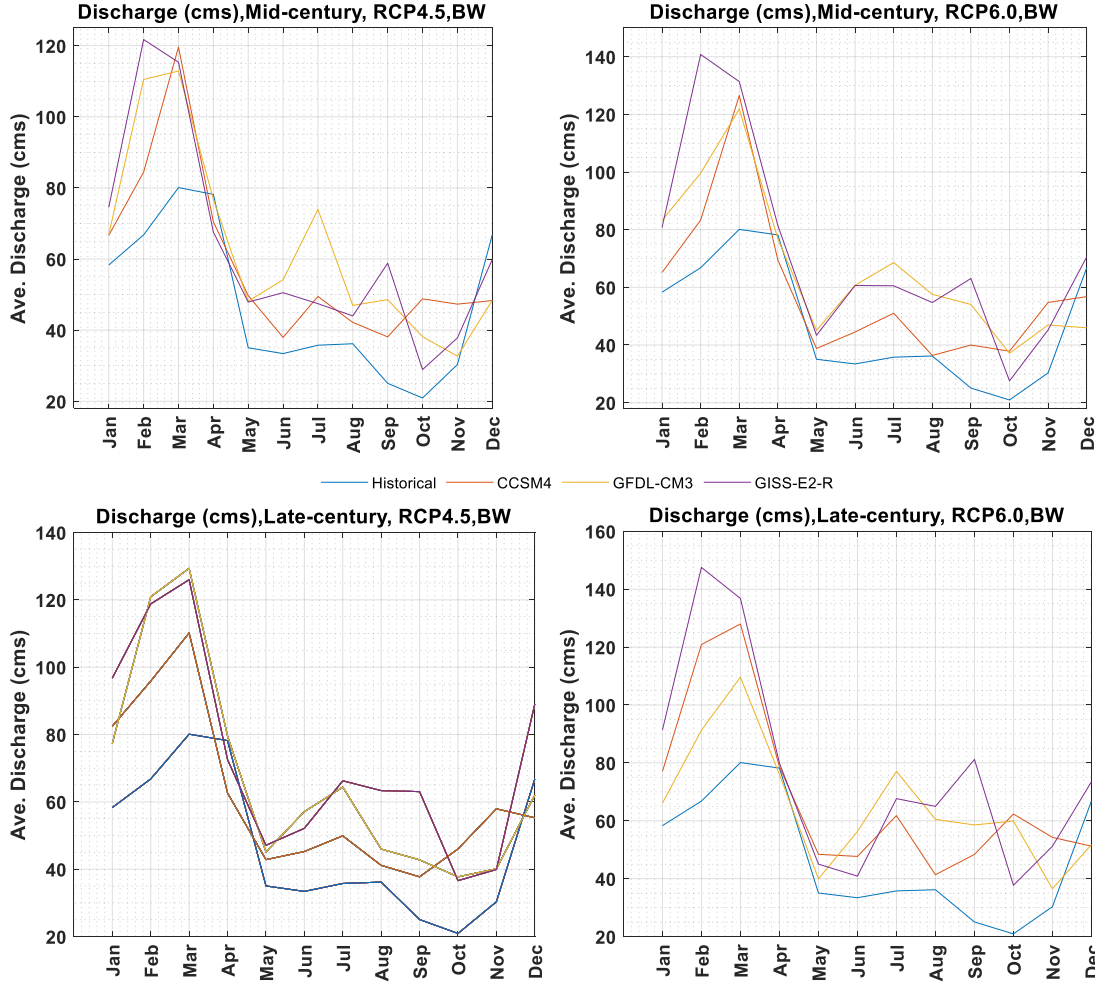


**Figure 10.** Discharge monthly average at Bellwood station based in the models and under RCP4.5 and RCP6.0.

Projected Winter rainfall has the shortest IQRs (smallest changes) compared to the other three seasons (both emission scenarios). For both scenarios, during the entire simulation period, IQRs and medians fall below zero line, meaning decreased amount of precipitation during Winter (Sunde et al., 2017). The direst Winter under severe emissions is projected to end of the mid-century (60s) where the median is -21.5%. Comparing the percent change variations for projected precipitation under both scenarios shows the largest changes in Summer and Winter when switching from RCP4.5 to RCP6.0. similar results were observed by Sunde et al. (2017).

Surface runoff variations, shows dramatic changes. For all seasons and under both scenarios, surface runoff is projected to increase up to several folds (Marhaento et al., 2018). For Spring surface runoff, under RCP4.5, the largest IQR is expected by end of the mid-century (60s)

ranging from 76.9% to 526.5%. Spring surface runoff, under RCP6.0, has overall length of IQR shorter than the that of RCP4.5 indicating less variations in percent changes. Comparison of Spring surface runoff under both scenarios shows significant differences during the beginning of the simulation where moderate emissions make shortest IQR while severe emissions make one the largest variations. Through the entire simulation period the overall IQR for Summer surface runoff under RCP6.0 is larger than that of Rcp4.5 indicating more variations under severe emissions. For fall surface runoff, the overall length for IQR varies through the simulation for both scenarios. The percent change values are also as high as Spring's and Summer's indicating several fold surface runoffs. For Winter surface runoff the overall length of IQR under moderate emissions is greater than that of sever emissions indicating more variation compared to the baseline period (Joh et al., 2011; Wang et al., 2014).

Water yield percent change variations indicates both increasing and decreasing amounts through all seasons (B. K. Pandey et al., 2019). Since the surface runoff and water yield are related, water yield follows the same pattern as the surface runoff does but due affected partitioning the level change differs (JG Arnold et al., 2013; Tamm et al., 2018; Wang et al., 2014). For Summer water yield, variations under RCP6.0 appears to be greater. This discrepancy is more obvious in the beginning and at the end of the simulation period. Under RCP4.5, the largest IQR ranging from -28.7% to 38.8% is projected at the beginning of the late-century period (70s). RCP4.5 has resulted in more outliers than RCP6.0 indicating higher chance of extreme amounts. For Fall water yield, medians under both scenarios show mild changes towards the end the century. The overall length of IQR under RCP6.0 is longer than that of RCP4.5, indicating more variations under severe emissions. The largest IQR under RCP4.5 is estimated during 50s (ranging from -24.6% to 63%). Under severe emissions, the largest variations are projected during 50s ranging from -62.2% to 30.4%. Winter water yield projections indicate decrease during the mid-century period and slight increase by end of the century under both emission scenarios (Villamizar et al., 2019).

ET has the smallest changes and variations compared to other hydrologic variables during all seasons (Y. Chen et al., 2019). Positive changes of ET during Spring show general increase (Georgakakos et al., 2014). Through the mid-century period ET decreases (RCP4.5) while during the late century it increases towards the end of the period. Under RCP6.0 during the late-century decreases are observed while RCP4.5 shows ET increase during the period. During Summer, ET

is expected to decrease always under RCP6.0. The largest (ranging from -4.6% to 3.9%) and the shortest (ranging from -1.99% to -0.02%) IQR are projected during 80s and 50s respectively. ET during Fall shows decrease for both scenarios and for the entire period. The projections indicate that the largest decrease is estimated during fall and under RCP6.0 up to -23.5% during 50s (McNulty et al., 2013). Projection for ET during Winter follows the same pattern as Summer (Villamizar et al., 2019; Vose et al., 2017).

### **2.6.3 Implications of Future Water Regime**

Here we integrated two types of projection: land use and climate data. Therefore, changes regarding land use and climate are the two main factors that affected the water regime (Wang et al., 2014). Results show consistency between the moderate and the severe emission scenarios regarding the projected hydrological variables. Through the simulation period precipitation increases, consequently, annual discharge increases. This increase is intensified by growing urbanization (Marhaento et al., 2018). Land use classes of URMD, URHD, and UIDU change from the mid-century period to the late-century period by 10%, 47%, and 12.5%, respectively. Therefore, even decreases of precipitation or attenuation in increase of rainfall towards the end of the century, is compensated by more increasing impermeable land covers (Sunde, He, Hubbart, & Urban, 2018). These land use changes are along with 23.1% decrease in forest cover (FRSE, FRSD, FRST), 14.7% hay cover (HAY) and 11.8% agricultural cover (AGRR). These changes affect regions microclimate impacting the water balance (Trail et al., 2013). RCP4.5 stabilizes atmospheric radiative forcing at  $4.5 \text{ W/m}^2$  (650 ppm CO<sub>2</sub> eq) in 2100 (Thomson et al., 2011; Van Vuuren, Edmonds, et al., 2011), however, by end of the mid-century period, the increase in the radiative forcing attenuates significantly. Unlike, RCP4.5, RCP6.0 keep increasing by end of the century and stabilizes the radiative forcing at  $6.0 \text{ W/m}^2$  (850 ppm CO<sub>2</sub> eq), however, GHG emissions declines after the end of the mid-century period (Van Vuuren, Edmonds, et al., 2011). Therefore, under RCP6.0 precipitation increases during the mid-century, and it declines during the late-century period. As a result, this decline is expected to reflect in discharge amount, but urban-oriented land use change results in increased discharge (Marhaento et al., 2018; Wang et al., 2014). Similarly, surface runoff and water yield increase in a same manner. However, since discharge and water yield have linked to groundwater (JG Arnold et al., 2013; Deb, Kiem, & Willgoose, 2019;

Neitsch et al., 2011), unlike surface runoff they are indirectly affected. Surface runoff projection increases are significantly greater for all types of monthly, seasonal, and annual values. Annual results, for instance, show at least 3 times higher compared to the baseline. Similar studies have concluded the same result in the region (Sunde et al., 2017; Wang et al., 2014). Increase in impermeable land covers (URMD, URHD, UIDU) decreases the amount of infiltration into the soil, and subsequently while baseflow contribution declines, surface runoff dramatically increases; this leads to more frequent and intense flooding (Huang, Cheng, Wen, & Lee, 2008; Rose & Peters, 2001; Wang et al., 2014). Combined effects of increasing in precipitation, and temperature as well as imperviousness leads in slight decrease in ET during mid and late century period. Chen et al. (2017) have reported the same result. This indicates increased urbanization compensates increased demand of evaporation and transpiration (Tamm et al., 2018). Since, the vegetation and tree cover decrease under the land use scenarios, much less transpiration and plant uptake are estimated. It can be concluded that the increase in evaporation due to increase in urbanization cannot be offset by decrease in transpiration (Marhaento et al., 2018; Wang et al., 2014). Also decline in soil water consumption and plant uptake due to less vegetation-covered lands can lead to increase in stream flow (Katie Price, 2011; Sunde et al., 2017). Seasonal percent change analysis (figure 11) indicates that most dramatic changes (more frequent extreme situations) to climate and hydrological variables is projected in the beginning of mid-century period when switching from the moderate to severe emissions. Seasonal behavior also agrees with annual changes; however, it indicates more changes in Winter and Summer. Similar results were reported by Sunde et al. 2017 and wang et al. 2013. In a study (Georgakakos et al., 2014) for the entire southeast region, decline in storm water has been projected. The general increase in this study can be attributed to urban-oriented land use change as well as the watershed specific characteristics like seasonality and storm frequencies (Hoyos et al., 2019; Sunde et al., 2017; Villarini & Smith, 2010).

Previous studies in the region have used CMIP3 or CMIP5 with general bias correction. CMIP5 with finer resolution and LOCA with more reliable climate data, now, have improved the future climate data projections (Ficklin, Letsinger, Stewart, & Maurer, 2016; D. W. Pierce et al., 2014). More realistic regional patterns of precipitation, better estimates of extreme events, and reduced number of light-precipitation days are the advantages of LOCA (D. W. Pierce et al., 2014). These improvements have reflected more reliable results in this study.

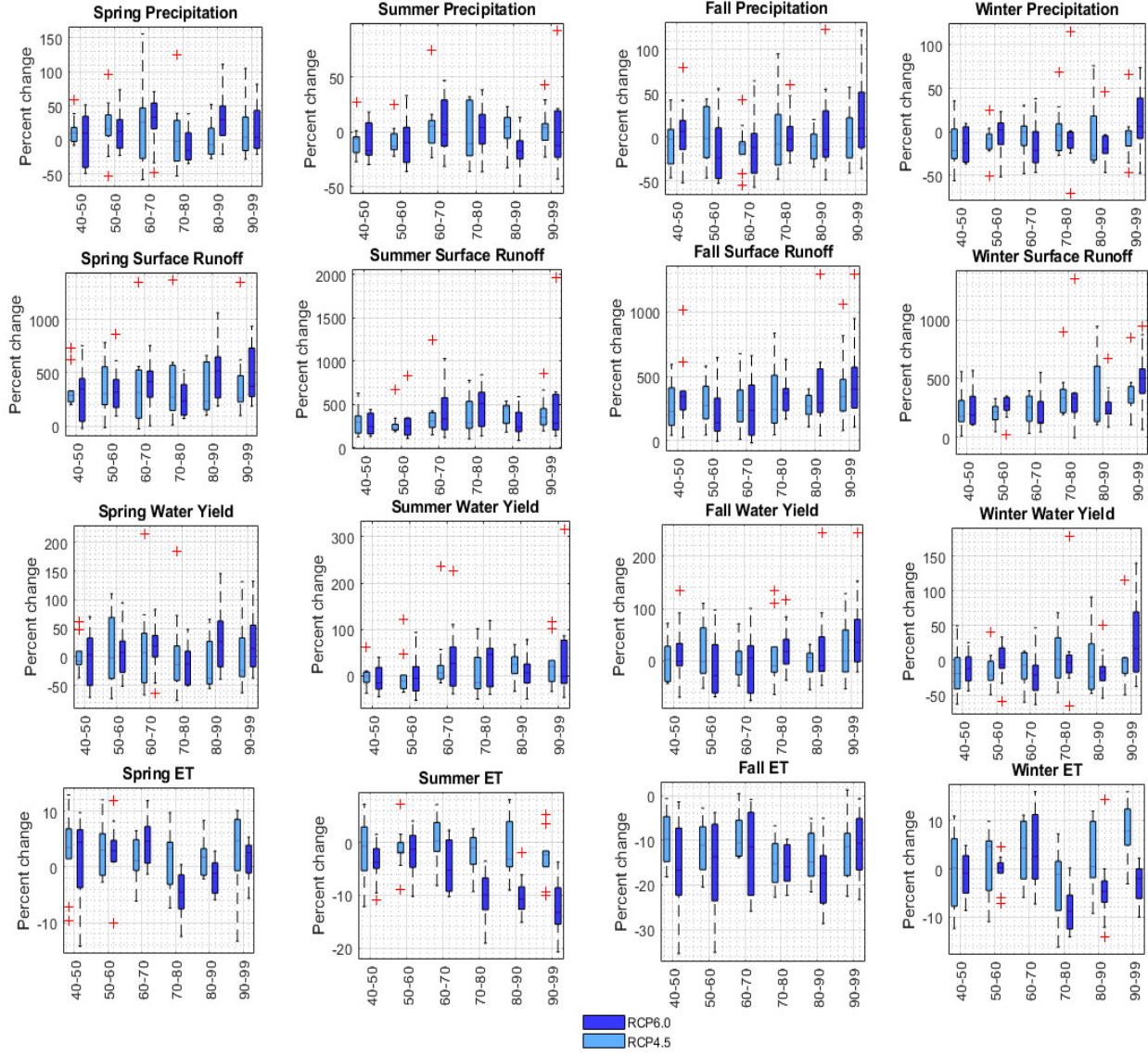


**Figure 11.** Seasonal variation of hydrological components based on the model and under both emission scenarios for entire simulation period.

This study helped to fill the current need to investigate the combined effects of the most recent downscaled and bias-corrected climate projections and the land use projections based on SSP of IPCC. LUC scenarios used here, are consistent with SSP and IPCC and couples improved demographic growth model and with a spatial allocation model. There have been very few studies of this type investigating the integrated effect of projected land use and climate data on hydrological responses in southeast US in this study's scale. UCS is mainly forested and agriculture which complicates the impacts and responses. More studies are required to investigate

the combined effect of this type of watersheds where notable level of humidity and proximity to the Gulf area which is exposed to more hurricanes and tropical storms effects the land use and hydrologic cycle. Wang et al. 2013 have studied an area close to UCS under CMIP3 and concluded the same results of this study. Because of the few numbers of research in the region where UCS locates and the also because of the approach used in this research, the result and projections brought here can be put into the overall research body and also can be served as a basis for comparison and decision-making process. The approach also can be utilized for other watersheds to investigate the integrate the land use and climate projections to study the hydrologic response. A few Native American Reservations are located within UCS; therefore, this study can also be used to research the future climate impact on the reservations' sustainability and the people. It should be noticed that we used SWAT weather generator to simulate wind speed, relative humidity, and solar radiation. The soil condition has not been changed i.e. for all models the current condition was used. Models also had challenges predicting the monthly average temperature, monthly average of maximum temperature, and monthly average of minimum temperature for months of Dec., Jan. and in some cases February.

The findings provide the basis to analyze combinations of what conservation practices and when and where may have the least impact on natural land cover, while incorporating socioeconomic planning. This study better integrates direct relation and feedbacks between future land use pattern and their influence on land cover and resulting changes in hydrological response (water balance variables). Mitigation activities and adaptation planning across related sectors can benefit from establishing this type of data and the findings. The results can be put into the overall research body and also can be served as a basis for comparison and decision-making process.

## CHAPTER 3

### TOPSOIL LOSS UNDER EXTREME RAINFALL; FINDING SOIL LOSS HOTSPOTS USING WEATHER RADAR DATA

#### 3.1 Introduction

Soil erosion is a common form of land degradation which can lead to decrease in crop productivity and increase in flood possibility (Admas et al., 2022; Borrelli et al., 2017; Pimentel & Burgess, 2013). It is a location-dependent widespread environmental hazard caused by water runoff (Xie, Nkonya, & Wielgosz, 2011). It exports nutrients which impairs river water quality and aquatic ecosystem habitat, and it causes and helps growing the dead zone in water bodies such as Gulf of Mexico (R. B. Alexander, Schwarz, & Smith, 1997; Inamdar et al., 2018; Q. Wang et al., 2021). It also removes soil organic matter required for food production from fertile topsoil (Fenta et al., 2021; Haregeweyn et al., 2017). Water induced erosion comprises 56% of world soil loss which cause almost 10 million ha agricultural land each year to be out of food production chain (Bouma & Batjes, 2000; Pimentel, 2006). Some underrepresented regions experienced and will probably experience increasing trend in cropland expansion and forest logging (Hansen et al., 2013; Hurtt et al., 2020); This vulnerability could be tied in increasing precipitation intensities and make the regions more erosion-prone (Borrelli et al., 2021). Erosion-prone parts of a watershed can be costly for the ecosystem and the environment. Identifying these areas are critical to introduce effective management practices. Conservation practices in agriculture which often referred as Best Management Practices (BMPs) are techniques and guidelines to improve water quality and agricultural productivity and to mitigate soil erosion and nutrient loss (Briak, Mrabet, Moussadek, & Aboumaria, 2019; Logan, 1993; Panagos et al., 2015; Zhou et al., 2016). BMPs' implementation, however, can be expensive; many studies have been focused on BMPs to mitigate soil erosion, however, site-specific BMPs are imperative for effective soil conservation (Admas et al., 2022). Determining the proper location for BMPs can also be challenging. Additionally, the unequivocal consequences of the warming climate can expose lands to Extreme Rainfalls (ERs) at regional and global scales. More frequent ERs generate high peak discharges quickly and create floods that can wash away soil active layer especially in growing season. Another associated risk

is sediment deposition; it affects the storage and hydropower generation capacity of the reservoirs. Dutta (2016) in a review study on reservoir sedimentation concluded that the impact of sediments on water quality and consequently water availability has remained unexplored (S. Dutta, 2016).

ERs' one main associated risk is topsoil loss. Scientific community now have robust confidence on increasing trends on ERs and more prominent intensification (Fischer, Beyerle, & Knutti, 2013; Fischer & Knutti, 2014; Pendergrass & Hartmann, 2014; Pfahl, O'Gorman, & Fischer, 2017) which is supported by robust agreement among them in theory, model results, and observational data (Fischer & Knutti, 2016; Guerreiro et al., 2018; Hoerling et al., 2016; Markonis, Papalexiou, Martinkova, & Hanel, 2019; Moustakis, Papalexiou, Onof, & Paschalis, 2021; Papalexiou & Montanari, 2019). Many others also reported the rise in frequency of extreme rainfalls including Kang et al 2009, Stone et al 2005 (Kang, Khan, & Ma, 2009; Stone, Hotchkiss, & Stone, 2005). Groisman et al. 2012 studied the changes in intensity of heavy precipitation in the central US and they reported significant increase in the frequency of very heavy rainfall and extreme precipitation events (%40 increase) (Groisman, Knight, & Karl, 2012; C. Lu et al., 2020). Westra et al. (2014) investigated short-duration ERs and concluded increase in magnitude and frequency of flash floods while emphasizing on local scale thermodynamic effects (Westra et al., 2014). Moustakias et al. 2021 have studied seasonality, intensity, and duration of Extreme rainfall events over the US and concluded that warming climate would intensify extreme precipitation events and storm depths; they predicted that a 20-year rainfall would become a 7-year rainfall on most part of the US (Moustakas et al., 2021). 1% increase in rainfall amount will increase the soil erosion up to 1.7% at multiple locations (Pruski & Nearing, 2002). Another associated risk of ERs is decline in crop productivity and eventually impacting the local and national economy. Kotz et al. (2022) in their study concludes that warming climate related changes in heavy rainfalls will affect the economic growth of the high-income countries (Kotz, Levermann, & Wenz, 2022). In southeast US observed changes in very heavy precipitation has increased 27% (Walsh et al., 2014a). This region has also the risk of experiencing tropical cyclone and North Atlantic hurricanes; the intensity, frequency and duration of the hurricanes have increased for four last decades (Knutson et al., 2021; Walsh et al., 2014b).

Extreme weather conditions including rain storms, flood, and drought or drastic changes in rainfall pattern are all cause of increasing air temperature (Abolverdi, Ferdosifar, Khalili, &

Kamgar-Haghghi, 2016; Q. Zhang, Xu, Gemmer, Chen, & Liu, 2009). For each degree of world temperature increase, the current most ER events are likely to double (Myhre et al., 2019). Hydrological extreme events will make challenges on food availability and environmental health (S. D. Donner & Scavia, 2007; Murdoch, Baron, & Miller, 2000; Rabalais, Turner, Wiseman, & Dortch, 1998). It is essential to understand sediment response to changing climate for preventing flood and drought, and for soil conservation and water resource management (Borrelli et al., 2021; Zan Xu, Zhang, & Yang, 2021). Runoff has a direct relation to erosion; with the increase in frequency of heavy precipitations, soil health and functionality can be significantly degraded. Parajuli et al in 2016 and Yasarer et al in 2017 studied the impact of climate change on sediment yield and concluded that the frequency of extreme rainfall events would increase in the future and that these changes would affect soil erosion and consequently crop productivity in multiple ways. (Parajuli, Jayakody, Sassenrath, & Ouyang, 2016; L MW Yasarer et al., 2017). In agricultural regions going through rapid land use change, climate variability, national resource conservation policies, and socioeconomic developments can contribute to soil health (Aghsaei et al., 2020; de Oliveira Serrão et al., 2022; Subhasri Dutta & Sen, 2018; Schiefer, Petticrew, Immell, Hassan, & Sonderegger, 2013).

A few important problems with soil-erosion modeling are result uncertainties, non-linear relation within parameters, and upscaling difficulties (De Vente and Poesen, 2005). Although, modeling obstacles accompanied with recent changes in climate impose challenges to our understanding of erosion process, ongoing advances in technology (e.g., data science), can offer decent solutions. For example, soil-erosion models have recently started using geospatial analysis tools in soil conservation and management practices (Panagos et al., 2015b). Here, we incorporate weather radar technology to capture spatially small-scale hydrologic extremes. Stream and rain gauges networks are often limited in capturing spatial variability of rainfall (L. V. Alexander et al., 2020; Lengfeld et al., 2020; Katie Price, Purucker, Kraemer, Babendreier, & Knightes, 2014). Weather radar technology can efficiently capture ERs especially short time (less than a day) ERs and is more accurate in smaller watersheds (J. Gao, Bieger, White, & Arnold, 2020; J. Gao, Sheshukov, Yen, & White, 2017; Lengfeld et al., 2020; K Price, Purucker, & Kraemer, 2011; Sexton, Sadeghi, Zhang, Srinivasan, & Shirmohammadi, 2010). In comparison to in-situ gauge,

hydrologic extremes are captured more than almost 1000 times by radar stations (Lengfeld et al., 2020).

Even though scientists have recommended many water management approaches to mitigate climate change impacts, most of them don't offer local solutions (Kang et al., 2009). Modeling soil erosion cannot be up or downscaled; In 2004 Vente et al. studied the soil erosion scale issues and they concluded that soil erosion at one scale cannot be applied for other scales (De Vente & Poesen, 2005). There is also a lack of knowledge on spatial distribution of the models (S. Pandey, Kumar, Zlatic, Nautiyal, & Panwar, 2021). Borrelli et al. ( 2021) carried out a global review and statistical analysis study (included 3030 modeling reports from 126 countries) and concluded that spatial aspect in less than half of one of the most common used models, was concern (Borrelli et al., 2021). Thus, it is crucial to study the soil erosion on finer scales. It is, also, important to investigate water balance parameters in each basin to adopt basin scale practices which sustainably addresses food security, energy, and biodiversity.

The relationship between topsoil loss and ERs is underrepresented, and there is a lack of understanding it (Admas et al., 2022; C. Lu et al., 2020; Parajuli et al., 2016; Zan Xu et al., 2021; X. C. Zhang & Nearing, 2005). There is no uniform conclusion adopted by the scientific community and lack of understanding caused by lack of quantitative studies (specially at the regional scale) points out the gap. Therefore, this chapter aims to address the understanding of interaction between soil erosion and ER spatial variation. Our objectives are to (i) investigate the relation between soil loss and ERs spatial variability by using weather radar data and (ii) find hotspots for soil loss. In this regard, we couple stage IV radar data with hydrologic modeling under variety of weather and management scenarios.

## 3.2 Materials and Methods

### 3.2.1 Method and Data Collection

we incorporated geospatial hydrological modeling to achieve the objectives. The required data including weather radar and land use data were obtained and utilized in Soil and Water Assessment Tool (SWAT+) (Jeff Arnold, 1994). The radar data were manipulated and converted to SWAT suitable format. The model, then, was calibrated for discharge and sediment after sensitivity analysis for parametrization. For detailed information please refer to (Makhtoumi et al.,

2020). Then the scenarios were developed considering future weather conditions and practiced human activities in the watershed. The model was run under the scenarios, and finally the output results were statistically and spatially analyzed. Following sections describes the steps. SWAT incorporates spatial and temporal data (Neitsch et al., 2011). Three types of spatial data are soil, land use and elevation data. Gridded gNATSGO (Gridded National Soil Survey Geographic Database) is used that allows up 5 soil horizons to be modelled with 10 m resolution (SoilSurvey, 2021a). The land use data us NLCD2019 and is obtained from Multi-Resolution Land Characteristics (MRLC) Consortiums (Dewitz, 2021)(see Appendix A for the detail).

Precipitation, temperature, solar radiation, wind speed, and humidity are the input data which SWAT requires daily timescale (Neitsch et al., 2011). For the last four, in-situ gauge station data were obtained. For precipitation, however, we used three types of data: stage IV NEXRAD radar (Klazura & Imy, 1993), Multi-Radar Multi-Sensor (MRMS) (J. Zhang et al., 2016), and in-situ rain gauge data. The National Weather Service (NWS) operates the US NEXRAD (Next Generation Radar) weather radar network which includes 160 high-resolution S-band Doppler weather radars. The network was installed in late 1980's comprising of WSR-88Ds (Weather Surveillance Radar, 1988 Doppler). In 2013, the network was upgraded to dual polarimetry technology (transmitting horizontal and vertical orientation of radio waves that supplies better estimate of shape and size of rainfall droplets) (Kumjian, 2013). This feature gives the ability of differentiating between ERs, hail, and snow. NEXRAD has multiple products or quality control levels (Stage I, II, III, and IV) (Crum & Alberty, 1993; Fulton, Breidenbach, Seo, Miller, & O'Bannon, 1998; Kitzmiller, Miller, Fulton, & Ding, 2013) and employs different QPE (Quantitative Precipitation Estimation) to drive the precipitation estimation including MPE (Multisensor Precipitation Estimation) which is the third level of quality control(Habib, Larson, & Graschel, 2009; He, Zhang, Kuligowski, Cifelli, & Kitzmiller, 2018; Kitzmiller et al., 2013; Y. Zhang, Reed, & Kitzmiller, 2011). The Stage IV data is derived based on the MPE (radar and rain gauge) hourly/6-hourly 'Stage III' data and unlike Stage II benefits from the manual quality control (QC). The 12 River Forecast Centers (RFCs) produces Stage III on gridded base with 4 km resolution for CONUS. It is then mosaicked by National Center for Environmental Protection (NCEP). While NEXRAD was being improved through time, many studies investigated the suitability of the data for different application, and they highlighted quantitative uncertainties

specially for ERs (Durrans, Julian, & Yekta, 2002; Eldardiry, Habib, & Zhang, 2015; Habib et al., 2009; Lengfeld et al., 2020; Katie Price et al., 2014). One of the main sources of uncertainties was the assumption on relationship between reflectivity and rainfall amount (Z/R assumption) (Katie Price et al., 2014). In 2015, Kirstetter et al. studied the issue and offered a probabilistic QPE solution as oppose to deterministic values which reads the radar measurements in the context of likelihood of observing precipitation (Kirstetter et al., 2015; Lengfeld et al., 2020). The Stage IV QPE data from 2016 to end of 2021 obtained from NWS website and used for scenario development. The MRMS data is the other rainfall data used in this study. It is a fully automated system of algorithms that incorporates multiple radar and ground and air observations, lightning detection system, satellite data, and forecasting models. It is developed to create severe weather and rainfall to assist with the decision-making process and real time hazardous weather warning. NOAA/National Severe Storm Laboratory (NSSL) collaborates with the University of Oklahoma to produce a quality-controlled radar data. The error sources such as beam blockage and range effect are corrected and then mosaicked onto a 3d grid to provide high resolution extreme weather and hydrological data such as rainfall type and rate (Lengfeld et al., 2020; J. Zhang et al., 2016). The system is connected to an automated rain gauge (Hydrometeorological Automated Data System -HADS; [www.nws.noaa.gov/oh/hads/](http://www.nws.noaa.gov/oh/hads/)) hourly and corrects the radar QPE biases in MRMS (Cisneros et al., 2014; J. Zhang et al., 2016). For the purpose of extreme rainfall studies, a high spatial (1km) and temporal (5 min) resolution of reanalysis MRMS was developed for the period of 2001 to 2011 (J. Zhang et al., 2016). This data is used for calibration and validation of the hydrological modeling. According to Price et al. 2014, rain gauge and radar data (NEXRAD) were the best options available for hydrologic modeling (Katie Price et al., 2014; Tobin & Bennett, 2009). Radar data is better in simulating daily stream flow and its frequency with more pronounced differences in smaller catchments (K Price et al., 2011). Additionally, for small catchments, higher rain station density results in better output, especially in sediment fluxes (Chaplot, 2005; Masih et al., 2011). Gridded version of NEXRAD which seamless dataset is better than ground-based weather stations; also, it has higher accuracy in capturing weather conditions in small watershed (J. Gao et al., 2020; J. Gao et al., 2017; Jayakrishnan, 2001; Moon, Srinivasan, & Jacobs, 2004). Therefore, we used the Stage IV QPE for the scenario development and the MRMS reanalysis for watershed hydrology and sediment processes modeling (see Appendix A for how to download and

convert to suitable format). Weather Radar data was large and needed to be converted to the SWAT desired format (text file.) To address this issue, we downloaded the data in grib and NetCDF format using Windows terminal. We, then, aggregated the 5 min data to daily timescale. Finally, we converted the aggregated data to .txt files. This procedure was done using Python and Jupyter Notebook (the codes are available upon request.) The streamflow, sediment discharge, and sediment concentrations data were collected from the National Water Dashboard of the US Geological Survey (USGS). The USGS site close to the outlet of the watershed that considered as the monitoring point for all variables is USGS 07277700 (see Appendix A for the detail).

### **3.2.2 Study Area**

We had three criteria to select the location: the target watershed includes pasture and agricultural land use; the second one was data availability specifically sediment discharge and concentration data and third, we wanted the target watershed to be small enough so we could consider as much detail as we could. It is also important to notice that we deliberately select that watershed so we could make sure that all sediment that passes through the monitoring point is originated from only the watershed itself. We intentionally avoided the reservoirs, since they have a major role in sediment transport and suspended sediment load processes (Zan Xu et al., 2021). The watershed is in northwestern Mississippi, approximately 50 km south of Memphis, TN (figure 12). It is one of Mississippi River basin subwatersheds. It encompasses 3 HUC 12 -080302040401 to 3 with the drainage area of 312 km<sup>2</sup>. The main river stream is called Hickahala Creek and is a tributary of the Coldwater River, upstream of Arkabutla Reservoir. Hereafter we will call the watershed Hickahala Creek Watershed (HCW). HCW is located between the -91 and -88.7 and latitudes 34 and 34.88. HCW hillsides are prone to erosion when there isn't or less natural vegetable cover; this sediments are deposited in the channels or drained into Arkabutla Reservoir and decrease the flood carrying capacity making the region prone to flooding under ERs ((Biedenharn, Watson, Smith, & Hubbard, 2004). The main land use is pasture (43%) and the second main is Forest-Deciduous (23%) (MRLC-Consortium, 2021). Agriculture land use is third with 14% of the HCW area. The main crops are soybean (*Glycine max* L., Merr, warm season annual legume), corn (*Zea mays* L., warm season annual), and cotton (USDA-NASS, 2007). Irrigated farming is not common in the area and only up 5% percent of farms are irrigated (USDA-

NASS, 2007). Collins and Flaya comprise the main soil cover. They both are silty texture and prone to erosion of any type if left bare. HCW climate is the humid subtropical, characterized by temperate winter and hot summer. Temporal heterogeneity of the rainfall makes northwestern MS subject to drought and flood. Destructive thunderstorms are expected for average period of two months each year. Annual mean temperature is 15.4°C. The lowest temperature recorded is -22.2°C in January and the highest recorded is 41.1°C in August. Average annual rainfall ranges from 1371 mm to 1423 mm. The wettest month is May and the driest is October.

### **3.2.3 Model Simulation and Performance Evaluation**

Soil and Water Assessment Tool (revised version known as SWAT+) was used(Jeff Arnold, 1994). It is a process-based and semi-distributed for river basin scale (J. G. Arnold et al., 1998; ASABE, Jun. 2017). Fortran language with more than 300 subroutines are used to model different parts of hydrological and biogeochemical processes on the surface and under the ground (JG Arnold et al., 2011; J. G. Arnold & Fohrer, 2005). It is efficient and be used for short- and long-term impact studies with good computational effectiveness (de Oliveira Serrão et al., 2022; Gassman et al., 2007). It allows to split the watershed into small parts of unique combination of soil, land use and slope (known Hydrologic Response Unit (HRU)) and used the properties of HRUs for the operation(J. G. Arnold et al., 2012; Gassman et al., 2007). This feature allows sediment loss and transport to be modeled at HRU level which results in quite good details (Neitsch et al., 2011). For details about equations see (Makhtoumi et al., 2020). Edivaldo Serrao et al. in recent study concluded that SWAT is a good estimator in hydro-sedimentological parameters that can be utilized for decision making applications(de Oliveira Serrão et al., 2022; Duru, Arabi, & Wohl, 2018; Mueller-Warrant, Phillips, & Trippe, 2019; Prabhanjan, Rao, & Eldho, 2015; ZX Xu, Pang, Liu, & Li, 2009; Zan Xu et al., 2021). The model is capable of detecting erosion-prone parts of the watershed (Subhasri Dutta & Sen, 2018). SWAT uses subbasin properties as the main source of soil erosion(Subhasri Dutta & Sen, 2018). Simulation in SWAT occurs in two phases: land phase and routing phase (Neitsch et al., 2011). At HRU level sediment loss is calculated and along with water and other nutrients is regulated into the main channel at subbasin level (Makhtoumi et al., 2020). Water and sediment routing is determined in the second phase where in-stream processes are simulated (J. G. Arnold et al., 2012).

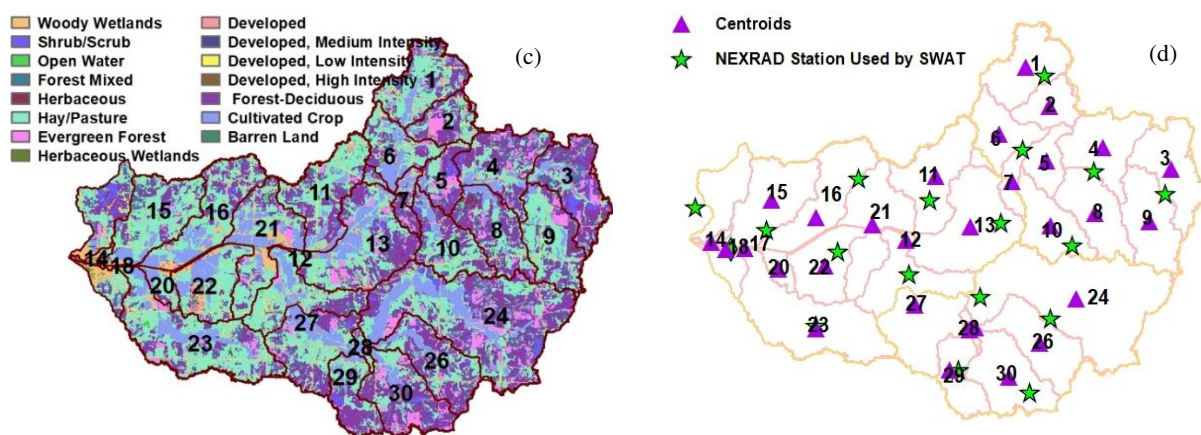
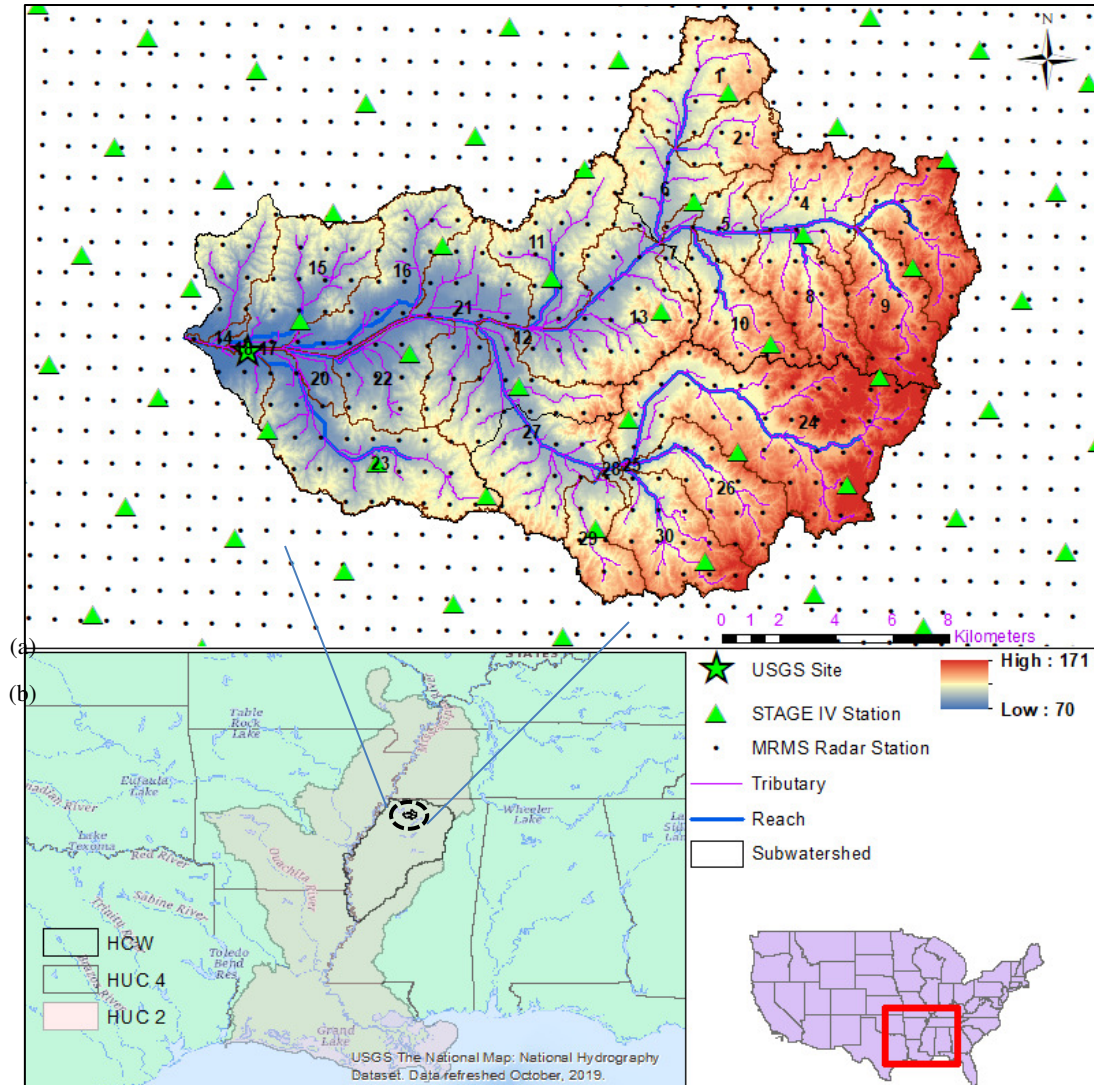


**Figure 12.** (a) location of the study area (HCW). (b) Hickahala Creek Watershed (HCW) relief map; the NEXRAD Stations (Stage IV and MRMS), and USGS site (USGS 07277700)

SWAT uses the modified USLE (Wischmeier & Smith, 1965, 1978) which utilizes the rainfall energy factor instead of a runoff factor. This enhances the sediment yield prediction, because runoff is a function of antecedent moisture condition and rainfall energy. It gets rid of the delivery ratio; and individual storm events can be studied (Neitsch et al., 2011). SWAT takes 4 main factors into account when modeling soil loss: soil erodibility, cover and management effect, support practice factor for specific practices such as counter tillage, stripcropping, and terrace, steepness effect, and the rock percentage in the first soil layer (Neitsch et al., 2011). The following is the equation used (Neitsch et al., 2011):

$$sed = 11.8 (Q_{surf} \cdot q_{peak} \cdot area_{hru})^{0.56} \cdot K_{USLE} \cdot C_{USLE} \cdot P_{USLE} \cdot LS_{USLE} \cdot CFRG \quad (1)$$

where  $sed$  is the sediment yield (ton),  $Q_{surf}$  is the surface runoff (mm H<sub>2</sub>O/ha),  $q_{peak}$  is the peak runoff rate (m<sup>3</sup>/s),  $area_{hru}$  is the area of the HRU (ha),  $K_{USLE}$  is the USLE soil erodibility factor (0.013 ton m<sup>2</sup>/(m<sup>3</sup> ton cm)),  $C_{USLE}$  is the USLE cover and management factor,  $P_{USLE}$  is the USLE support practice factor,  $LS_{USLE}$  is the USLE topographic factor, CFRG is the coarse fragment factor (Neitsch et al., 2011). We used simplified Bagnold method (Bagnold, 1977) for the entrainment and deposition of the particles. The following are the equations used (J. G. Arnold, Williams, & Maidment, 1995; Neitsch et al., 2011; J. Williams & Berndt, 1977):

$$conc_{sed,ch,mx} = c_{sp} \cdot v_{ch,pk}^{spexp} \quad (2)$$

$$sed_{dep} = (conc_{sed,ch,i} - conc_{sed,ch,mx}) \cdot V_{ch} \quad (3)$$

$$sed_{deg} = (conc_{sed,ch,mx} - conc_{sed,ch,i}) \cdot V_{ch} \cdot K_{ch} \cdot C_{ch} \quad (4)$$

$$sed_{out} = (sed_{ch,i} - sed_{dep} + sed_{deg}) \cdot \frac{V_{out}}{V_{ch}} \quad (5)$$

where  $conc_{sed,ch,mx}$  is the maximum concentration of sediment that can be transported by the water (kg/L),  $c_{sp}$  is the linear coefficient defined by the user (SPCON),  $v_{ch,pk}$  is the peak channel velocity (m/s),  $spexp$  is the exponent coefficient defined by the user,  $sed_{dep}$  is the amount of sediment deposited (ton),  $conc_{sed,ch,i}$  is the initial sediment concentration (kg/L),  $V_{ch}$  is the volume of water in the segment (m<sup>3</sup> H<sub>2</sub>O),  $sed_{deg}$  is the amount of reentrained sediment (ton),  $K_{ch}$  is the channel erodibility factor,  $C_{ch}$  is the channel cover factor,  $sed_{ch,i}$  is the amount of initial suspended sediment in the segment (ton),  $sed_{out}$  is the amount of sediment transported out of the

segment (ton), and  $V_{out}$  is the volume of outflow during the time step ( $\text{m}^3 \text{ H}_2\text{O}$ ) (Neitsch et al., 2011).

We evaluated accuracy of the model output with graphical comparison and statistical metrics (J. G. Arnold et al., 2012; Gassman et al., 2007; Tan, Gassman, Liang, & Haywood, 2021). To calibrate the model, we used combination of manual and auto calibration (D. Moriasi et al., 2012). We carried out calibration and validation using split-sample strategy (D. Moriasi et al., 2012) and Latin hypercube sampling. Latin hypercube sampling is considered more advantageous than monte-Carlo; the former makes sure the whole range of a given parameter is sampled while the later performs random sampling which could result in samples clustered in one part of the parameter range. To parametrize, we carried out a Sensitivity Analysis (SA) (J. G. Arnold et al., 2012; Saltelli et al., 2004) and then utilized the Sequential Uncertainty Fitting version algorithm (SUFIT2) within SWAT-CUP (SWAT Calibration and Uncertainty Program)(K. C. Abbaspour et al., 2004; Makhtoumi et al., 2020; Santhi et al., 2001) which was the only open source algorithm. We performed global and one-at-a-time SA several times based on baseline period (2000-2010) and filtered out insensitive parameters (K. C. Abbaspour, Vejdani, et al., 2007; Ghoraba, 2015; Saltelli et al., 2004). The model first was calibrated for flow and then calibrated for sediment while flow parameters were included. For accuracy quantification, our objective function includes Nash–Sutcliffe Efficiency (NSE), Percent Bias (PBAIS), and RMSE-observations standard deviation ratio (RSR) (see Appendix A for the detail) (K. Abbaspour, 2015; Gupta et al., 1999; Legates & McCabe Jr, 1999; D. N. Moriasi et al., 2007). Table 10 presents the final calibration results including satisfactory thresholds from the literature (K. C. Abbaspour et al., 2015; Legates & McCabe Jr, 1999). See Appendix A for the final parameters chosen based on SA (relative significance and significance of sensitivity (K. C. Abbaspour, Yang, et al., 2007)) for further analysis. We did not consider the elevation band and laps rate, since the target watershed is in low elevation area. Small portion of HCW is wetland and it was modeled. We didn't see any sensitivity in streamflow for wetland related parameter (WET\_FR, WET\_NSA, WET\_VOL, and WET\_K) (Jalowska & Yuan, 2019; Melles et al., 2010; Rahman, Thompson, & Flower, 2016). This can be due to small area of the wetland. We modeled snow melt and it appeared to be insignificant. The average annual snow fall and the amount of snow melt, both, is 19 mm. SWAT underestimates biomass in pasture land use; to counteract inadequate residue we set USLE\_P to a higher value

(Vigiak, Malagó, Bouraoui, Vanmaercke, & Poesen, 2015). We found that average rain fall does not necessarily match with the flow discharge or sediment discharge. This is due to the heterogeneity of the precipitation. The same amount of rain can occur over a subbasin where is more capable of generating surface run off or more prone to sediment loss and subbasins that are less prone to them. We found that calibration at month level is different from daily calibration. Many parameters are responsive on a daily basis, however, at monthly scale the daily dynamicity diminishes. If ephemeral and intermittent streams exist in watershed, they can play key roles in the hydrology and the sediment transport of the watershed. Perennial rivers with some degree of intermittency can make calibration challenging and it could require more inclusive methodology with less computational efforts.

### **3.3 Scenario Development**

SWAT allows to model plant growth, agricultural (such as crop rotation, tillage, irrigation, fertilizer application) and grazing practices. With planting date, maturity date, base temperature and mean daily temperature, the total number of heat units needed to bring a crop to maturity can be calculated (Neitsch et al., 2011). For forest or range, the start of the growing season is the time when the buds start developing and the end of the growing season is the time when the plant seeds reach maturity (Neitsch et al., 2011). we used specific dates rather than heat units to reduce the uncertainty. Since, when using heat units, we can't know if the application of fertilizer or pesticide scheduled by heat units is on a rainy day or not, and if it does coincide, significant amount of nutrient would be transported with surface runoff (Neitsch et al., 2011). There are four growth constraints parameters that can impact plant growth reversely: extreme temperatures, an insufficient water, nitrogen or phosphorus(Neitsch et al., 2011). Plant Operation requires specific information in SWAT. This information includes but not limited to total number of heat units for a given land cover, the timing of the operation, and the given land cover. The curve number for moisture condition II can be manipulated during the growth process. This can be done during setting the plant operation, tillage operation and harvest and kill operation(Neitsch et al., 2011).

In this study, scenarios include management operations under different weather condition. Main management operations are farming soybean/corn, crop rotation, irrigation, fertilizer application, and grazing.

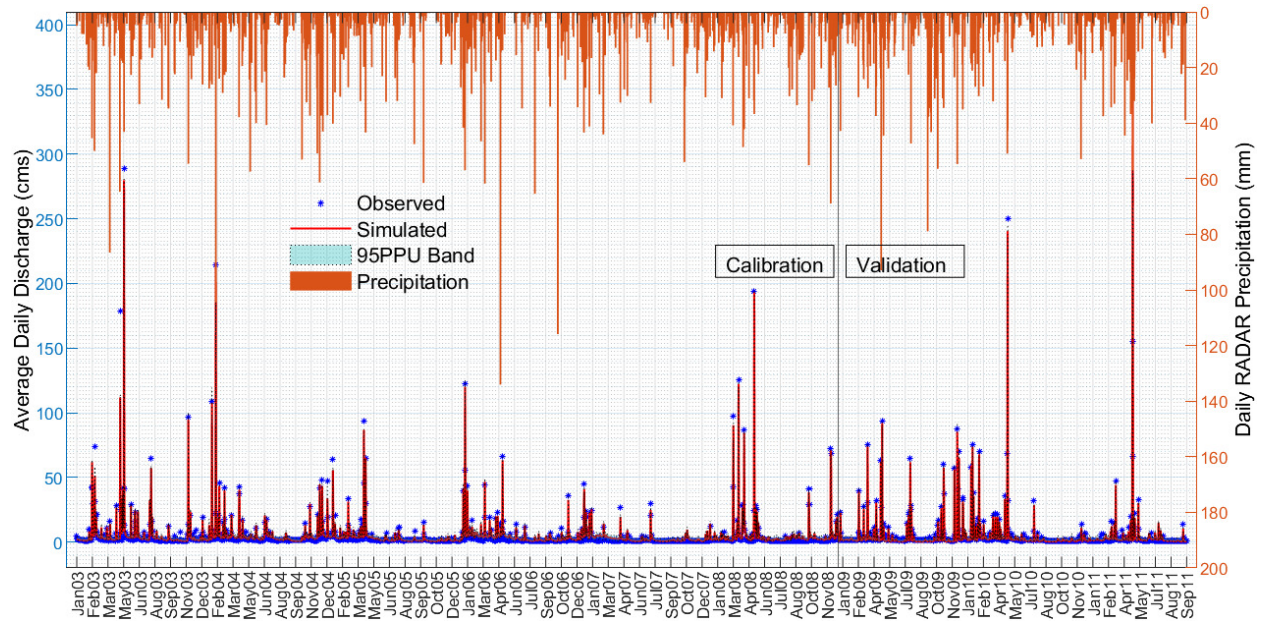


**Figure 13.** Flow calibration and validation result for USGS 07277700 site.

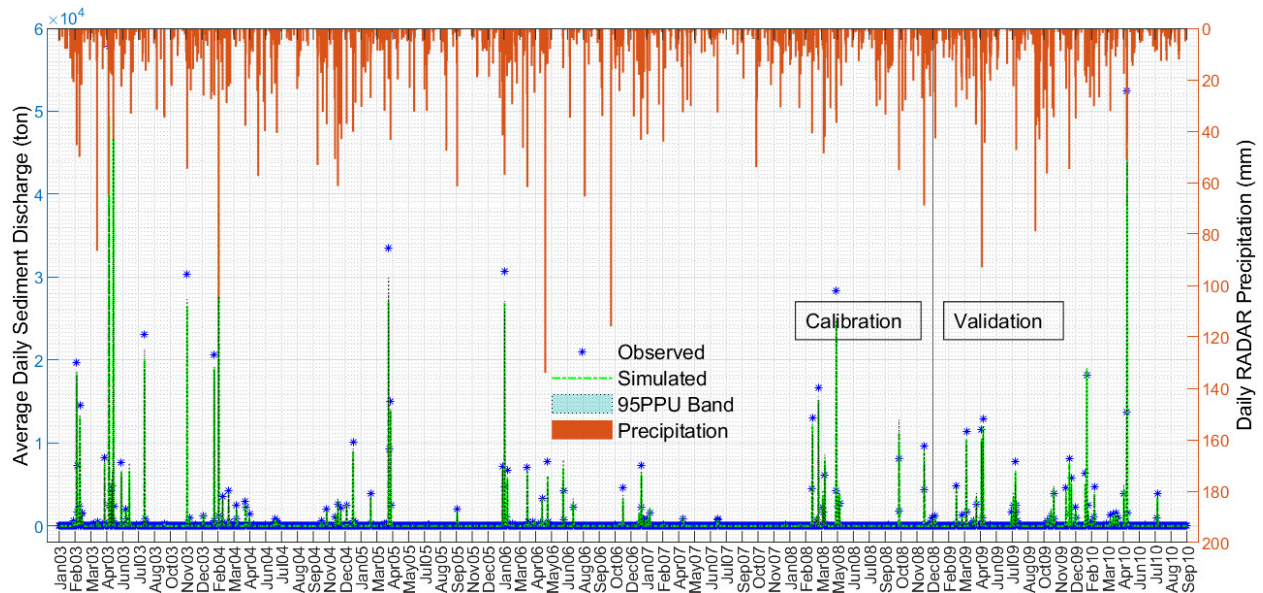


**Figure 14.** Sediment calibration and validation result for USGS 07277700 site.

**Table 10.** Model efficiency evaluation metrics.

Metrics	Satisfactory Threshold		Flow		Sediment	
	Flow / Sediment		Calibration Period	Validation Period	Calibration Period	Validation Period
NSE	> 0.5		0.62	0.58	0.51	0.48
PBIAS	$\pm 25\%$		3.9%	6.4%	-14%	-16%
RSR	$\leq 0.7$		0.43	0.48	0.53	0.61

The scheduling management operation were selected based on several studies (Cao, Lu, & Yu, 2018; Her, Chaubey, Frankenberger, & Smith, 2016; C. Lu et al., 2020; Pignotti, Rathjens, Cibin, Chaubey, & Crawford, 2017; Q. Wang et al., 2021). Table 11 presents more details about the operations. Tile drainage are not practiced in the county (Tate county, MS) where HCW locates (N. Nakagaki, 2016; Valayamkunnath, Barlage, Chen, Gochis, & Franz, 2020). **Fertilizer:** Primary nutrient content in fertilizer used in US are Nitrogen, Phosphate, and Potash (USDA-ERS, 2019; USDA-NASS, 2009). The main used fertilizer in the area are urea and ammonia (C. Lu et al., 2020). From the inventories and Cao et al. (2018) very insignificant amount is used for soybean (Cao et al., 2018). Therefore, the fertilizer wasn't used when growing soybean. **Tillage:** If the soil is infrequently disturbed, biological mixing can be significant. SWAT models this process to a depth of 300 mm (Neitsch et al., 2011). According to the CTIC (Conservation Technology Information Center) conservation tillage (No-Till) is mainly practiced in the county (EPA, 2022). According to local farmers and USDA, late March through mid-April is good time to plant and mid- august to mid- September to harvest soybean/corn in MS (MSPB, 2021), (USDA-NCRS, 1999). We didn't set any value to LAI\_INIT (initial leaf area index), instead we made sure that by end of the warmup period (2 years), the leaf area index was in normal range. **Irrigation:** In terms of irrigation, we tried two options: auto irrigation and manual irrigation. Although the later allows to implement major growth stages of crop development and although SWAT auto irrigation has limitation, we used auto irrigation based on soil water content; it is not easy to schedule and in reality there isn't a fixed time for irrigation and farmers irrigate based on soil water content (Allen, Pereira, Raes, & Smith, 1998; Y. Chen, Marek, Marek, Brauer, & Srinivasan, 2017, 2018; Kebede, Fisher, Sui, & Reddy, 2014). The irrigation amount for corn and soybean are 3100 and 2800  $m^3 ha^{-1}$ , respectively (Massey et al., 2017; Lindsey MW Yasarer, Taylor, Rigby, & Locke, 2020). Based on USDA-NASS 2007 census only around 5% of the farms are irrigated (USDA-NASS, 2009). **Grazing:** In the pastureland, in north Mississippi tall fescue is grown. The grazing parameter values were selected according to the literature and ((JG Arnold et al., 2013; Chiang, Chaubey, Gitau, & Arnold, 2010; Park, Ale, Teague, & Dowhower, 2017; Sheshukov, Douglas-Mankin, Sinnathamby, & Daggupati, 2016). Based on USDA-NASS 2007 and ASABE Standards 2005, the stocking rate at the county level is 0.7UA/ha (ASAE, 2005; Pai, Saraswat, & Daniels, 2011; Sheshukov et al., 2016; USDA-NASS, 2009).

**Table 11.** Management Operation

Grazing		Crop	
<b>Land Use</b>	Pasture	<b>Rotation</b>	-Soybean-Corn, Annually
<b>Duration</b>	300 days	<b>Irrigation</b>	-Major growth stages/ only 7% irrigated
<b>Fertilizer</b>	Anhydrous ammonia	<b>Fertilizer</b>	-Anhydrous ammonia/ 4 times during major growth stages
<b>Vegetation</b>	Fescue Grass	<b>Plant Beginning</b>	
<b>Stocking Rate</b>	0.7 AU*	<b>Harvest and kill</b>	-April 5 <sup>th</sup> -August 15 <sup>th</sup>

\*Animal Unit

Regions going through soil erosion could have increases in the intensity and frequency of ERs under warming climate (Verma et al., 2015; Q. Wang et al., 2021). South and Southeastern US receives maximum rain during summer and most of the ERs occurs in this time (figure 15). The ER changes in south US has rose 27% in last few decades (Mondal, Mishra, & Leung, 2020; Walsh et al., 2014b). This changes for Mississippi river basin can increase 17% in rainfall and 32% in runoff, in flash flood- producing ERs (Dougherty & Rasmussen, 2021). Studies also indicate that the total annual precipitation for the region won't change (Groisman et al., 2012). To account for these changes, we developed the weather scenarios as follows.

In this study we have five scenarios; one is without any management operations (nomgt) and one is with the scheduled management practices (S0) and the other three are with the practices under intensified rainfalls (S1, S2, S3). Table 13 shows the scenarios details. Three types of extreme rainfall scenarios were developed by changing the rainfall concentration indices while the total annual rainfall kept constant. These indices were used to characterize the spatial and temporal distribution of the ER events (Y. Lu et al., 2019; Zan Xu et al., 2021). We obtained the Stage IV QPE data for the years 2016 to 2021. We analyzed this data to determine the base year for further scenario development. To select a base year as a representative year that could account for the changes in rainfall behavior, we used daily rainfall concentration index (CI) (Abolverdi et al., 2016; Martin-Vide, 2004) and the monthly rainfall concentration (PCI) indices(De Luís et al., 2001; Oliver, 1980). Table 12 and 13 show the results. The following are the equations used for the scenario development:

$$PCI = 100 \times \left( \sum_{i=1}^{12} p_i^2 \right) / \left( \sum_{i=1}^{12} p_i \right)^2 \quad (6)$$

where  $p_i$  is the monthly rainfall amount of month i. PCI ranges from around 8 to 100; if annual rainfall of a given year is concentrated in a single month, PCI becomes 100, and if the rainfall is evenly distributed throughout the year, then the PCI equals to a value around 8 (Y. Lu et al., 2019; Oliver, 1980). PCI values that are less than 10 indicates a uniform distribution; PCI values between 10 to 15 indicates moderate seasonal concentration. PCI values between 15 to 20 indicate quite irregularity in the rainfall event distribution where rainfall occurs only in a few months; and PCI values greater than 20 shows substantial rainfall concentration. Our PCI result show that most of the years from 2016 to 2021 falls moderate concentration class and only year 2017 falls in slightly below 10.

The daily concentration index (CI) is used to evaluate the contribution of individual ER events to i.e. variation of proportion of daily rainfall compared to the cumulative precipitation of the year (X. Li, Jiang, Li, & Wang, 2011). It can be used to quantitatively assess the largest ERs' relative or percentage contribution (Brooks & Carruthers, 1953). To calculate CI, the daily rainfall values should be classified based on class limits. Contribution of the classes to the annual rainfall amount is associated with the exponential curve called normalized rainfall curve (Jolliffe & Hope, 1996). The curve can be determined as equation 6 fitting the values of  $(X_i, Y_i)$  (Martin-Vide, 2004); the equation can generate polygonal line known as concentration curve or Lorenz curve and widely used in many area (W. Chen et al., 2015; Coscarelli & Caloiero, 2012; Vélez, Martin-Vide, Royé, & Santaella, 2019; Wheeler & Shaw, 1994; Zubieta, Saavedra, Silva, & Giráldez, 2017). After determining the classes, the number of rainy days and corresponding amount of rain for each class is calculated; then the accumulated percentage of precipitation days (X) and the associative accumulated percentage of precipitation (Y) are calculated; then curve is derived.

$$Y = X \times \exp(-b(100 - X)^a) \quad (7)$$

$$\ln a = \frac{\sum X_i^2 \sum \ln Y_i + \sum X_i \sum X_i \ln X_i - \sum X_i^2 \sum \ln X_i - \sum X_i \sum X_i \ln Y_i}{N \sum X_i^2 - (\sum X_i)^2} \quad (8)$$

$$b = \frac{N \sum X_i \ln Y_i + \sum X_i \sum \ln X_i - N \sum X_i \ln X_i - \sum X_i \sum \ln Y_i}{N \sum X_i^2 - (\sum X_i)^2} \quad (9)$$

$$S = 5000 - \int_0^{100} Y \quad (10)$$

$$CI = \frac{S}{5000} \quad (12)$$

where a and b are regression coefficients by the least-square method; N is the number of classes with non-zero frequency; S is the area enclosed by the bisector of the quadrant and the curve. CI is the fraction of S and ranges from 0 to 1; the larger the area, the higher the CI indicating greater concentration degree; and the greater CI means more rainfall occur in fewer days. Our result for the Stage IV QPE data from 2016 to 2021, shows that the CI for HCW fall these years ranges approximately from 0.6 to 0.7 with 2017 being the highest (Table 12). Based on Table 12, and to ensure that the changes in the scenario rainfall events are within the acceptable range we accepted the year 2021 as the base year for scenario development. This was because 2021 has the second to the highest CI and third in the annual rainfall amount. It also has the highest amount of one day precipitation (146.57 mm in June) among the six year (2016-2021.)

Using equation 7 and 8, we created rainfall values for scenario S1, S2, S3. This method makes sure that the total annual rainfall would stay constant while four top highest rainy days become more intensified rainfall events (Zan Xu et al., 2021). . We concentrated 3, 6, and 9 % of the cumulative precipitation of the year to top 4 daily precipitations in the base year (2021). Equation 14 was applied to the rest of the days to lower the rainfall amount corresponding each day. Figure 15 shows the developed rainfall series as scenarios.

$$R_{ii} = R_i + \sum_{i=5}^{365} c (1 - c)^{j-1} R_j \quad (13)$$

$$R_{jj} = (1 - c)^4 R_j \quad (14)$$

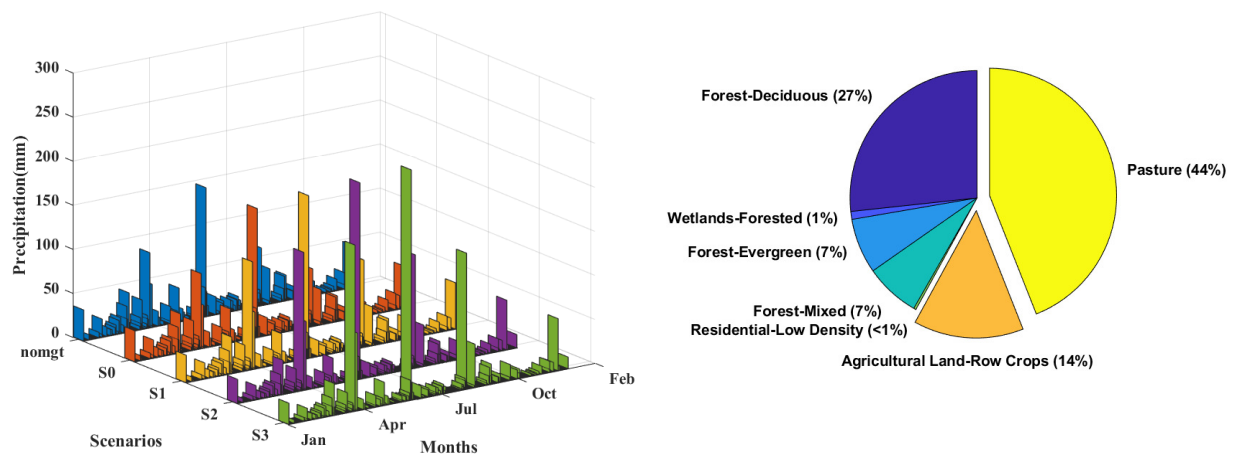
where  $R_{ii}$  the new value for the four topmost rainy days in 2021;  $R_{jj}$  is the new rainfall series for each scenario (361 remaining values);  $R_j$  is the rainfall value for the corresponding day in the base year; i= 1, 2, 3, 4; and j= 5, 6, 7,..., 365. We didn't force the scenarios through the 17 stations within the HCW; instead, we calculated the average for the study area and forced the average basin rainfall values through one station at the centroid of the watershed. Forcing the scenario values through the 17 stations could be too much of arbitrary values which are too specific for the stations that are 4km away each other. Because assigning scenario values to specific stations that are not far from each other (4km) could go against heterogeneity of precipitation which could lead to overfocusing on certain subbasins. In our development we didn't alter the temporal or spatial distribution of the representative year. Table 13 shows CI and PCI and the percentage of increases for them as well as the concentration ratio corresponding each scenario.

**Table 12.** Rainfall statistics from 2016 to 2021

	<b>2016</b>	<b>2017</b>	<b>2018</b>	<b>2019</b>	<b>2020</b>	<b>2021</b>
<b>CI</b>	0.63	0.66	0.59	0.59	0.58	0.63
<b>PCI</b>	11.53	9.43	10.27	10.26	9.95	10.82
<b>Annual rainfall (mm)</b>	1314.3	1297.7	1775.1	1802	1550.8	1628.5
<b>Mean (mm)</b>	3.59	3.55	4.81	4.94	4.24	4.46

**Table 13.** Scenario Development

	<b>nomgt</b>	<b>S0</b>	<b>S1</b>	<b>S2</b>	<b>S3</b>
<b>Management practices</b>	No	Yes	Yes	Yes	Yes
<b>Precipitation</b>	Historical	Historical	Concentrated	Concentrated	Concentrated
<b>CI</b>	0.63	0.63	0.66	0.69	0.73
<b>PCI</b>	10.82	10.82	12.19	13.78	15.51
<b>CI increase (%)</b>	-	-	4.7	9.5	15.9
<b>Concentration ratio (c)</b>	-	-	3%	6%	9%

**Figure 15.** Left panel shows the rainfall distribution over the year for the scenarios. Right panel shows the land use percentage in HCW

### **3.4 Results and Discussion**

For soil erosion simulation, SWAT uses the MUSLE model which has a few limitations; for example it is an empirical model in contrary to physical models such as Water Erosion Prediction Project (WEPP) (Flanagan, Gilley, & Franti, 2007). However, studies show that using other models instead of MUSLE wouldn't necessarily result in lower uncertainties and that MUSLE provides certain information which other models simply cannot (Alewell, Borrelli, Meusburger, & Panagos, 2019; Nearing, 2013).

Hydrological simulation of HCW indicated that for streamflow, the most sensitive parameters were CNOP, ESCO, RCHRG\_DP, and SOL\_AWC (Makhtoumi et al., 2020; Parajuli et al., 2016). HCW is located in outcrop region where Sparta Sand aquifer is exposed at the surface (unconfined); thus, the groundwater table is close to the surface and facilitates transmission loss making RCHRG\_DP responsive (McKee & Hays, 2002). The model indicates that the most influential land use change that controls sediment loss is grazing. This result was expected, but the sensitivity was remarkably high. The pasture management (grazing) parameters (BIO\_EAT, BIO\_TRMP, and MANURE\_KG) are the most sensitive ones throughout sediment parametrization and modeling (Chiang et al., 2010; Park et al., 2017). The second responsive process was sediment routing process including parameters such as SPCON, SPEXP, and PRF (Aghsaei et al., 2020; Razad, Shamsuddini, Setu, & Sidek, 2021). Third sensitive process was topsoil loss where parameters such as USLE\_K, USLE\_C, USLE\_P, and SOL\_ROCK play role (Halecki, Kruk, & Ryczek, 2018). Calibration for both streamflow and sediment were challenging, and the satisfactory metrics were at the lower side of the acceptable range; this can be due to small size of HCW; HCW drains inly 312km<sup>2</sup> and there is no upstream inlet; this makes the amount of daily discharge, sometimes, less than 1 cms indicating some degree of intermittency(Reynolds, Shafrroth, & Poff, 2015). On the other hand, there are days were both streamflow and sediment discharge were high (figure 13 ,14); this implies that HCW is flash-flood prone and easily eroded (Biedenharn et al., 2004; Dougherty & Rasmussen, 2021). Streamflow and sediment yield were calculated for the base year to investigate the effect of extreme rainfall events on topsoil loss. We divided HCW into 30 subbasins to spatially investigate the characteristics of ERs and each subbasins underlying surface condition in these small hydrologic units. Since there is no major reservoir in HCW that could interfere with the transport processes of suspended sediment, we were

able to study the upland sediment concentration (Heimann, Sprague, & Blevins, 2011). According to the in-situ gauge data, mean annual flow discharge at the monitoring point is 2122 cms and the mean annual sediment discharge is 102974 (metric) ton or 3.3 ton per hectare. Figure 16 shows the spatial distribution of the agricultural and pasture management practices within HCW. The distributions indicate irregularity among subbasins, however, subbasins located on the south of HCW experience more than other regions (USDA-NASS, 2009). Initial analysis shows that adding the management operation increases the surface runoff, average upland sediment yield, and instream sediment change by 8.3%, 1206%, and 1397%.

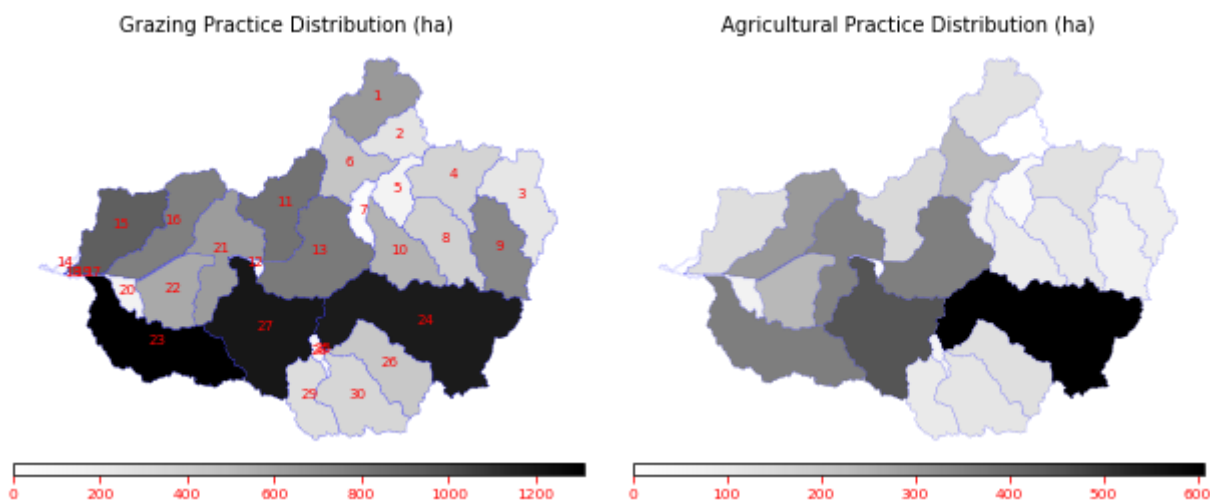


**Figure 16.** Left panel shows grazing practice distribution. Right panel shows agricultural practice distribution in HCW.

Soil erosion at the watershed was originally high; however, under a few management projects, appropriate management practices were implemented (Biedenharn et al., 2004; H. C. W. I. T.-. MDEQ, 2009). Although, the BMPs controlled the topsoil loss and the deterioration at some degree; recent emergent weather and climate irregularities appose another threat to the soil, crop production and livestock. HCW drains into lake Arkabutla and therefore can endanger many lakes economic opportunities. Topsoil loss can inflict both on-site and off-site costs. the later can be due to water quality deterioration. Here we mainly study the on-site consequences. To do so, we analyzed different water and sediment variable under severe conditions. We compared the variables under nomgt (no management), S0 (with management but no change in rainfall), S1 (3% ER concentration), S2 (6% ER concentration), and S3 (9% ER concentration). S0 is our baseline

scenario. Figure 17 shows the distribution of annual rainfall, water yield, sediment yield, sediment concentration in the reaches, soil available water content, and ET for each subbasin. We used Stage IV Radar data with 4km resolution, and it allows us to see how much rainfall occurs in each subbasin. Figure 17a indicates that under all scenarios, annual rainfall ranges from 1560 to 1720 mm; subbasins located at the north receives more rainfall (subbasins: 5, 6, 7, 16, 15, 2, and 4) than subbasins at the south of the watershed (subbasins: 23, 22, and 27). Spatial distribution difference between S0 and S1 and between S1, S2, and S3 are interesting, our weather scenario development model redistributes rainfall to subbasins 5, 6, 7 under S1 ( $c=3\%$ ); however, as  $c$  (concentration ratio) increases (S2 and the S3) more annual rainfall goes to subbasin 16. Since subbasin 16 is heavily grazed (figure 16 left), this subbasin can be more vulnerable to soil degradation due to high erosion (J. C. Ritchie, McHenry, & Schiebe, 1978). SWAT mechanism to allocate rainfall forces uncertainties; if averaging methods such as Thiessen polygon is used, it might help distributing rainfall amount smoother, however, it will create unrealistic rainfall records for some of the points; this could lead to error in finding the soil erosion hotspots (Zeiger & Hubbart, 2017). On the other hand, if fine gridded data such as NEXRAD Stage IV or MRMS is applied, it might assign two different rainfall amounts to neighboring subbasins where they, in reality, received approximately the same amount of rain. This is due to the SWAT mechanism that assign rainfall from stations whichever is the closes to the centroid of the subbasin (Ruan et al., 2016; Zeiger & Hubbart, 2017).

Annual water yield ( $WYLD = Q_{surface} + Q_{lateral} + Q_{groundwater} - transmission\ loss$ ) distribution is different than that of rainfall (Neitsch et al., 2011). It shows clear trend from nomgt scenario to S3 (figure 17b). It indicates that underlying conditions on the watershed surface has bigger contribution to WYLD than precipitation (Makhtoumi et al., 2020). Comparing ‘nomgt’ to ‘S0’ where the difference is only management practices in S0 indicates that grazing and farming soybean/corn yields more surface runoff which could increase the risk of flood (Parajuli et al., 2016; Park et al., 2017). Subbasins 6 and 16 are reflects 8.5% and 11.2% increase in WYLD when the management practices are added. The increases rise further for most of the subbasins as the concentration ( $c$ ) increases; (Zan Xu et al., 2021).

Figure 17c presents the mean daily soil water content (SWC) throughout the watershed. SWC ranges from 130 in subbasin 17 to around 300 mm in subbasin 3. Comparing nomgt to S0

reveals that the added management slightly increases the soil's water holding capacity (Park et al., 2017). Comparing SWC distribution to rainfall and WYLD indicates that subbasins that received more rainfall and produced more WYLD (generally north part of HCW) have less water holding capacity than subbasins located at the south. Increasing CI is associated with less SWC throughout HCW. This means more severe rainfall will deteriorate the infiltration rate and water holding capacity of the soil which could lead to drought or flood (Gavahi, Abbaszadeh, & Moradkhani, 2022; Ho-Hagemann, Hagemann, & Rockel, 2015; Wasko & Nathan, 2019; Wasko, Nathan, Stein, & O'Shea, 2021).

figure 17d presents evapotranspiration (ET) distribution for the scenarios. ET decreases when adding the management operations (S0) or severe rainfalls (S1, S2, S3). Vasquez et al. (2020) and Zesu et al. (2016) also reported the same results (Vázquez, Nieto, Liberato, & Gimeno, 2020; Z. Yang, Zhang, & Hao, 2016). ET ranges from 600 to more than 830 mm throughout the subbasins under different scenarios. The lowest ET values are under S3, and the highest ET amounts are under nomgt scenario. Comparing nomgt and S0 reveals that practicing grazing (44% area) and farming (14% area) in the watershed decreases ET. The highest ETs occurs in subbasins 15, 22, 23 and it decreases 15%, 12%, and 14% respectively when the grazing and farming added. Subbasin 7 under all scenarios had high ET, this is due to the irrigation. The model doesn't allow SWC would fall below a set threshold and irrigates cultivated crop land use, therefore ET stays higher than many other subbasins despite scenario changes (Y. Chen et al., 2018; Verstraeten, Veroustraete, & Feyen, 2008). Changing the land use (nomgt to S0) inflicts bigger change than increasing rainfall CI (Makhtoumi et al., 2020).

Figure 17e shows the annual soil loss distribution. It indicates that both the management operations and ERs exacerbate the topsoil loss (Admas et al., 2022; Halecki et al., 2018; Zan Xu et al., 2021; L MW Yasarer et al., 2017; X. C. Zhang & Nearing, 2005). Topsoil loss under the scenarios, ranges from 0 to above 350 ton/ha. The lower range associated with nomgt and baseline (S0); as the rainfall CI increase the erosion worsens throughout the watershed with more erosion for some subbasins, subbasins 15, 16, 9, 10, and 23. HCW is in Coldwater River watershed and it is considered impaired due to siltation (M. D. o. E. Q. MDEQ, 2003); the amount of sediment load was almost 5 times higher than other north Mississippi watersheds (McHenry, Ritchie, & Schieber, 1977). HCW is in Mississippi Valley Loess Plains (MVP). In 2002, Simon et al. studied sediment

transport in MVLP and reported annual sediment yield (topsoil loss) ranges from 90 (ton/ha) to 3650 (ton/ha) (Simon, Kuhnle, Knight, & Dickerson, 2001). Based on these studies in the region we classified topsoil loss in HCW as follows: low (< 10 ton/ha), moderate (10 to 40 ton/ha), severe (40 to 90 ton/ha), very severe (90 to 150), and extremely severe (>150 ton/ha) (T. Chen, Niu, Li, Zhang, & Du, 2011; Lemma et al., 2019; Simon et al., 2001) (See Appendix A for details). Before adding any management operations (nomgt) most of the subbasins are in the low class except subbasins 6, 7, 16, 22 where they fall in the lower side of the moderate class. Under S0, however, increases are manifold in all the subbasins with biggest increase (3600%) in subbasin 2 and the smallest change (96%) in subbasin 14 putting most of the watershed in very or extremely severe class. This indicates how pasture management (grazing) and farming can be significant in terms of soil degradation (Pai et al., 2011; Parajuli et al., 2016; Sheshukov et al., 2016). Comparing S1, S2, and S3 to the baseline (S0) indicates the further increase as rainfall CI grows (Verma et al., 2015; Zan Xu et al., 2021). Under S1 with CI of 0.66, subbasins 6, 9, 10, 15, 23, and 27 yield more than 150 ton/ha (extremely severe). Under S2 with CI of 0.69, subbasins 1, 13, 16, 22 also fall into extremely severe category yielding approximately 200 ton/ha. Under S3 with CI 0.73, subbasins 2, 5, 8, 11, 12, 17, 20, 21, 24 also are in Extremely severe class yielding more than 200 ton/ha. In figure 17e when moving from left to right, the emergence of severe and extremely severe classes can be seen (Admas et al., 2022; M. D. o. E. Q. MDEQ, 2003; Zan Xu et al., 2021). Subbasins 9, 10, 11, 15, 16, and 23 are the hotspots to be considered and prioritized.

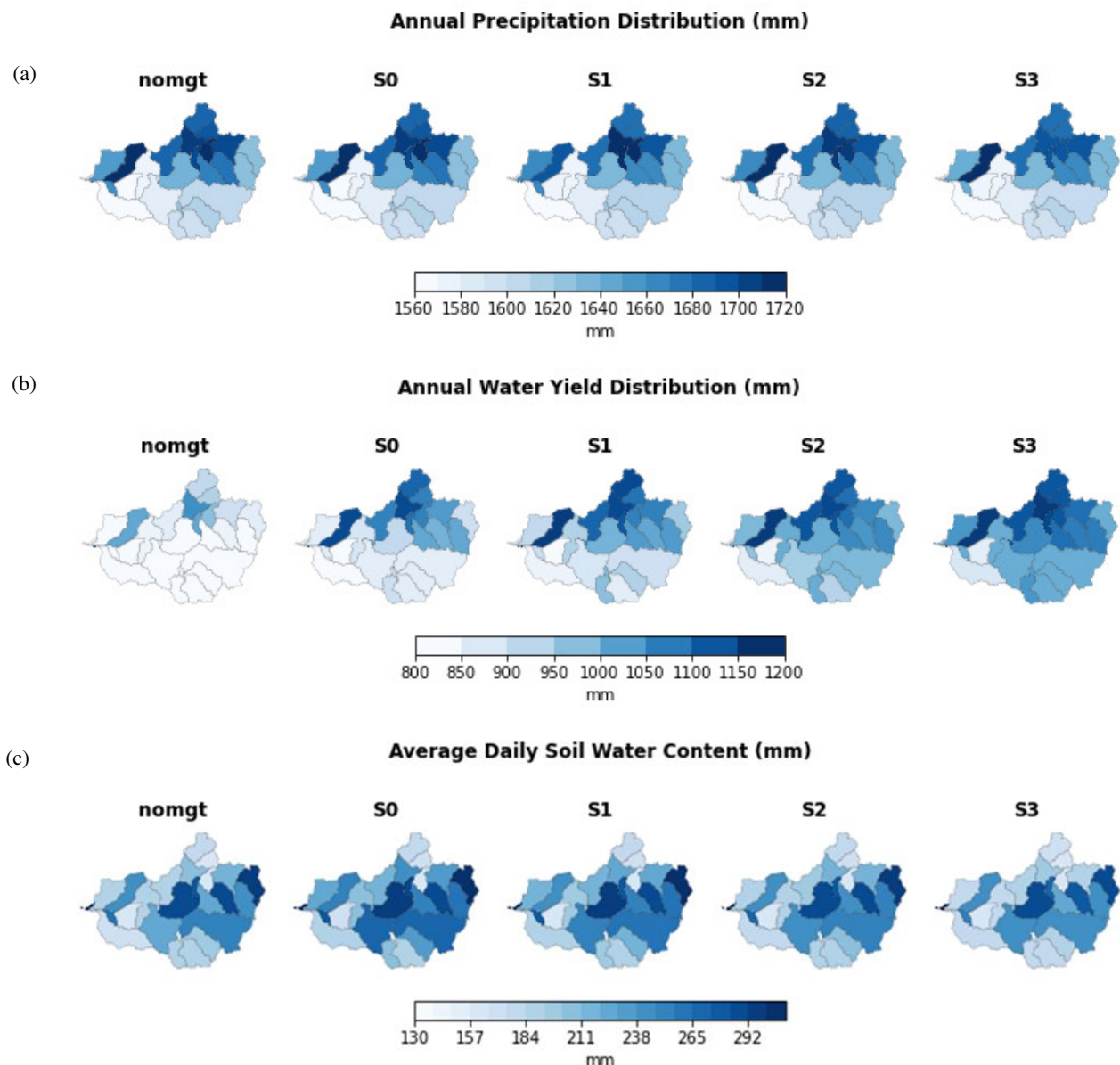
Figure 17f illustrates the sediment concentration in the reach segment of each subbasin. Suspended Sediment Concentration (SSC) in HCW were measured at the monitoring point (the USGS site, reach 19 fig. 1) from 1986 to 2003. According to the measured data, mean daily SS in the period was 137.4 (mg/L), and the mean annual was 55563 (mg/L). McHenry also studied the SS load in north Mississippi lakes and reported that annual mean SS at Arkabutla lake surface water was 73000 (mg/L) approximately (McHenry et al., 1977); our findings regarding SS matches with the reports. Comparing nomgt to S0, shows substantial increase in SS when the grazing and corn/soybean farming are practiced (Biedenharn et al., 2004). The biggest changes occur in subbasins 1, 2, 3, 8, 9, 10, 15, 16, 22, 23, 24, 26, 29, and 30 (dark subbasins in fig.6f). The highest SS values under S0 is from subbasins 15, 23, and 16 with over than 1 million (mg/L). These subbasins can be considered and prioritized for water quality and impaired turbidity hotspots

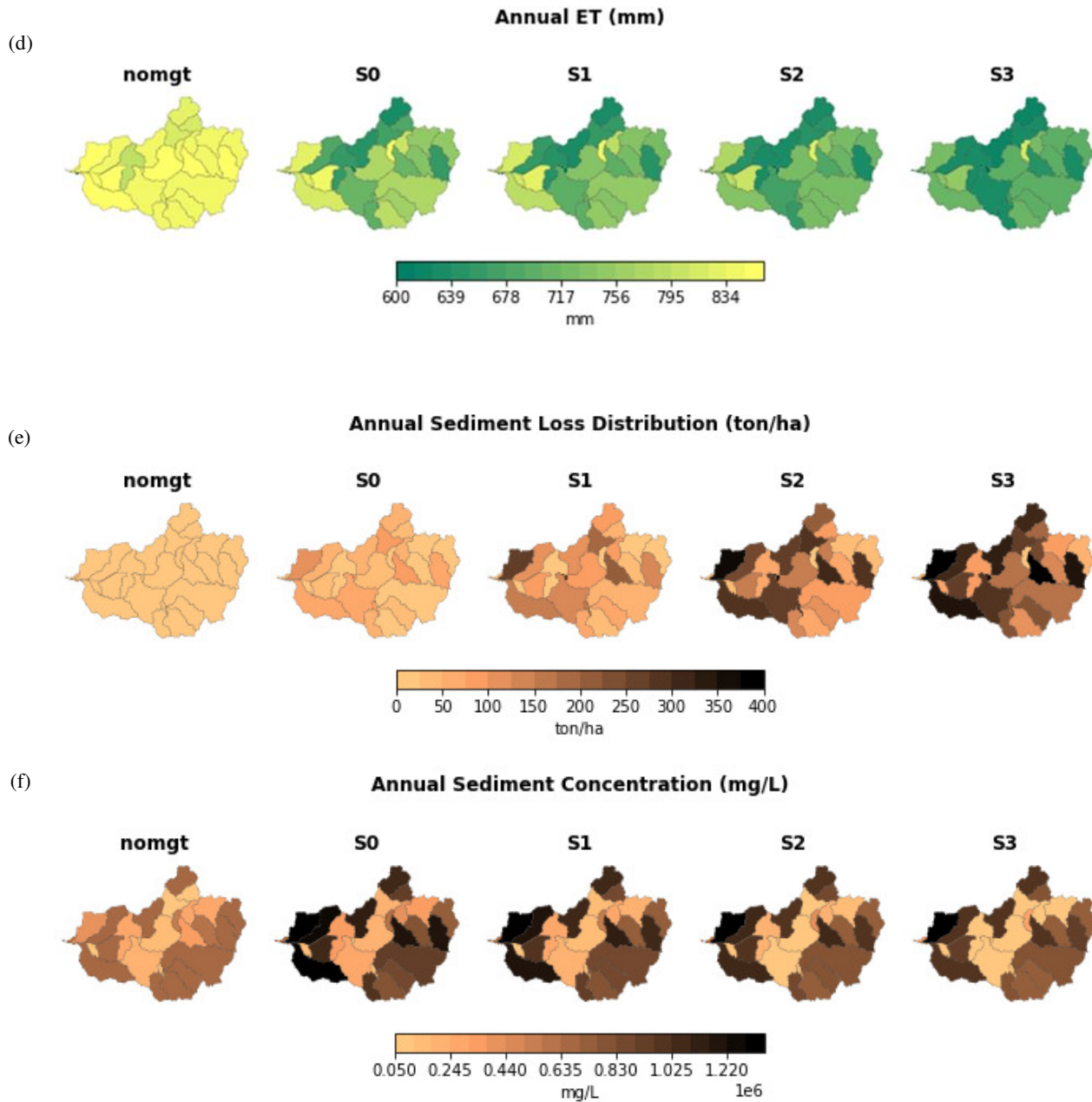
(Halecki et al., 2018; C. Lu et al., 2020; Q. Wang et al., 2021; L MW Yasarer et al., 2017). Comparing baseline scenario (S0) to S1, S2, and S3 indicates that as rainfall CI increases the SS throughout HCW decreases slightly. This could be the result of scenario value generation which means less precipitation on normal rainy days (not top four rainy days). This could also indicate that as CI increases the raindrops can wash away bigger soil particles that can be easily settled in the reach (S. Dutta, 2016; Neitsch et al., 2011; Wischmeier & Smith, 1965, 1978). Subbasins 4, 5, 6, 13, 21, and 27 are the lowest under S1, S2, and S3 with mean daily of 63 (mg/L). Comparing sediment yield and SS distribution shows that the hotspots are the same Subbasins (9, 10, 11, 15, 16, and 23). Table 14 shows the annual soil loss w.r.t. % change in CI. This result indicates that up to 9.5% increase in CI could increase soil loss up to 72.3% (in subbasin 11).

Figure 18 demonstrates changes over the year period for the variables (Flow discharge (Q), SYLD, SSC, ET, and SWC) under the scenarios. Since the runoff generation and consequently, soil erosion depends on soil conditions, the time when the ERs occur can play a role (Q. Wang et al., 2021). Figure 18a shows that the top four rainy day in baseline scenario which happen in Spring and Summer (two in March, June, and August) and values for all four days increases as CI grows (S0 to S3). For the rest of the days (normal days), however, the opposite occurs where S3 has least daily discharge throughout the year. This can imply that the cumulative effect of normal day rain on SS can be higher than the effect of top four days on SS, hence, figure 17f shows decrease in SSC throughout the watershed as CI increases. Comparing nomgt daily discharge to S0 reveals that grazing and corn/soybean farming increase runoff noticeably (Adimassu, Tamene, & Degefie, 2020; Parajuli et al., 2016). Figure 18b illustrates the daily sediment discharge at the monitoring point. Daily sediment discharge shows the same pattern as flow discharge (Simon et al., 2001). The greater amount of sediment is transported during the flood season specially from March to May, therefore this time of the year should be considered and prioritized in decision making (Makhtoumi et al., 2020; Zan Xu et al., 2021). The transported sediment amount on the top four days is extremely high. Table 15 shows the percent changes regarding changes to the baseline scenario. Figure 18c illustrates mean daily SSC. For the normal days SSC follows the same pattern as SYLD and Q. On the four topmost rainy days, it shows irregularities. For example, on March 31, S2 generate highest SSC rather than S3; or on August 28, S0 generates the highest SSC.

**Table 14.** Percent change in annual soil loss under changes in rainfall concentration ratio

Subbasin	9	10	11	15	16	23
CI %change						
<b>4.7</b>	34.7%	27.0%	36.9%	34.5%	34.4%	33.0%
<b>9.5</b>	72.4%	56.2%	76.3%	72.3%	70.5%	68.5%
<b>15.9</b>	108.8%	95.4%	112.7%	110.4%	109.5%	103.7%

**Figure 17.** (a) Annual rainfall distribution. (b) Annual water yield distribution. (c) Annual soil water content.



**Figure 17.** -continued (d) Annual Evapotranspiration. (e) Annual soil loss distribution. (f) Annual suspended sediment concentration

This could be due to soil preconditions and/or heterogeneity of the rain (Ho-Hagemann et al., 2015; Wasko & Nathan, 2019; Zan Xu et al., 2021). Also timing the management practices can play a role (Park et al., 2017). Figure 18d and 18e demonstrate ET and SWC through the year. SWC shows more variability from March to late August. Comparing nomgt to S0 shows that under S0 soil has more ability of holding more water (Park et al., 2017; Pulley & Collins, 2020); however,

under S1, S2, and S3 it holds less water throughout the year. ET under nomgt shows higher values during Spring, Summer, and Fall (Makhtoumi et al., 2020); however, under other scenarios the watershed ET doesn't show noticeable variability. MUSLE allows to study single storm events (Neitsch et al., 2011; Wischmeier & Smith, 1978). In table 15 we showed percent change of rainfall amount (pcp), Q, SYLD, and SSC in respect to the baseline scenario (S). the topmost rainy days are March 28, March 31, June 9, and August 20 with 85.5, 49.3, 146.6, and 65.7 mm respectively. Table 15 indicates that without any management operation Q, SYLD, and SSC depending on the amount of rain and the time of the year it occurs. ERs in March generate slightly more flow and sediment under nomgt ERs in summer generate less flow and sediment. This could be due to the timing and type of the operation as well as vegetation cover (Table 11) (Pulley & Collins, 2020); Wang et al. (2021) studied the effect of ERs in different seasons and reported the same findings (L. Wang et al., 2021).

**Under S1**, the highest increase in pcp was on August 20<sup>th</sup> by 51.2%; this induced 78.1%, 16.3%, -34.7% changes in Q, SYLD, and SSC respectively. The decrease in SSC could imply the importance of the management operations. Under S1, the highest SYLD and SSC increase occurred on March 28<sup>th</sup> by 93.8% and 21.4% respectively.

**Table 15.** % Change in flow (Q), Sediment Yield (SYLD), and Suspended Sediment Concentration (SSC) on the topmost rainy days

Scenarios	Variables	3/28	3/31	9/09	8/20
<b>nomgt</b>	Pcp	0	0	0	0
	Q	0.2	0.45	-1.7	-12
	SYLD	0.39	0.9	-3.27	-16.3
	SSC	0.2	0.45	-1.7	-4.6
<b>S1</b>	Pcp	43.2	31.8	26.1	51.2
	Q	59.6	47	31.6	78.1
	SYLD	93.8	69.8	46	16.3
	SSC	21.4	15.5	10.9	-34.7
<b>S2</b>	Pcp	83.4	58.1	52.2	96
	Q	116.8	89.7	63.3	148.5
	SYLD	194.82	27.65	97.6	86.1
	SSC	36	-32.7	21	-25.11
<b>S3</b>	Pcp	120.7	79.5	78.3	134.9
	Q	170.5	125.7	94.8	207.8
	SYLD	302.3	61.6	152.7	150.9
	SSC	48.7	-28.4	29.8	-18.5

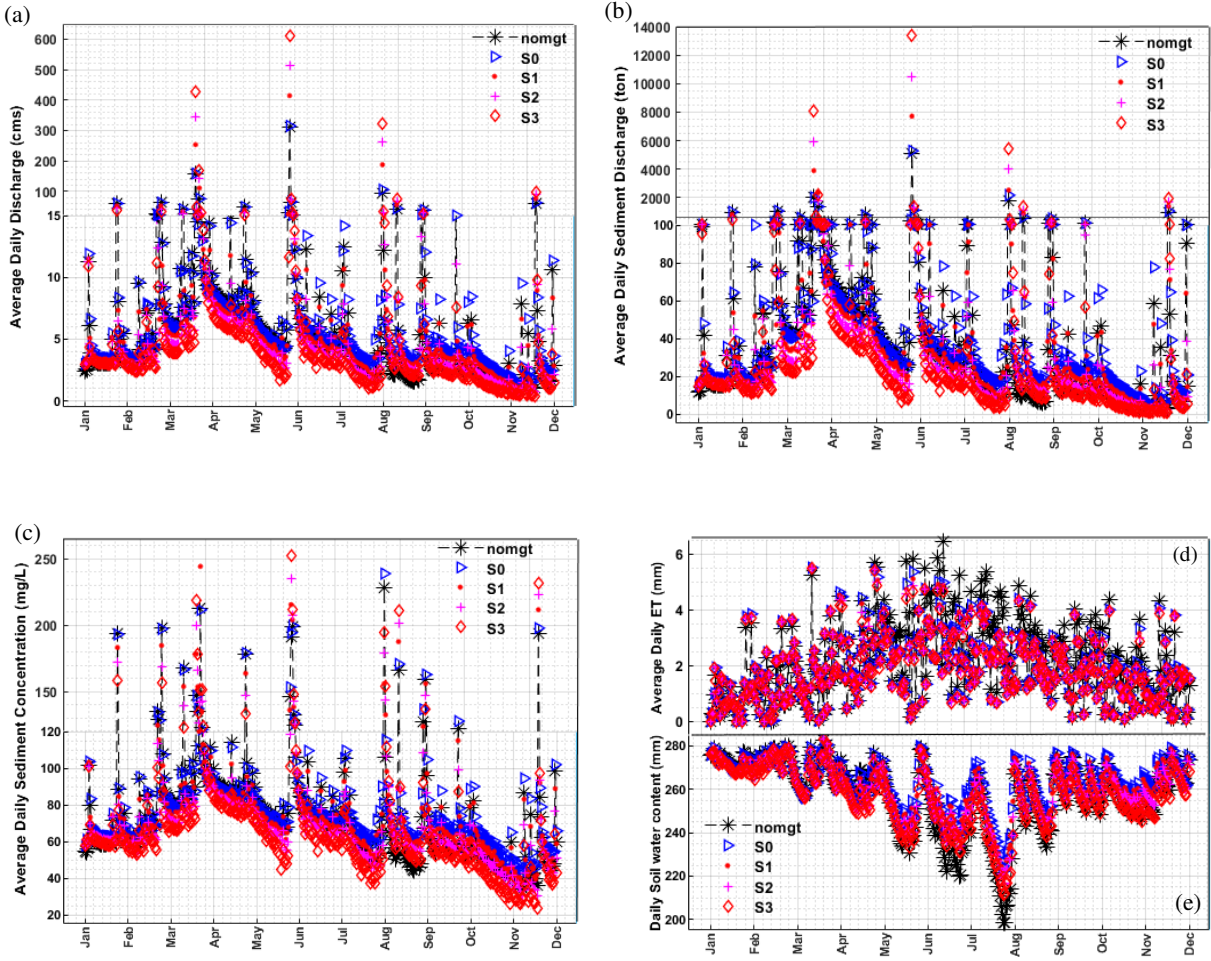


**Figure 18.** (a) Daily flow discharge time series for all scenarios at the monitoring point (USGS 07277700). (b) Daily sediment discharge time series for all scenarios at the monitoring point. (c) Daily suspended sediment concentration time series for all scenarios at the monitoring point. (d) Daily ET for the entire watershed. (e) Daily soil water content for the entire watershed.

**Under S2,** the highest increase in pcp was on August 20<sup>th</sup> by 96% followed by rainfall on March 28<sup>th</sup> with increase of 83.4%; this induced 148.5%, 86.1%, -25.1% changes in Q, SYLD, and SSC respectively on August 20<sup>th</sup> and 116.8%, 194.8%, 36% changes in Q, SYLD, and SSC respectively on March 28<sup>th</sup>. Under S2 and on June 9<sup>th</sup> which has the highest rainfall in base scenario, the SYLD and SSC increase was 97.6% and 21%. **Under S3** which has the highest concentration ratio (c), August 20<sup>th</sup> has the highest increase in pcp, Q, and SYLD by 134.9%, 207.8%, and 150.9%; SSC declines by 18.5%. Although, March 28<sup>th</sup> has the second highest change, it generates highest changes SYLD and SSC under S3. On March 31<sup>st</sup>, under S1, 31.8%

increase in pcp results in 47%, 69.8%, and 15.5% increase in Q, SYLD, and SSC respectively. On June 9<sup>th</sup>, under S3, 78.3% increase in pcp results in 94.8%, 152.7%, and 29.8% increase in Q, SYLD, and SSC respectively. Table 15 which represents percent changes for the variables, reveals different trends for each ERs emphasizing the necessity of studying each storm individually. For example, SSC increases under all scenarios on March 28<sup>th</sup>, but it declines on March 31<sup>st</sup>. This indicates the significance of underlying conditions in the watershed such as SWC and Management operations' timing and type as well as heterogeneity of individual rainfall (Park et al., 2017; Peleg, Skinner, Ramirez, & Molnar, 2021; Pulley & Collins, 2020; L. Wang et al., 2021; Zhu, Wright, & Yu, 2018).

Studies have shown that rainfalls spatial variability could explain 20-30% of the runoff generation variability in urban watersheds and even higher in rural watersheds (Peleg, Blumensaat, Molnar, Fatichi, & Burlando, 2017; Peleg et al., 2021; Zhu et al., 2018). Here we inspect spatial properties of the top four rainfall events under the scenarios and their effect on the sediment generation. Figure 19a shows the Stage IV QPE radar data over Mississippi for the four days. June 9<sup>th</sup> has the highest rainfall amount, followed by March 28<sup>th</sup>, followed by August 20<sup>th</sup> and March 31<sup>st</sup> ER has the last rank. According to the figure 19b the rainfall amount ranges from 36 to 168 mm among these four days. All the subbasins on June 9<sup>th</sup> received above 141 mm with the highest in subbasin 23 with 168 mm and only subbasins 30, 24, and 26 received lower amount (118, 128, and 128 mm respectively). on March 28<sup>th</sup>, received rainfall ranges from 67 to 94 mm; on August 20<sup>th</sup>, received rainfall ranges from 25 to 86mm. on March 31<sup>st</sup>, received rainfall amount ranges from 39 to 58mm. ER on August 20<sup>th</sup> shows the highest spatial variability. This variability could partially explain why despite increase in total rainfall the SSC declined (table 15). Subbasins 8 and 10 experienced most rain followed by subbasin 4 and 29. The second highest variability occurs on March 28<sup>th</sup>, where according to the figure 19b more rain received on the east of the watershed. Subbasin 30 with 68 mm has the least amount of rain, however, subbasins 11,15, 16, 20, 21, 22, and 23 received more than 90 mm. March 31<sup>st</sup> has the lowest amount and variability compared to others. The rainband covered east side mostly where subbasins 15, 16, 20, 21, 22, and 23 are located. This rainfall structure (spatial and temporal variability) presented here could company with watershed propensities and produce a complex hydrologic and sediment processes (L. Chen,

Sela, Svoray, & Assouline, 2016; A. Y. Sun, Xia, Caldwell, & Hao, 2018; Zhu et al., 2018). In the following two figures we examine the SYLD and SSC response in HCW.

Figure 20 demonstrates distribution of topsoil loss (SYLD) under the scenarios. Topsoil loss ranges from less than 1 ton/ha (nomgt- March 28) to 130 ton/ha (S3-June 9) in subbasin 15. Comparing nomgt to S0 reveals that in all four ER events SYLD almost doubled due to pasture management and agricultural practices (Parajuli et al., 2016; Park et al., 2017). This increase is larger in Summer ERs (June 9 and August 20). Comparing S0 to S1, S2, and S3 indicates that as CI increases vulnerable subbasins emerge; however, the emergence depends on the severity and spatial variability of the ERs (Zan Xu et al., 2021). ERs in March and June affected east side (darker than the west side); these subbasins are 15, 16, 23, 27, 6, 9, 11, and 10. However, on August 20, the west side was affected (figure 19b). As a result, most of the subbasins on the west side including 8, 9, 10, and 29 generated the highest SYLD on that day. This implies the significance of spatial variability of individual ERs (Peleg et al., 2021; L. Wang et al., 2021).

Our result in figure 20 emphasizes the direct relationship between severity of an ER and the emergence of the subbasins with severe soil loss (Zan Xu et al., 2021). If the same classification for annual SYLD used here, for the individual ERs, under nomgt almost all the subbasin are in the low class. However, under S0 almost all fall into the moderate class generating between 10 to 40 ton/ha which emphasizes the significance of anthropogenic activities in regulating under the related processes (Cerdan et al., 2010; Halecki et al., 2018; Parajuli et al., 2016). Under S1, S2, and S3 fall into the high, severe, and extreme severe classes depending on the amount of rain received on that day which runoff generation mechanism is sensitive to these changes (Wei, Zhang, & Wang, 2007). The topsoil loss hotspots can be listed as follows: subbasins 15, 16, 23, 9, 10, 11.

Sediment is the major pollutant in streams and reservoirs and in US reservoirs water storage capacity declines 0.2% each year due sedimentation (S. Dutta, 2016; McHenry et al., 1977). Figure 21 illustrates the Suspended Sediment Concentration (SSC) in the reach segment of each subbasin. Spatial distribution of SSC is expected to show the same pattern as SYLD (Figure 20); it also reveals some valuable insights as well. Comparing nomgt to S0 indicates that SSC increases significantly when adding pasture management and farming activities. The percent change under S0 is higher than that of S1, S2, and S3. Subbasins 15, 16, and 9 have remarkably high values of 63600, 61450, and 62770 (mg/L) respectively.

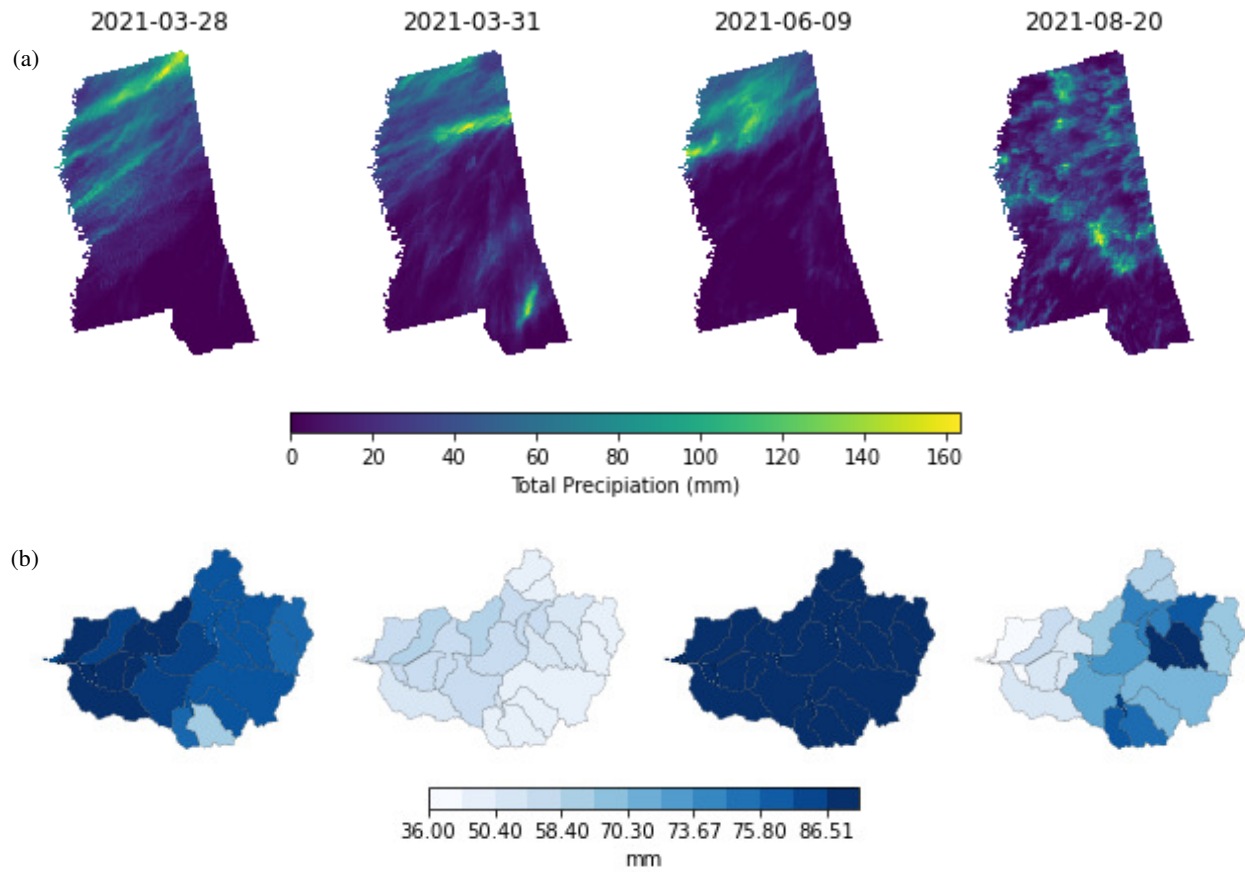


**Figure 19.** (a) Stage IV QPE radar rainfall over Mississippi on March 28<sup>th</sup>, March 31<sup>st</sup>, June 9<sup>th</sup>, and August 20<sup>th</sup>. (b) distribution of rainfall occurred on corresponding days

Different ERs impact different subbasins due to differences in spatial variability. Subbasins 4, 5, 6, 13, and 27 reflect less amount of SSC; this could be due to the fact that suspended particles are more likely to settle in bigger reaches (Baronas et al., 2020; Biedenharn et al., 2004). Biedenharn et al. (2004) carried out an erosion control project and reported significant amount of sediment settlement in HCW (Biedenharn et al., 2004). Under the ERs as CI increases (from S1 to S3) SSC increase throughout the watershed affecting some subbasins more than others. Subbasins on the west (subbasins 9, 10, 24, and 26) and subbasins on the east (subbasins 15, 16, 23, and 11) generate the highest SSC. Overall, subbasins that can be Considered SSC hotspots are: 15, 16, 23, 9, 10, 11.

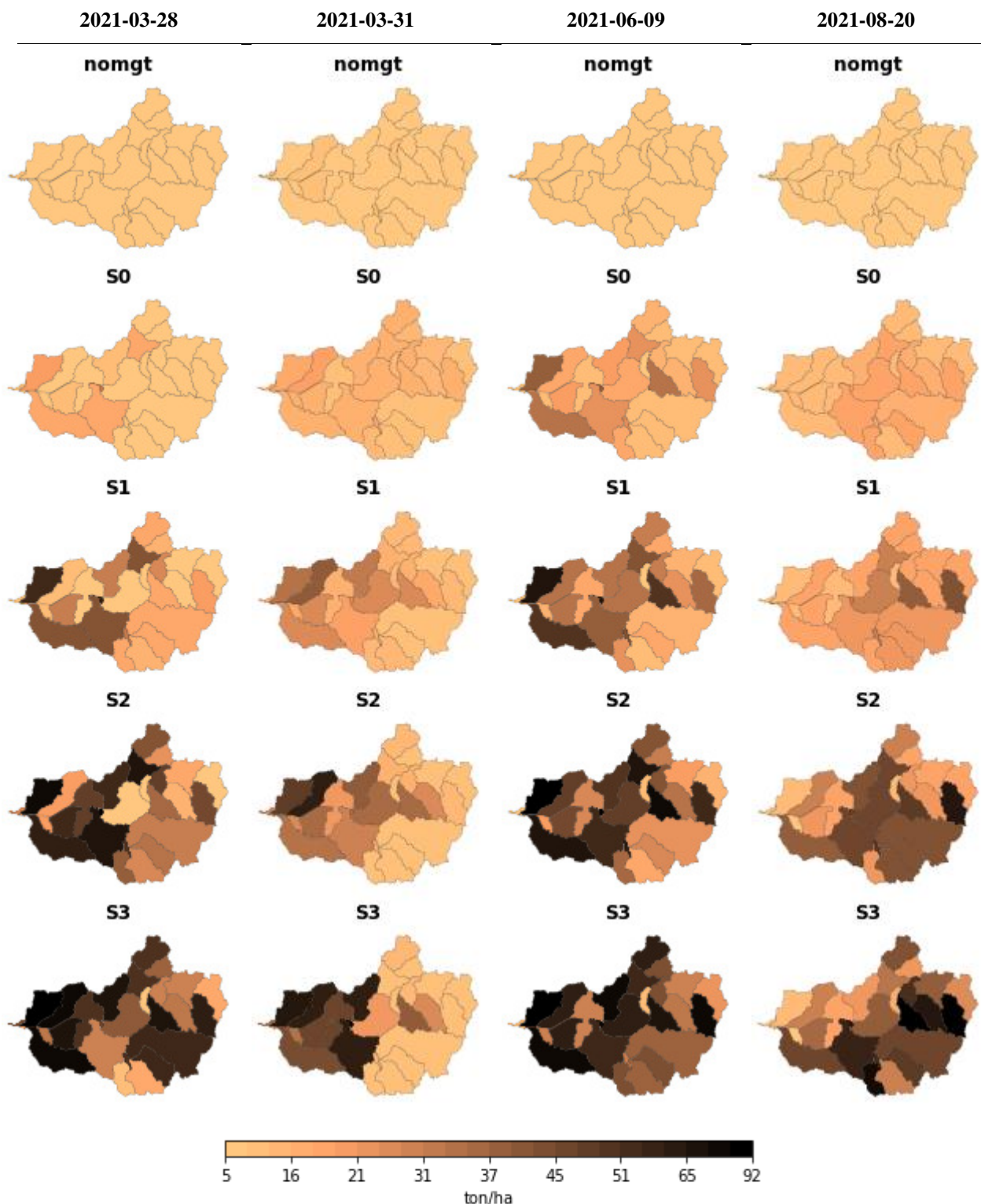


**Figure 20.** Distribution of soil loss caused by extreme rainfalls on March 28<sup>th</sup>, March 31<sup>st</sup>, June 9<sup>th</sup>, and August 20<sup>th</sup> over HCW under all scenarios.

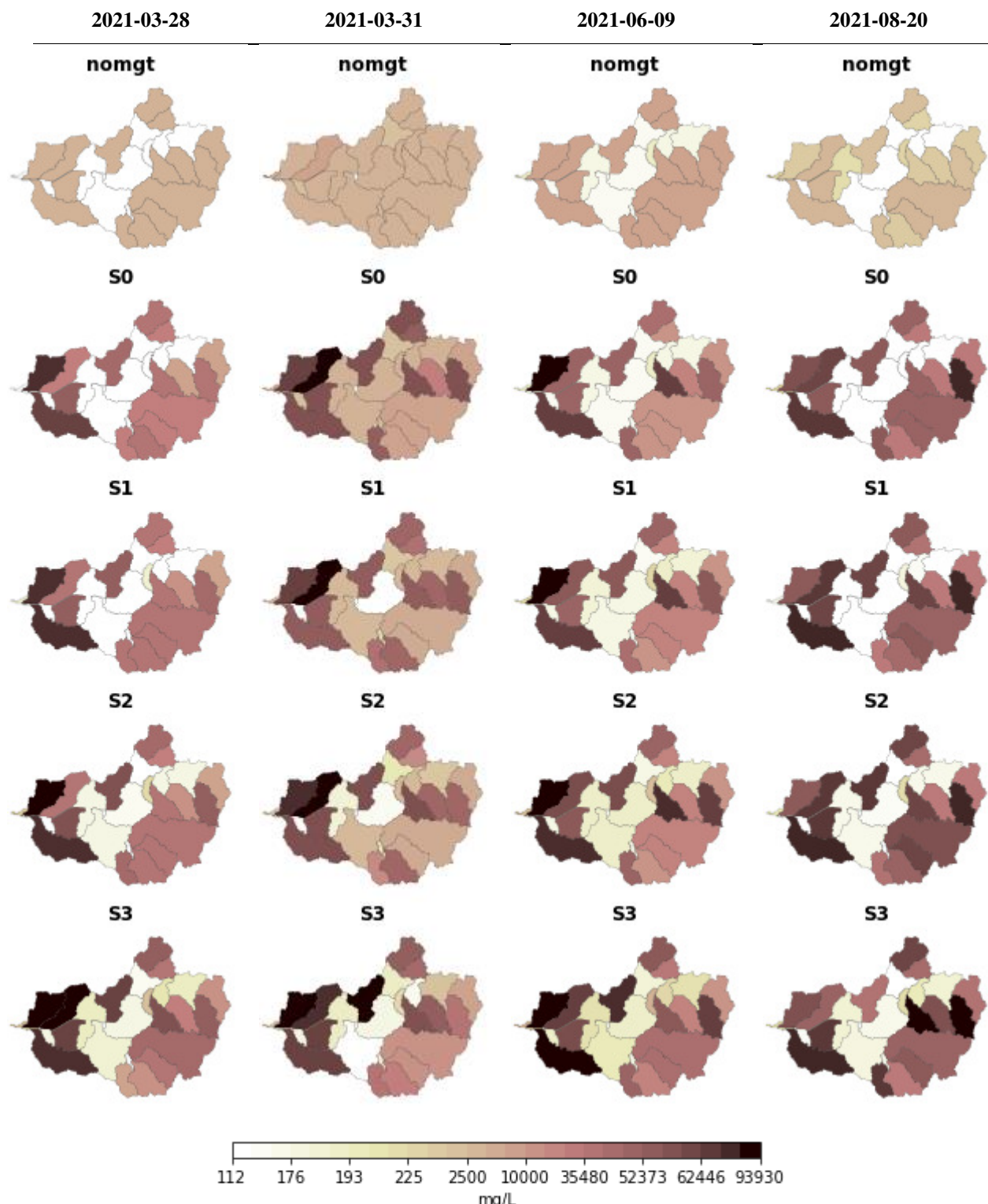


**Figure 21.** Distribution of suspended sediment concentration in reaches caused by extreme rainfalls on March 28<sup>th</sup>, March 31<sup>st</sup>, June 9<sup>th</sup>, and August 20<sup>th</sup> under all scenarios

## **CHAPTER 4**

### **CONCLUSIONS**

Land use change has transformed the Earth more than any other environmental change. On the other hand, changing climate rivals with mounting pressure on environment, ecosystem, hydrological cycle, soil health and communities. There is a need to better understand the combined effects of land use and climate change to identify adaptable practices and to build resilient communities (Ahmadisharaf et al., 2020). Towards that end, we studied the impact of land use and climate change on water balance variables and soil erosion at local scale. In the second chapter we presented a method that integrated future climate and land use projection with a hydrologic model to investigate the water balance under combined effect of climate change and land use change. To address some level of uncertainty with the approach, we used three CMIP5 GCM outputs under two emission scenarios (RCP4.5 and RCP6.0.) The future time period was split in two time period (mid-century and late-century). Calibration and sensitivity analyses were carried out to make sure the hydrologic model output is reliable. Results show increase in temperature and precipitation. Annual maximum and minimum temperature are projected to increase up to 30% especially during summer and winter. Rainfall will also increase by around 11%, however different emission scenarios showed different trend through the simulation period. surface runoff, water yield, and discharge at the two stations were estimated to increase. However, surface runoff changes were the largest. Increases in discharge during summer and fall are more extreme than other seasons. ET has the modest changes and is expected to decrease. This chapter can be helpful as an example for areas that mainly comprised of forest and agricultural cover. Additionally, it can provide information for investigating how future climate data and land use projections could impact hydrological processes in Southeastern watersheds. This region has not been under focus for climate and land use management studies. Moreover, data and results shown here can provide help in sustainable management especially for Native American Reservations located within Upper Choctawhatchee subbasin. The model used here, showed satisfactory performance that can be further used to study best management practices, water quality modelling (NPS and PS pollution)

and also to track extreme weather footprint such as hurricane and tropical storms, and droughts which have been more frequent recently.

In the third chapter, we assessed the response of a small watershed on topsoil loss under combined effects of land use and climate change. We showed that resolution of rainfall data is crucial in studying the soil loss. Our results indicate pasture management by itself can exacerbate soil loss; and if accompanied with extreme rainfalls, soil loss accelerates impacting different subbasins each time. We found that spatial heterogeneity can be more significant in individual extreme rainfalls, however, over a year, soil moisture and type of the management practices (grazing and farming) could contribute more to topsoil loss. We classified the subbasins into different classes of soil loss severity and then determined the hotspots for soil loss which are: subbasins 15, 16, 23, 9, 10, 11. Soil loss can go as high as 350 (ton/ha/yr) under extreme rainfalls. Adding only the management practices can increase erosion 3600% in subbasin 2. Under S1 with CI of 0.66, subbasins 6, 9, 10, 15, 23, and 27 yield more than 150 ton/ha/yr (extremely severe). Under S2 with CI of 0.69, subbasins 1, 13, 16, 22 also fall into extremely severe category yielding approximately 200 ton/ha/yr. Under S3 with CI 0.73, subbasins 2, 5, 8, 11, 12, 17, 20, 21, 24 also are in Extremely severe class yielding more than 200 ton/ha/yr. We found that in hotspots, up to 10% increase in CI can increase soil loss up to 75% in annual SYLD. single ER can generate up to 35% of annual soil loss. Under one ER event hotspot subbasins can lose up to 160 ton/ha/day (subbasin 15). The results reveal that adding grazing and farming (S0) under one ER event can increase soil loss by 95%; 32% and 80% increase in rainfall amount in one ER event can increase soil loss by 94% and 285% respectively. Our results suggest the importance of site-specific managements to mitigate the soil loss and all the consequences. It is essential to consider the varying sensitivity of subbasins for the sustainability of the agricultural landscapes. our study can help in better soil loss management implementation. Insights of our study may also help in water quality control and flood mitigation planning efforts. This study can be applied in agro-ecosystem resiliency research and BMP implementation decision making, as well as flood mitigation and water quality planning. Sediment process studies also offer understanding of microplastic processes in aquatic environments (Horton & Dixon, 2018; Waldschläger et al., 2022).

This study is not free of limitations. In the study of water balance variables, we used three models to present future projections. Although, we made sure they would be representative of the

region, more models would ensure less uncertainties. Another limitation is that we applied land use based on only SSP5 scenarios. Using other SSP scenarios are potential area of future research. A further limitation of this study is that land use change projections can impact on the simulated hydrological outputs. In the study of soil loss simulation, also, limitations exist. One of the limitations is the use of a single empirical model to simulate soil loss. An ensemble modeling approach is recommended to assess the model-induced uncertainty (Ahmadisharaf et al., 2020; Huisman et al., 2009; Sharifi et al., 2017).

## APPENDIX A

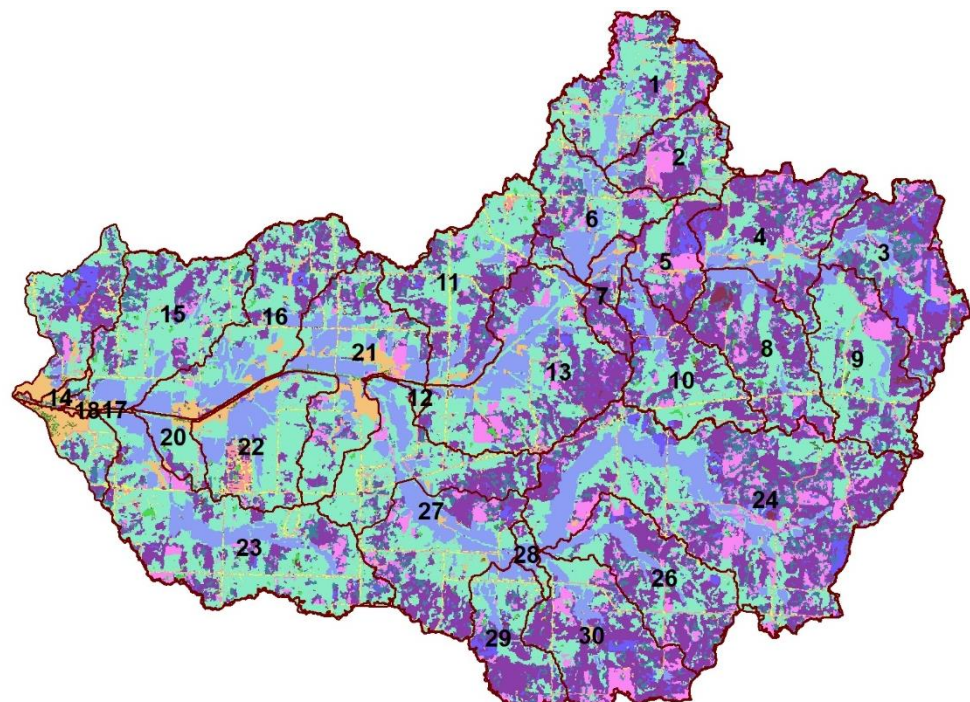
### SUPPORTING INFORMATION FOR CHAPTER 3

Land use, soil, and elevation data (Digital Elevation Model (DEM)) are in a gridded format. For soil both State Soil Geographic Database (STATSGO) and gridded Soil Survey Geographic Databases (gSSURGO) were used through gNATSGO (gridded National Soil Survey Geographic Databases) (SoilSurvey, 2021b). It was derived from United States Department of Agriculture (USDA) (Winchell et al., 2013). Since gNATSGO combine gSSURGO and STATSGO and includes greater detail and better performance (SoilSurvey, 2021a). HCW soil map has more than 50 soil classes (figure1, 2). The elevation and land use data sets were derived from US Geological Survey (USGS) and Multi-Resolution Land Characteristics (MRLC) Consortiums, respectively. The Digital Elevation Model (DEM) of 1/3 arc-second (approximately 10m resolution for the study area) was used. It is a 3DEP (3D Elevation Program) map (U.S.GeologicalSurvey, 2017).The data extent is  $1 \times 1$  degree. The land use data set is NLCD2019 in 30 m resolution (L. Yang et al., 2018), and the corresponding 2001–2006 lookup table was used.

**Table 16.** Soil and Water Assessment Tool (SWAT) Input Data.

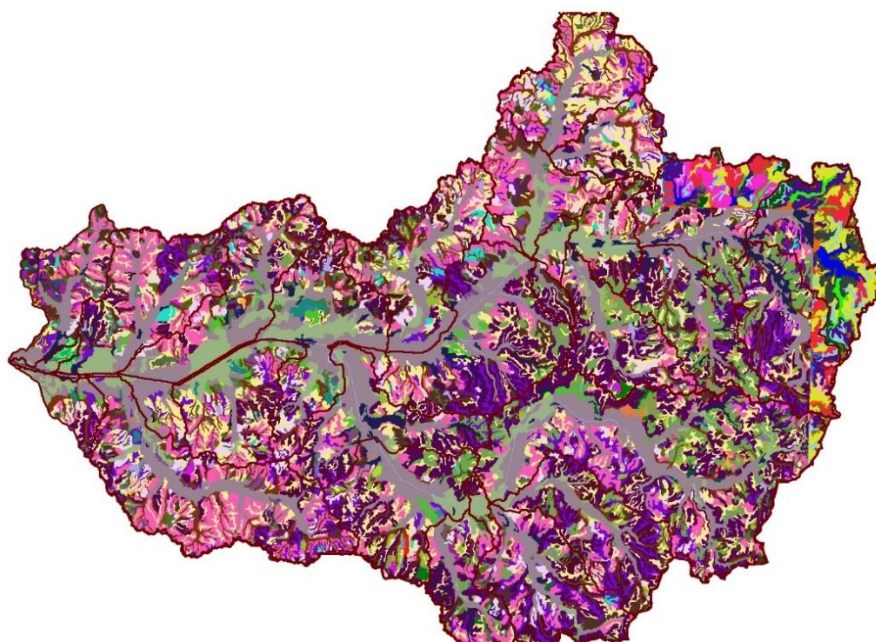
Data Type	Description	Available Source	Spatial Resolution
Soil	gNATSGO: US gridded soil map	<a href="#">Geospatial Data Gate</a>	10 m × 10 m
Elevation	3DEP-DEM 1/3 arcsecond	<a href="#">The National Map</a>	10 m × 10 m
Land Cover	NLCD2019	<a href="#">Multi-Resolution Land Characteristics (MRLC) Consortium</a>	30 m × 30 m
Observed water discharge	Discharge, cubic feet per second (Mean)	<a href="#">National Water Information System</a>	Daily
Observed sediment discharge	Sediment Load, short tons per day (Mean)	<a href="#">National Water Dashboard</a>	Daily
Observed suspended sediment	Suspended sediment concentration, milligram per liter (Mean)	<a href="#">National Water Dashboard</a>	Daily
In-situ climate data	Daily measured rainfall and temperature.	<a href="#">National Center for Environmental Information</a>	Daily
Weather Radar data	NEXRAD (MRMS, Stage IV QPE)	<a href="#">National Center for Environmental Information</a>	5 min/24h

(a)



Woody Wetlands	Forest Mixed	Evergreen Forest	Developed, Medium Intensity	Forest-Deciduous
Shrub/Scrub	Herbaceous	Herbaceous Wetlands	Developed, Low Intensity	Cultivated Crop
Open Water	Hay/Pasture	Developed	Developed, High Intensity	Barren Land

(b)



MUKEY	1602290	568271	568282	568298	568563	568571	568576	568581	568587	568593	568601	
	1018779	568265	568273	568283	568300	568564	568572	568577	568582	568588	568595	568604
	1456912	568266	568274	568284	568559	568565	568573	568578	568583	568590	568598	
	1602281	568269	568275	568289	568561	568569	568574	568577	568579	568585	568591	568599
	568270	568276	568294	568562	568570	568575	568580	568586	568592	568600		

**Figure 22.** (a) Land use map. (b) soil map

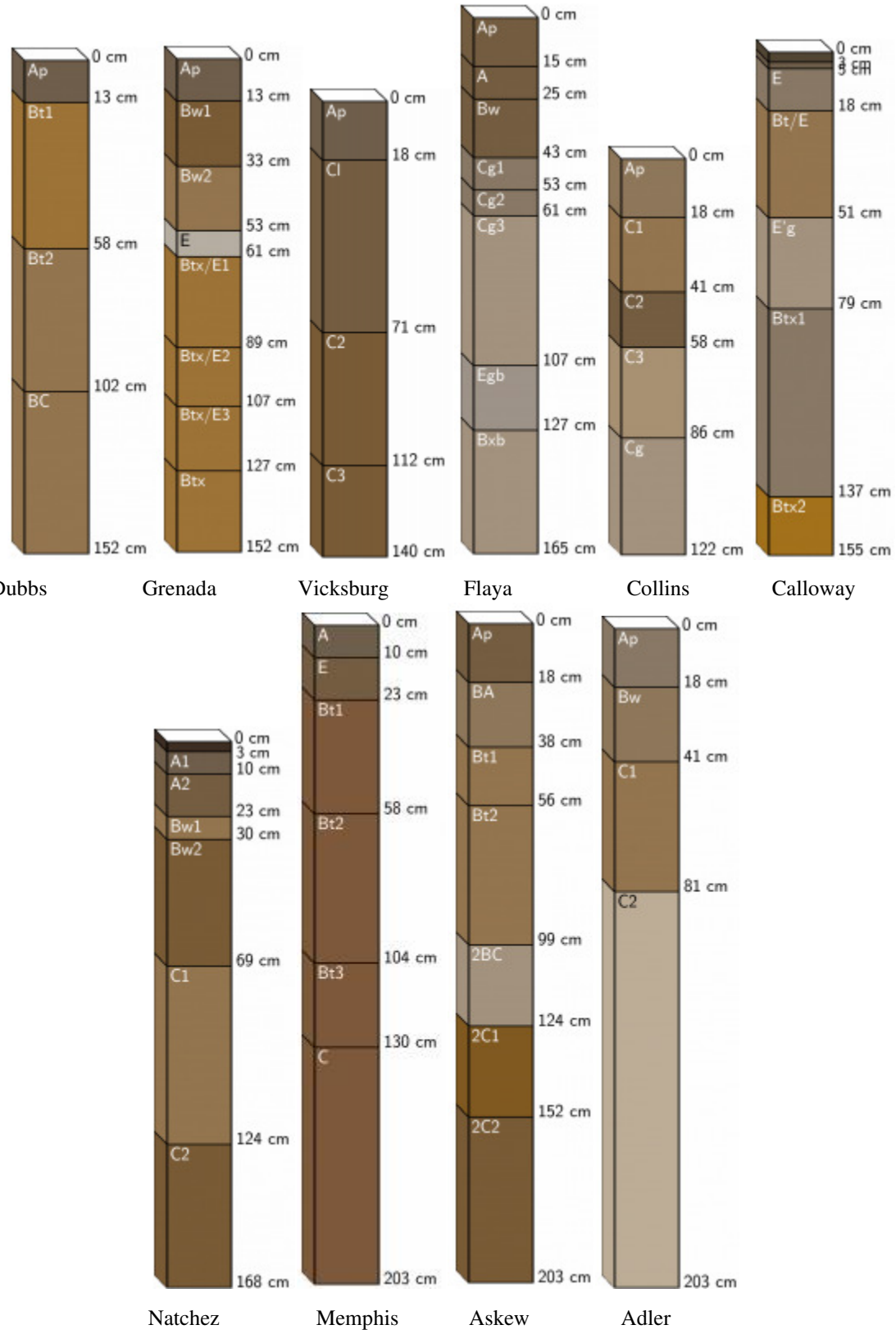


**Figure 23.** Main soil types and associated horizons

For accuracy quantification of the model, our objective function includes Nash–Sutcliffe efficiency (NSE), Percent Bias (PBAIS), and RMSE-observations standard deviation ratio (RSR) (Gupta et al., 1999; Legates & McCabe Jr, 1999; D. N. Moriasi et al., 2007; Nash & Sutcliffe, 1970). Following are the equations used in model performance evaluation.

$$\text{NSE} = 1 - \left[ \frac{\sum_{i=1}^n (Y_i^{obs} - Y_i^{sim})^2}{\sum_{i=1}^n (Y_i^{obs} - Y^{mean})^2} \right], \quad -\infty < \text{NSE} \leq 1 \quad (1)$$

$$\text{PBAIS} = \left[ \frac{\sum_{i=1}^n (Y_i^{obs} - Y_i^{sim}) \times (100)}{\sum_{i=1}^n (Y_i^{obs})} \right], \quad -\infty < \text{PBAIS} < +\infty \quad (2)$$

$$\text{RSR} = \frac{\left[ \sqrt{\sum_{i=1}^n (Y_i^{obs} - Y_i^{sim})^2} \right]}{\left[ \sqrt{\sum_{i=1}^n (Y_i^{obs} - Y^{mean})^2} \right]}, \quad 0 \leq \text{RSR} < +\infty \quad (3)$$

where  $Y_i^{obs}$  is the  $i$ th measured stream flow;  $Y_i^{sim}$  is  $i$ th simulated stream flow;  $Y^{mean}$  is the mean of observed stream flow data;  $Y^{simmean}$  is the mean of simulated data, and  $n$  the total number of observations.

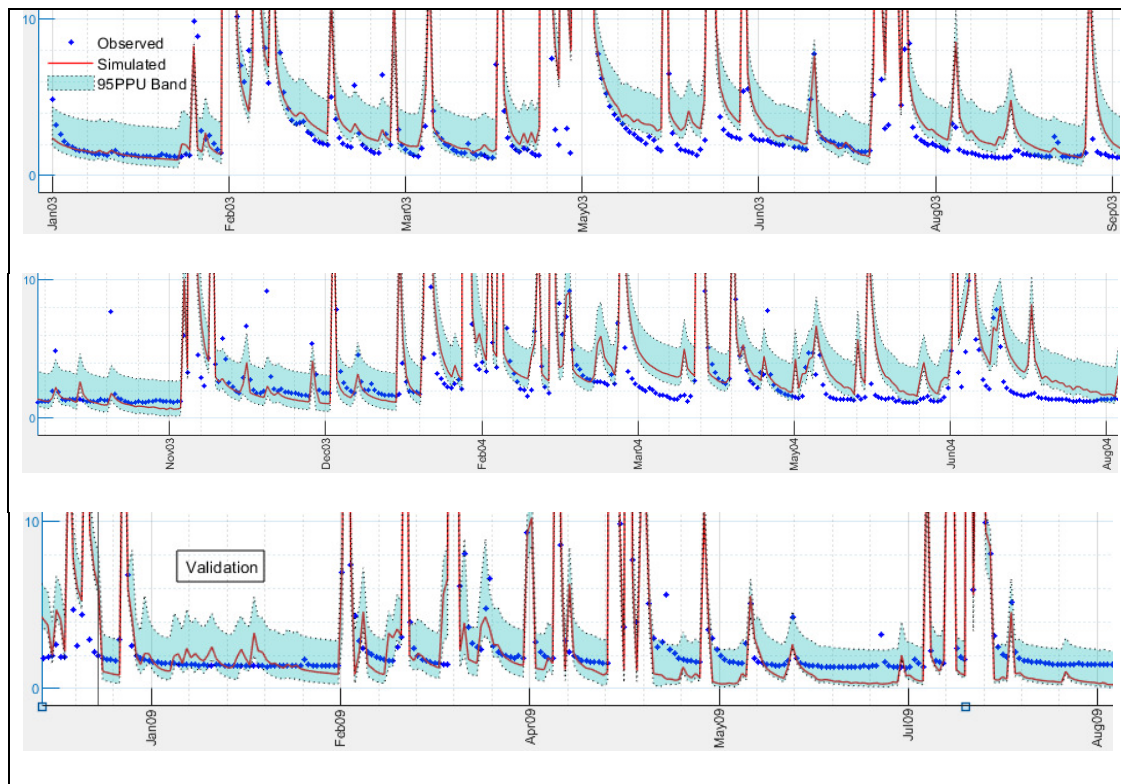


**Figure 24.** Calibration and validation result for days no or less amount of rainfall.

**Table 17.** Sensitive Parameters

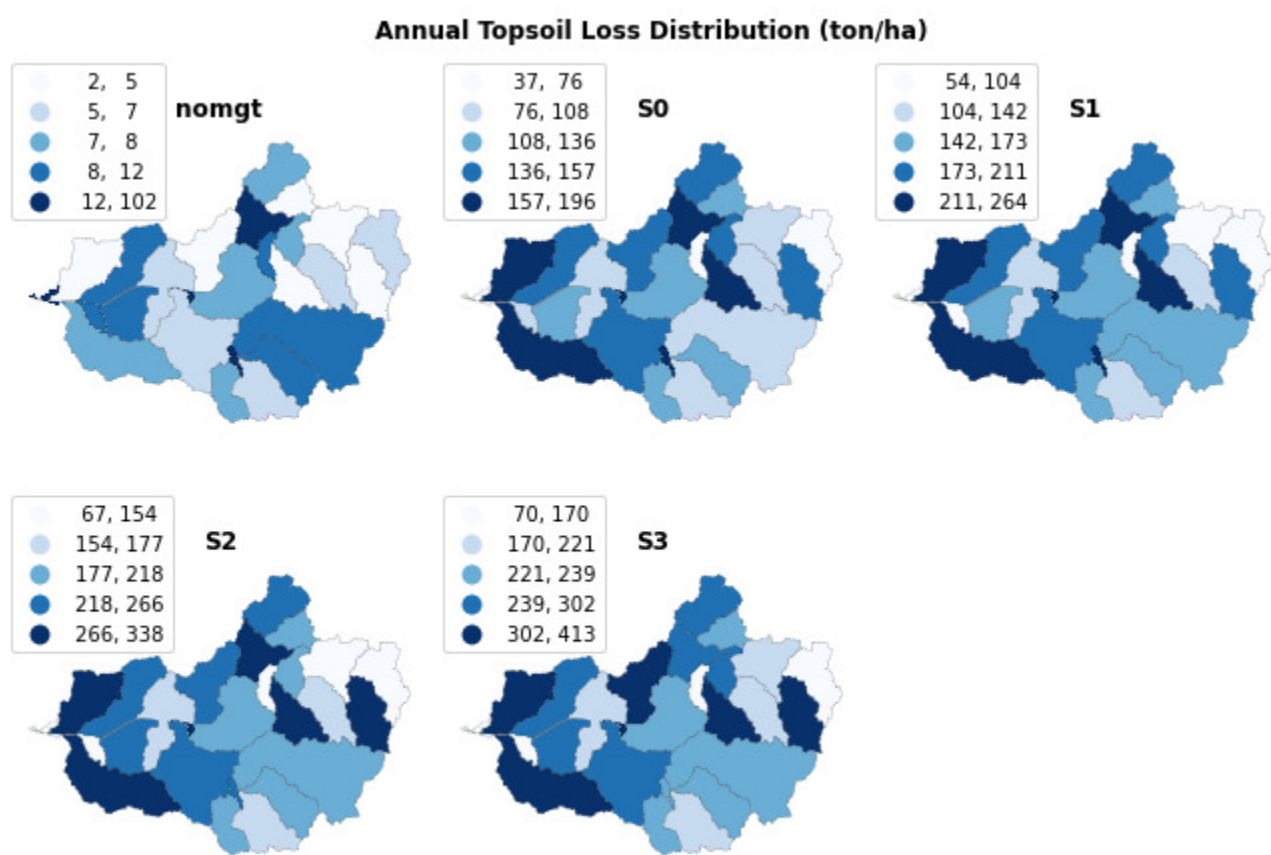
	Name	description	method	Max	min	Input file
Streamflow	CNOP	CN2 SCS runoff curve number for moisture condition II	r	0.07	0.12	.mgt
	SOL_AWC	Available water capacity of the soil layer	r	0.17	0.32	.sol
	SLUSUBBSN	Saturated hydraulic conductivity	r	-0.32	-0.52	.hru
	ESCO	Soil evaporation compensation factor	v	0.65	0.82	.hru
	GWQMN	Threshold depth of water in the shallow aquifer required for return flow to occur	v	973	1112	.gw
	REVAPMN	Threshold dept. of shallow aquifers for evaporation/deep aquifer percolation	v	729	815	.gw
	RCHRG_DP	Deep aquifer percolation fraction	v	0.28	0.39	.gw
	CH_K1	Effective hydraulic conductivity in tributary channel	v	8	17	.sub
	CH_K2	Effective hydraulic conductivity in main channel alluvium	v	1	5	.rte
	CANMX	Maximum canopy storage	v	1	3	.hru
Sediment	ALPHA_BF	Baseflow recession constant	v	0.051	0.059	.gw
	ALPHA_BF_D	Baseflow recession constant for deep aquifer	v	0.014	0.025	.gw
	SPCON	Linear parameter for calculating the channel sediment routing	v	0.0008	0.0011	.bsn
	SPEXP	Exponent parameter for calculating the channel sediment routing	v	0.71	0.92	.bsn
	PRF	peak rate adjustment factor for sediment routing in the main channel	v	0.98	1.21	.bsn

**Table 17** -continued

Name	description	method	Max	min	Input file
ADJ_PKR	Peak rate adjustment factor for sediment routing in the subbasin (tributary channels)	v	1.32	1.74	.bsn
USLE_K	USLE equation soil erodibility (K) factor	v	0.46	0.61	.sol
SOL_ROCK	rock percentage in the first soil layer	r	0.59	0.96	.sol
USLE_P	support practice factor	v	0.33	0.44	.mgt
USLE_C {12}	cover and management effect- PASTURE	v	0.26	0.32	.plant
USLE_C {7}	cover and management effect- FRSD	V	0.03	0.1	.plant
USLE_C {2}	cover and management effect- AGRR	V	0.06	0.14	.plant
USLE_C {19}	cover and management effect- CORN	V	0.08	0.19	.plant
USLE_C {59}	cover and management effect- SOYBEAN	V	0.14	0.18	.plant
USLE_C {16}	cover and management effect- RNGB	V	0.07	0.12	.plant
BIO_EAT	Dry weight of biomass consumed daily	v	5	7.1	.mgt
BIO_TRMP	Dry weight of biomass consumed daily	v	5.8	7.7	.mgt
MANURE_K G	Dry weight of manure deposited daily	v	5.2	6.2	.mgt
CH_COV1	Channel erodibility factor	V	0.48	0.56	.rte
CH_COV2	Channel cover factor	V	0.4	0.49	.rte

**Table 18.** Water Balance Ratios

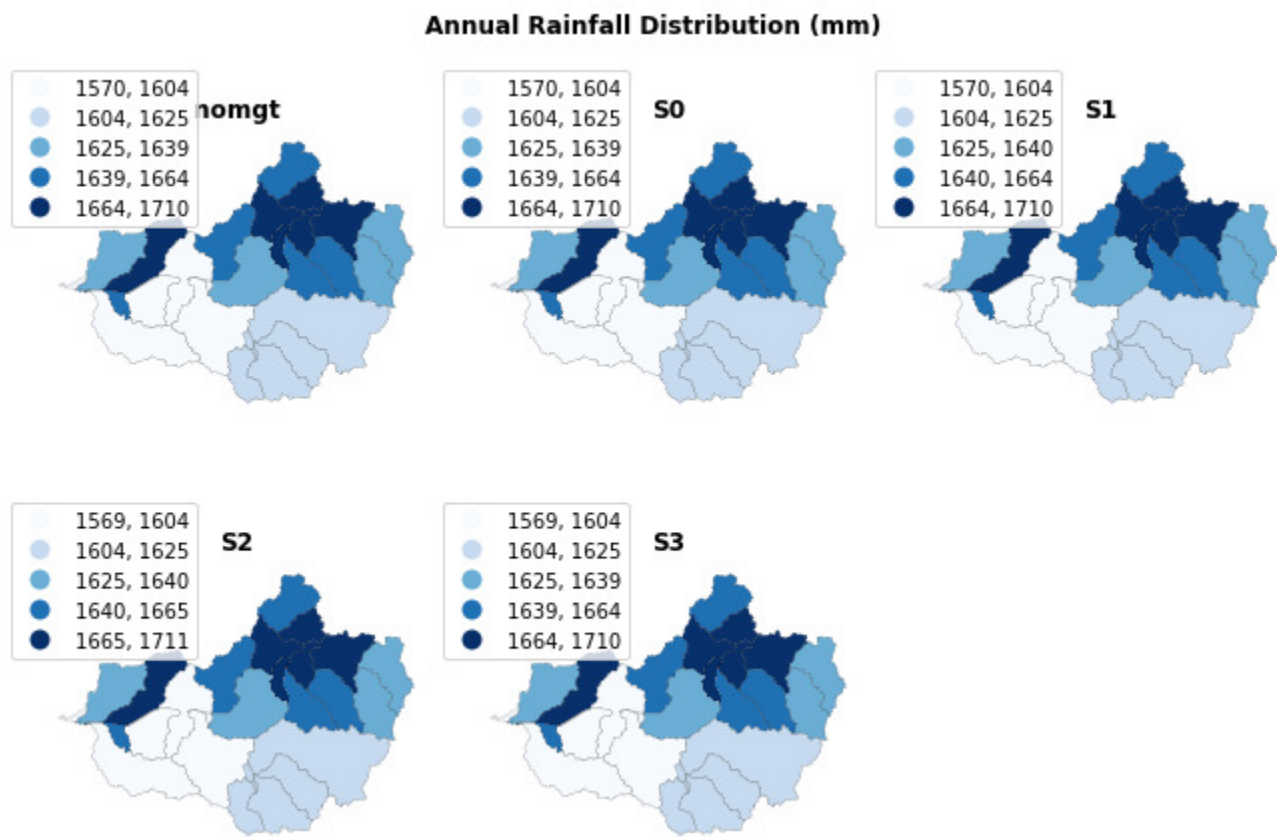
Variable ratio	Ratio
Streamflow/Precipitation	0.17
Baseflow/Total Flow	0.48
Surface Runoff/ Total Flow	0.52
Percolation / Precipitation	0.25
Deep Recharge/ Precipitation	0.1
Evapotranspiration/ Precipitation	0.64



**Figure 25.** Annual sediment loss distribution

**Table 19.** Topsoil loss classification

Class	Class (metric ton/ha)	Description
1	< 10	Low
2	10 to 40 ton/ha	Moderate
3	40 to 90 ton/ha	High
4	90 to 150	Severe
5	>150	Extremely Severe

**Figure 26.** Annual rainfall distribution

## REFERENCES

- Abbaspour, K. (2015). SWAT Calibration and Uncertainty Programs—A User Manual. *Swiss Federal Institute of Aquatic Science and Technology: Eawag, Switzerland.*
- Abbaspour, K. C., Johnson, C., & Van Genuchten, M. T. (2004). Estimating uncertain flow and transport parameters using a sequential uncertainty fitting procedure. *Vadose Zone Journal*, 3(4), 1340-1352.
- Abbaspour, K. C., Rouholahnejad, E., Vaghefi, S., Srinivasan, R., Yang, H., & Kløve, B. (2015). A continental-scale hydrology and water quality model for Europe: Calibration and uncertainty of a high-resolution large-scale SWAT model. *Journal of Hydrology*, 524, 733-752.
- Abbaspour, K. C., Vejdani, M., Haghishat, S., & Yang, J. (2007). *SWAT-CUP calibration and uncertainty programs for SWAT*. Paper presented at the MODSIM 2007 international congress on modelling and simulation, modelling and simulation society of Australia and New Zealand.
- Abbaspour, K. C., Yang, J., Maximov, I., Siber, R., Bogner, K., Mieleitner, J., . . . Srinivasan, R. (2007). Modelling hydrology and water quality in the pre-alpine/alpine Thur watershed using SWAT. *Journal of Hydrology*, 333(2-4), 413-430.
- Abolverdi, J., Ferdosifar, G., Khalili, D., & Kamgar-Haghghi, A. A. (2016). Spatial and temporal changes of precipitation concentration in Fars province, southwestern Iran. *Meteorology and Atmospheric Physics*, 128(2), 181-196.
- Adimassu, Z., Tamene, L., & Degefe, D. T. (2020). The influence of grazing and cultivation on runoff, soil erosion, and soil nutrient export in the central highlands of Ethiopia. *Ecological Processes*, 9(1), 1-11.
- Admas, B. F., Gashaw, T., Adem, A. A., Worqlul, A. W., Dile, Y. T., & Molla, E. (2022). Identification of soil erosion hot-spot areas for prioritization of conservation measures using the SWAT model in Ribb watershed, Ethiopia. *Resources, Environment and Sustainability*, 100059.
- Agency, U. S. E. E. P. (2017). *Updates To The Demographic And Spatial Allocation Models To Produce Integrated Climate And Land Use Scenarios (ICLUS) (Final Report, Version 2)*. Retrieved from
- Aghsaei, H., Dinan, N. M., Moridi, A., Asadolahi, Z., Delavar, M., Fohrer, N., & Wagner, P. D. (2020). Effects of dynamic land use/land cover change on water resources and sediment yield in the Anzali wetland catchment, Gilan, Iran. *Science of the total environment*, 712, 136449.

- Ahmadisharaf, E., Lacher, I. L., Fergus, C., Benham, B. L., Akre, T., & Kline, K. S. (2020). Projecting land use change impacts on nutrients, sediment and runoff in multiple spatial scales: Business-as-usual vs. stakeholder-informed scenarios. *Journal of Cleaner Production*, 257, 120466.
- Alamdari, N., Claggett, P., Sample, D. J., Easton, Z. M., & Yazdi, M. N. (2022). Evaluating the joint effects of climate and land use change on runoff and pollutant loading in a rapidly developing watershed. *Journal of Cleaner Production*, 330, 129953.
- Aleweli, C., Borrelli, P., Meusburger, K., & Panagos, P. (2019). Using the USLE: Chances, challenges and limitations of soil erosion modelling. *International Soil and Water Conservation Research*, 7(3), 203-225.
- Alexander, L. V., Bador, M., Roca, R., Contractor, S., Donat, M. G., & Nguyen, P. L. (2020). Intercomparison of annual precipitation indices and extremes over global land areas from in situ, space-based and reanalysis products. *Environmental Research Letters*, 15(5), 055002.
- Alexander, R. B., Schwarz, G. E., & Smith, R. A. (1997). *Regional transport of point and nonpoint-source nitrogen to the gulf of Mexico*: Gulf of Mexico Program Office.
- Allen, R. G. (1986). A Penman for all seasons. *Journal of Irrigation and Drainage Engineering*, 112(4), 348-368.
- Allen, R. G., Jensen, M. E., Wright, J. L., & Burman, R. D. (1989). Operational estimates of reference evapotranspiration. *Agronomy journal*, 81(4), 650-662.
- Allen, R. G., Pereira, L. S., Raes, D., & Smith, M. (1998). Crop evapotranspiration-Guidelines for computing crop water requirements-FAO Irrigation and drainage paper 56. *Fao, Rome*, 300(9), D05109.
- Andersson, J. C., Zehnder, A. J., Wehrli, B., & Yang, H. (2012). Improved SWAT Model Performance With Time-Dynamic Voronoi Tessellation of Climatic Input Data in Southern Africa 1. *JAWRA Journal of the American Water Resources Association*, 48(3), 480-493.
- Arnell, N. W., & Gosling, S. N. (2013). The impacts of climate change on river flow regimes at the global scale. *Journal of Hydrology*, 486, 351-364.
- Arnold, J. (1994). SWAT-soil and water assessment tool.
- Arnold, J., Kiniry, J., Srinivasan, R., Williams, J., Haney, E., & Neitsch, S. (2011). Soil and Water Assessment Tool input/output file documentation: Version 2009. *Texas Water Resources Institute Technical Report*, 365.
- Arnold, J., Kiniry, J., Srinivasan, R., Williams, J., Haney, E., & Neitsch, S. (2013). *SWAT 2012 input/output documentation*. Retrieved from

- Arnold, J. G., & Fohrer, N. (2005). SWAT2000: current capabilities and research opportunities in applied watershed modelling. *Hydrological Processes: An International Journal*, 19(3), 563-572.
- Arnold, J. G., Moriasi, D. N., Gassman, P. W., Abbaspour, K. C., White, M. J., Srinivasan, R., . . . Van Liew, M. W. (2012). SWAT: Model use, calibration, and validation. *Transactions of the ASABE*, 55(4), 1491-1508.
- Arnold, J. G., Srinivasan, R., Muttiah, R. S., & Williams, J. R. (1998). Large area hydrologic modeling and assessment part I: model development 1. *JAWRA Journal of the American Water Resources Association*, 34(1), 73-89.
- Arnold, J. G., Williams, J. R., & Maidment, D. R. (1995). Continuous-time water and sediment-routing model for large basins. *Journal of Hydraulic engineering*, 121(2), 171-183.
- ASABE, A. S. o. A. a. B. E. (Jun. 2017). Guidelines for Calibrating, Validating, and Evaluating Hydrologic and Water Quality (H/WQ) Models. In. 2950 Niles Road, St. Joseph, MI, US.
- ASAE, A. (2005). Manure production and characteristics. *American Society of Agricultural and Biological Engineers St Joseph*.
- Bagnold, R. (1977). Bed load transport by natural rivers. *Water Resources Research*, 13(2), 303-312.
- Baronas, J. J., Stevenson, E. I., Hackney, C. R., Darby, S. E., Bickle, M. J., Hilton, R. G., . . . Tipper, E. T. (2020). Integrating suspended sediment flux in large alluvial river channels: Application of a synoptic Rouse-based model to the Irrawaddy and Salween rivers. *Journal of Geophysical Research: Earth Surface*, 125(9), e2020JF005554.
- Biedenham, D. S., Watson, C. C., Smith, J. B., & Hubbard, L. C. (2004). Application of a regional sediment approach to Hickahala Creek watershed, Northern Mississippi.
- Bierwagen, B. G., Theobald, D. M., Pyke, C. R., Choate, A., Groth, P., Thomas, J. V., & Morefield, P. (2010). National housing and impervious surface scenarios for integrated climate impact assessments. *Proceedings of the National Academy of Sciences*, 107(49), 20887-20892.
- Borrelli, P., Alewell, C., Alvarez, P., Anache, J. A. A., Baartman, J., Ballabio, C., . . . Chalise, D. (2021). Soil erosion modelling: A global review and statistical analysis. *Science of the total environment*, 780, 146494.
- Borrelli, P., Robinson, D. A., Fleischer, L. R., Lugato, E., Ballabio, C., Alewell, C., . . . Ferro, V. (2017). An assessment of the global impact of 21st century land use change on soil erosion. *Nature communications*, 8(1), 1-13.
- Bouma, J., & Bates, N. (2000). Trends of world-wide soil degradation. In *Bodenschutz* (pp. 33-43): [sn].

- Briak, H., Mrabet, R., Moussadek, R., & Aboumaria, K. (2019). Use of a calibrated SWAT model to evaluate the effects of agricultural BMPs on sediments of the Kalaya river basin (North of Morocco). *International Soil and Water Conservation Research*, 7(2), 176-183.
- Brooks, C. E. P., & Carruthers, N. (1953). Handbook of statistical methods in meteorology. *Handbook of statistical methods in meteorology*.
- Bureau of Reclamation, C. A. G., Climate Central, Lawrence Livermore National Laboratory, Santa Clara University, Scripps Institution of Oceanography, U.S. Army Corps of Engineers, U.S. Geological Survey. (2013). Downscaled CMIP3 and CMIP5 Climate and Hydrology Projections. Retrieved from <https://gdo-dcp.ucar.edu/>. Retrieved 30 Nov. 2019 <https://gdo-dcp.ucar.edu/>
- Cao, P., Lu, C., & Yu, Z. (2018). Historical nitrogen fertilizer use in agricultural ecosystems of the contiguous United States during 1850–2015: application rate, timing, and fertilizer types. *Earth System Science Data*, 10(2), 969-984.
- Carter, L. M., Jones, J. W., Berry, L., Burkett, V., Murley, J. F., Obeysekera, J., . . . Wear, D. (2014). *Southeast and the Caribbean*. Retrieved from
- Cecílio, R. A., Pimentel, S. M., & Zanetti, S. S. (2019). Modeling the influence of forest cover on streamflows by different approaches. *Catena*, 178, 49-58.
- Cerdan, O., Govers, G., Le Bissonnais, Y., Van Oost, K., Poesen, J., Saby, N., . . . Auerswald, K. (2010). Rates and spatial variations of soil erosion in Europe: a study based on erosion plot data. *Geomorphology*, 122(1-2), 167-177.
- Chanapathi, T., Thatikonda, S., & Raghavan, S. (2018). Analysis of rainfall extremes and water yield of Krishna river basin under future climate scenarios. *Journal of Hydrology: Regional Studies*, 19, 287-306.
- Chaplot, V. (2005). Impact of DEM mesh size and soil map scale on SWAT runoff, sediment, and NO<sub>3</sub>-N loads predictions. *Journal of Hydrology*, 312(1-4), 207-222.
- Chen, J., Brissette, F. P., Poulin, A., & Leconte, R. (2011). Overall uncertainty study of the hydrological impacts of climate change for a Canadian watershed. *Water Resources Research*, 47(12).
- Chen, L., Sela, S., Svoray, T., & Assouline, S. (2016). Scale dependence of Hortonian rainfall-runoff processes in a semiarid environment. *Water Resources Research*, 52(7), 5149-5166.
- Chen, Q., Chen, H., Wang, J., Zhao, Y., Chen, J., & Xu, C. (2019). Impacts of Climate Change and Land-Use Change on Hydrological Extremes in the Jinsha River Basin. *Water*, 11(7), 1398.

- Chen, T., Niu, R.-q., Li, P.-x., Zhang, L.-p., & Du, B. (2011). Regional soil erosion risk mapping using RUSLE, GIS, and remote sensing: a case study in Miyun Watershed, North China. *Environmental Earth Sciences*, 63(3), 533-541.
- Chen, W., Chen, C., Li, L., Xing, L., Huang, G., & Wu, C. (2015). Spatiotemporal analysis of extreme hourly precipitation patterns in Hainan Island, South China. *Water*, 7(5), 2239-2253.
- Chen, Y., Ale, S., Rajan, N., & Srinivasan, R. (2017). Modeling the effects of land use change from cotton (*Gossypium hirsutum* L.) to perennial bioenergy grasses on watershed hydrology and water quality under changing climate. *Agricultural Water Management*, 192, 198-208.
- Chen, Y., Marek, G. W., Marek, T. H., Brauer, D. K., & Srinivasan, R. (2017). Assessing the efficacy of the SWAT auto-irrigation function to simulate irrigation, evapotranspiration, and crop response to management strategies of the Texas High Plains. *Water*, 9(7), 509.
- Chen, Y., Marek, G. W., Marek, T. H., Brauer, D. K., & Srinivasan, R. (2018). Improving SWAT auto-irrigation functions for simulating agricultural irrigation management using long-term lysimeter field data. *Environmental Modelling & Software*, 99, 25-38.
- Chen, Y., Marek, G. W., Marek, T. H., Moorhead, J. E., Heflin, K. R., Brauer, D. K., . . . Srinivasan, R. (2019). Simulating the impacts of climate change on hydrology and crop production in the Northern High Plains of Texas using an improved SWAT model. *Agricultural Water Management*, 221, 13-24.
- Chiang, L., Chaubey, I., Gitau, M. W., & Arnold, J. G. (2010). Differentiating impacts of land use changes from pasture management in a CEAP watershed using the SWAT model. *Transactions of the ASABE*, 53(5), 1569-1584.
- Cho, J., Bosch, D., Lowrance, R., Strickland, T., & Vellidis, G. (2009). Effect of spatial distribution of rainfall on temporal and spatial uncertainty of SWAT output. *Transactions of the ASABE*, 52(5), 1545-1556.
- Christensen, J. H., & Christensen, O. B. (2007). A summary of the PRUDENCE model projections of changes in European climate by the end of this century. *Climatic change*, 81(1), 7-30.
- Cisneros, J., BE, T. O., Arnell, N. W., Benito, G., Cogley, J. G., Döll, P., . . . Gerten, D. (2014). Freshwater resources. In.
- Clarke, L., Edmonds, J., Jacoby, H., Pitcher, H., Reilly, J., & Richels, R. (2007). Scenarios of greenhouse gas emissions and atmospheric concentrations.
- Coscarelli, R. a., & Caloiero, T. (2012). Analysis of daily and monthly rainfall concentration in Southern Italy (Calabria region). *Journal of Hydrology*, 416, 145-156.

- Crum, T. D., & Albert, R. L. (1993). The WSR-88D and the WSR-88D operational support facility. *Bulletin of the American Meteorological Society*, 74(9), 1669-1688.
- De Luís, M. n., García-Cano, M. F., Cortina, J., Raventós, J., González-Hidalgo, J. C., & Sánchez, J. R. (2001). Climatic trends, disturbances and short-term vegetation dynamics in a Mediterranean shrubland. *Forest ecology and management*, 147(1), 25-37.
- de Oliveira Serrão, E. A., Silva, M. T., Ferreira, T. R., de Ataide, L. C. P., dos Santos, C. A., de Lima, A. M. M., . . . Gomes, D. J. C. (2022). Impacts of land use and land cover changes on hydrological processes and sediment yield determined using the SWAT model. *International Journal of Sediment Research*, 37(1), 54-69.
- De Vente, J., & Poesen, J. (2005). Predicting soil erosion and sediment yield at the basin scale: scale issues and semi-quantitative models. *Earth-science reviews*, 71(1-2), 95-125.
- Deb, P., & Kiem, A. S. (2020). Evaluation of rainfall-runoff model performance under non-stationary hydroclimatic conditions. *Hydrological Sciences Journal*, 1-18.
- Deb, P., Kiem, A. S., & Willgoose, G. (2019). A linked surface water-groundwater modelling approach to more realistically simulate rainfall-runoff non-stationarity in semi-arid regions. *Journal of hydrology*, 575, 273-291.
- Dewitz, J., and U.S. Geological Survey. (2021). *National Land Cover Database (NLCD) 2019 Products* (ver. 2.0, June 2021). Retrieved from: <https://doi.org/10.5066/P9KZCM54>
- Diffenbaugh, N. S., Scherer, M., & Trapp, R. J. (2013). Robust increases in severe thunderstorm environments in response to greenhouse forcing. *Proceedings of the National Academy of Sciences*, 110(41), 16361-16366.
- Diffenbaugh, N. S., Swain, D. L., & Touma, D. (2015). Anthropogenic warming has increased drought risk in California. *Proceedings of the National Academy of Sciences*, 112(13), 3931-3936.
- Dile, Y. T., & Srinivasan, R. (2014). Evaluation of CFSR climate data for hydrologic prediction in data-scarce watersheds: an application in the Blue Nile River Basin. *JAWRA Journal of the American Water Resources Association*, 50(5), 1226-1241.
- Donner, L. J., Wyman, B. L., Hemler, R. S., Horowitz, L. W., Ming, Y., Zhao, M., . . . Schwarzkopf, M. D. (2011). The dynamical core, physical parameterizations, and basic simulation characteristics of the atmospheric component AM3 of the GFDL global coupled model CM3. *Journal of Climate*, 24(13), 3484-3519.
- Donner, S. D., & Scavia, D. (2007). How climate controls the flux of nitrogen by the Mississippi River and the development of hypoxia in the Gulf of Mexico. *Limnology and oceanography*, 52(2), 856-861.

- Dougherty, E., & Rasmussen, K. L. (2021). Variations in flash flood-producing storm characteristics associated with changes in vertical velocity in a future climate in the Mississippi River basin. *Journal of Hydrometeorology*, 22(3), 671-687.
- Durrans, S. R., Julian, L. T., & Yekta, M. (2002). Estimation of depth-area relationships using radar-rainfall data. *Journal of Hydrologic Engineering*, 7(5), 356-367.
- Duru, U., Arabi, M., & Wohl, E. E. (2018). Modeling stream flow and sediment yield using the SWAT model: a case study of Ankara River basin, Turkey. *Physical Geography*, 39(3), 264-289.
- Dutta, S. (2016). Soil erosion, sediment yield and sedimentation of reservoir: a review. *Modeling Earth Systems and Environment*, 2(3), 123. doi:10.1007/s40808-016-0182-y
- Dutta, S., & Sen, D. (2018). Application of SWAT model for predicting soil erosion and sediment yield. *Sustainable Water Resources Management*, 4(3), 447-468.
- Eldardiry, H., Habib, E., & Zhang, Y. (2015). On the use of radar-based quantitative precipitation estimates for precipitation frequency analysis. *Journal of Hydrology*, 531, 441-453.
- Emanuel, K. A. (2013). Downscaling CMIP5 climate models shows increased tropical cyclone activity over the 21st century. *Proceedings of the National Academy of Sciences*, 110(30), 12219-12224.
- EPA, U.-N. (2022). CTIC (Conservation Technology Information Center) Retrieved from <https://www.ctic.org/>
- Fenta, A. A., Tsunekawa, A., Haregeweyn, N., Tsubo, M., Yasuda, H., Kawai, T., . . . Sultan, D. (2021). Agroecology-based soil erosion assessment for better conservation planning in Ethiopian river basins. *Environmental Research*, 195, 110786.
- Ficklin, D. L., & Barnhart, B. L. (2014). SWAT hydrologic model parameter uncertainty and its implications for hydroclimatic projections in snowmelt-dependent watersheds. *Journal of Hydrology*, 519, 2081-2090.
- Ficklin, D. L., Letsinger, S. L., Stewart, I. T., & Maurer, E. P. (2016). Assessing differences in snowmelt-dependent hydrologic projections using CMIP3 and CMIP5 climate forcing data for the western United States. *Hydrology Research*, 47(2), 483-500.
- Field, C. B., Barros, V., Stocker, T. F., & Dahe, Q. (2012). *Managing the risks of extreme events and disasters to advance climate change adaptation: special report of the intergovernmental panel on climate change*: Cambridge University Press.
- Fischer, E. M., Beyerle, U., & Knutti, R. (2013). Robust spatially aggregated projections of climate extremes. *Nature Climate Change*, 3(12), 1033-1038.

- Fischer, E. M., & Knutti, R. (2014). Detection of spatially aggregated changes in temperature and precipitation extremes. *Geophysical Research Letters*, 41(2), 547-554.
- Fischer, E. M., & Knutti, R. (2016). Observed heavy precipitation increase confirms theory and early models. *Nature Climate Change*, 6(11), 986-991.
- Flanagan, D. C., Gilley, J. E., & Franti, T. G. (2007). Water Erosion Prediction Project (WEPP): Development history, model capabilities, and future enhancements. *Transactions of the ASABE*, 50(5), 1603-1612.
- Flato, G., Marotzke, J., Abiodun, B., Braconnot, P., Chou, S. C., Collins, W., . . . Eyring, V. (2014). Evaluation of climate models. In *Climate change 2013: the physical science basis. Contribution of Working Group I to the Fifth Assessment Report of the Intergovernmental Panel on Climate Change* (pp. 741-866): Cambridge University Press.
- Fowler, H. J., Blenkinsop, S., & Tebaldi, C. (2007). Linking climate change modelling to impacts studies: recent advances in downscaling techniques for hydrological modelling. *International Journal of Climatology: A Journal of the Royal Meteorological Society*, 27(12), 1547-1578.
- Fu, G., Charles, S. P., Chiew, F. H., Teng, J., Zheng, H., Frost, A. J., . . . Kirshner, S. (2013). Modelling runoff with statistically downscaled daily site, gridded and catchment rainfall series. *Journal of Hydrology*, 492, 254-265.
- Fujino, J., Nair, R., Kainuma, M., Masui, T., & Matsuoka, Y. (2006). Multi-gas mitigation analysis on stabilization scenarios using AIM global model. *The Energy Journal*(Special Issue# 3).
- Fuka, D. R., Walter, M. T., MacAlister, C., Degaetano, A. T., Steenhuis, T. S., & Easton, Z. M. (2014). Using the Climate Forecast System Reanalysis as weather input data for watershed models. *Hydrological Processes*, 28(22), 5613-5623.
- Fulton, R. A., Breidenbach, J. P., Seo, D.-J., Miller, D. A., & O'Bannon, T. (1998). The WSR-88D rainfall algorithm. *Weather and forecasting*, 13(2), 377-395.
- Galván, L., Olías, M., Izquierdo, T., Cerón, J., & de Villarán, R. F. (2014). Rainfall estimation in SWAT: An alternative method to simulate orographic precipitation. *Journal of Hydrology*, 509, 257-265.
- Gao, J., Bieger, K., White, M. J., & Arnold, J. G. (2020). Development and accuracy assessment of a 12-digit hydrologic unit code based real-time climate database for hydrologic models in the US. *Journal of Hydrology*, 586, 124817.
- Gao, J., Sheshukov, A. Y., Yen, H., & White, M. J. (2017). Impacts of alternative climate information on hydrologic processes with SWAT: A comparison of NCDC, PRISM and NEXRAD datasets. *Catena*, 156, 353-364.

- Gao, Y., Leung, L. R., Lu, J., & Masato, G. (2015). Persistent cold air outbreaks over North America in a warming climate. *Environmental Research Letters*, 10(4), 044001.
- Gassman, P. W., Reyes, M. R., Green, C. H., & Arnold, J. G. (2007). The soil and water assessment tool: historical development, applications, and future research directions. *Transactions of the ASABE*, 50(4), 1211-1250.
- Gavahi, K., Abbaszadeh, P., & Moradkhani, H. (2022). How does precipitation data influence the land surface data assimilation for drought monitoring? *Science of the total environment*, 831, 154916.
- GCX, G. C. E. (2020). ICLUS v2.1 land use projections for the Fourth National Climate Assessment (SSP5). Retrieved from <https://www.epa.gov/gcx/iclus-fourth-national-climate-assessment>. Retrieved 1 Jan. 2020, from U.S. EPA (Environmental Protection Agency) <https://www.epa.gov/gcx/iclus-fourth-national-climate-assessment>
- Gent, P. R., Danabasoglu, G., Donner, L. J., Holland, M. M., Hunke, E. C., Jayne, S. R., . . . Vertenstein, M. (2011). The community climate system model version 4. *Journal of Climate*, 24(19), 4973-4991.
- Georgakakos, A., Fleming, P., Dettinger, M., Peters-Lidard, C., Richmand, T. C., Reckhow, K., . . . Yates, D. (2014). Chapter 3: Water resources. *Climate Change Impacts in the United States: The Third National Climate Assessment* Retrieved from
- Ghoraba, S. M. (2015). Hydrological modeling of the Simly Dam watershed (Pakistan) using GIS and SWAT model. *Alexandria Engineering Journal*, 54(3), 583-594.
- Green, C., & Van Griensven, A. (2008). Autocalibration in hydrologic modeling: Using SWAT2005 in small-scale watersheds. *Environmental Modelling & Software*, 23(4), 422-434.
- Groisman, P. Y., Knight, R. W., Easterling, D. R., Karl, T. R., Hegerl, G. C., & Razuvayev, V. N. (2005). Trends in intense precipitation in the climate record. *Journal of Climate*, 18(9), 1326-1350.
- Groisman, P. Y., Knight, R. W., & Karl, T. R. (2012). Changes in intense precipitation over the central United States. *Journal of Hydrometeorology*, 13(1), 47-66.
- Guerreiro, S. B., Fowler, H. J., Barbero, R., Westra, S., Lenderink, G., Blenkinsop, S., . . . Li, X.-F. (2018). Detection of continental-scale intensification of hourly rainfall extremes. *Nature Climate Change*, 8(9), 803-807.
- Gupta, H. V., Sorooshian, S., & Yapo, P. O. (1999). Status of automatic calibration for hydrologic models: Comparison with multilevel expert calibration. *Journal of Hydrologic Engineering*, 4(2), 135-143.

- Habib, E., Larson, B. F., & Graschel, J. (2009). Validation of NEXRAD multisensor precipitation estimates using an experimental dense rain gauge network in south Louisiana. *Journal of Hydrology*, 373(3-4), 463-478.
- Halecki, W., Kruk, E., & Ryczek, M. (2018). Loss of topsoil and soil erosion by water in agricultural areas: A multi-criteria approach for various land use scenarios in the Western Carpathians using a SWAT model. *Land Use Policy*, 73, 363-372.
- Hansen, M. C., Potapov, P. V., Moore, R., Hancher, M., Turubanova, S. A., Tyukavina, A., . . . Loveland, T. R. (2013). High-resolution global maps of 21st-century forest cover change. *Science*, 342(6160), 850-853.
- Haregeweyn, N., Tsunekawa, A., Poesen, J., Tsubo, M., Meshesha, D. T., Fenta, A. A., . . . Adgo, E. (2017). Comprehensive assessment of soil erosion risk for better land use planning in river basins: Case study of the Upper Blue Nile River. *Science of the total environment*, 574, 95-108.
- He, Y., Zhang, Y., Kuligowski, R., Cifelli, R., & Kitzmiller, D. (2018). Incorporating satellite precipitation estimates into a radar-gauge multi-sensor precipitation estimation algorithm. *Remote Sensing*, 10(1), 106.
- Heimann, D. C., Sprague, L. A., & Blevins, D. W. (2011). *Trends in suspended-sediment loads and concentrations in the Mississippi River Basin, 1950-2009*: US Department of the Interior, US Geological Survey.
- Her, Y., Chaubey, I., Frankenberger, J., & Smith, D. (2016). Effect of conservation practices implemented by USDA programs at field and watershed scales. *Journal of Soil and Water Conservation*, 71(3), 249-266.
- Hidalgo León, H. G., Dettinger, M. D., & Cayan, D. R. (2008). Downscaling with constructed analogues: Daily precipitation and temperature fields over the United States.
- Hinson, A. S., Rogers, A. L., & Cook, M. R. (2015). *Choctawhatchee, Pea and Yellow Rivers Comprehensive Watershed Management Plan*. Retrieved from
- Ho-Hagemann, H. T. M., Hagemann, S., & Rockel, B. (2015). On the role of soil moisture in the generation of heavy rainfall during the Oder flood event in July 1997. *Tellus A: Dynamic Meteorology and Oceanography*, 67(1), 28661.
- Hoerling, M., Eischeid, J., Perlitz, J., Quan, X.-W., Wolter, K., & Cheng, L. (2016). Characterizing recent trends in US heavy precipitation. *Journal of Climate*, 29(7), 2313-2332.
- Horton, A. A., & Dixon, S. J. (2018). Microplastics: An introduction to environmental transport processes. *Wiley Interdisciplinary Reviews: Water*, 5(2), e1268.

- Hoyos, N., Correa-Metrio, A., Jepsen, S. M., Wemple, B., Valencia, S., Marsik, M., . . . Velez, M. I. (2019). Modeling Streamflow Response to Persistent Drought in a Coastal Tropical Mountainous Watershed, Sierra Nevada De Santa Marta, Colombia. *Water*, 11(1), 94.
- Huang, H. j., Cheng, S. j., Wen, J. c., & Lee, J. h. (2008). Effect of growing watershed imperviousness on hydrograph parameters and peak discharge. *Hydrological Processes: An International Journal*, 22(13), 2075-2085.
- Huisman, J., Breuer, L., Bormann, H., Bronstert, A., Croke, B., Frede, H.-G., . . . Kite, G. (2009). Assessing the impact of land use change on hydrology by ensemble modeling (LUCHEM) III: Scenario analysis. *Advances in water resources*, 32(2), 159-170.
- Hurtt, G. C., Chini, L., Sahajpal, R., Frolking, S., Bodirsky, B. L., Calvin, K., . . . Klein Goldewijk, K. (2020). Harmonization of global land use change and management for the period 850–2100 (LUH2) for CMIP6. *Geoscientific Model Development*, 13(11), 5425-5464.
- Inamdar, S., Johnson, E., Rowland, R., Warner, D., Walter, R., & Merritts, D. (2018). Freeze-thaw processes and intense rainfall: the one-two punch for high sediment and nutrient loads from mid-Atlantic watersheds. *Biogeochemistry*, 141(3), 333-349.
- Ingram, K. T., Dow, K., Carter, L., & Anderson, J. (2013). Forests and climate change in the Southeast USA. In *Climate of the Southeast United States* (pp. 165-189): Springer.
- Jalowska, A. M., & Yuan, Y. (2019). Evaluation of SWAT impoundment modeling methods in water and sediment simulations. *JAWRA Journal of the American Water Resources Association*, 55(1), 209-227.
- Jayakrishnan, R. (2001). *Effect of rainfall variability on hydrologic simulation using WSR-88D (NEXRAD) data*: Texas A&M University.
- Joh, H.-K., Lee, J.-W., Park, M.-J., Shin, H.-J., Yi, J.-E., Kim, G.-S., . . . Kim, S.-J. (2011). Assessing climate change impact on hydrological components of a small forest watershed through SWAT calibration of evapotranspiration and soil moisture. *Transactions of the ASABE*, 54(5), 1773-1781.
- Jolliffe, I. T., & Hope, P. B. (1996). Representation of daily rainfall distributions using normalized rainfall curves. *International Journal of Climatology*, 16(10), 1157-1163.
- Kang, Y., Khan, S., & Ma, X. (2009). Climate change impacts on crop yield, crop water productivity and food security—A review. *Progress in natural Science*, 19(12), 1665-1674.
- Karl, T. R., Melillo, J. M., Peterson, T. C., & Hassol, S. J. (2009). *Global climate change impacts in the United States*: Cambridge University Press.

- Katz, R. W., Parlange, M. B., & Tebaldi, C. (2003). Stochastic modeling of the effects of large-scale circulation on daily weather in the southeastern US. In *Issues in the Impacts of Climate Variability and Change on Agriculture* (pp. 189-216): Springer.
- Kebede, H., Fisher, D. K., Sui, R., & Reddy, K. N. (2014). Irrigation methods and scheduling in the Delta region of Mississippi: Current status and strategies to improve irrigation efficiency. *American Journal of Plant Sciences*, 5(20), 2917.
- Khalid, K., Ali, M. F., Rahman, N. F. A., Mispan, M. R., Haron, S. H., Othman, Z., & Bachok, M. F. (2016). Sensitivity analysis in watershed model using SUFI-2 algorithm. *Procedia Eng*, 162, 441-447.
- Kirstetter, P. E., Gourley, J. J., Hong, Y., Zhang, J., Moazamigoodarzi, S., Langston, C., & Arthur, A. (2015). Probabilistic precipitation rate estimates with ground-based radar networks. *Water Resources Research*, 51(3), 1422-1442.
- Kitzmiller, D., Miller, D., Fulton, R., & Ding, F. (2013). Radar and multisensor precipitation estimation techniques in National Weather Service hydrologic operations. *Journal of Hydrologic Engineering*, 18(2), 133-142.
- Klazura, G. E., & Imy, D. A. (1993). A description of the initial set of analysis products available from the NEXRAD WSR-88D system. *Bulletin of the American Meteorological Society*, 74(7), 1293-1312.
- Knutson, T. R., Chung, M. V., Vecchi, G., Sun, J., Hsieh, T.-L., & Smith, A. J. (2021). Climate change is probably increasing the intensity of tropical cyclones. In *Critical issues in climate change science: ScienceBrief Review*.
- Kotz, M., Levermann, A., & Wenz, L. (2022). The effect of rainfall changes on economic production. *Nature*, 601(7892), 223-227. doi:10.1038/s41586-021-04283-8
- Kumjian, M. R. (2013). Principles and Applications of Dual-Polarization Weather Radar. Part I: Description of the Polarimetric Radar Variables. *Journal of Operational Meteorology*, 1.
- Kundzewicz, Z. W., Mata, L. J., Arnell, N., Doll, P., Kabat, P., Jimenez, B., . . . Shiklomanov, I. (2007). Freshwater resources and their management.
- Legates, D. R., & McCabe Jr, G. J. (1999). Evaluating the use of “goodness-of-fit” measures in hydrologic and hydroclimatic model validation. *Water Resources Research*, 35(1), 233-241.
- Lemma, H., Frankl, A., van Griensven, A., Poesen, J., Adgo, E., & Nyssen, J. (2019). Identifying erosion hotspots in Lake Tana Basin from a multisite Soil and Water Assessment Tool validation: Opportunity for land managers. *Land Degradation & Development*, 30(12), 1449-1467.

- Lengfeld, K., Kirstetter, P.-E., Fowler, H. J., Yu, J., Becker, A., Flamig, Z., & Gourley, J. (2020). Use of radar data for characterizing extreme precipitation at fine scales and short durations. *Environmental Research Letters*, 15(8), 085003.
- Li, H., Sheffield, J., & Wood, E. F. (2010). Bias correction of monthly precipitation and temperature fields from Intergovernmental Panel on Climate Change AR4 models using equidistant quantile matching. *Journal of Geophysical Research: Atmospheres*, 115(D10).
- Li, X., Jiang, F., Li, L., & Wang, G. (2011). Spatial and temporal variability of precipitation concentration index, concentration degree and concentration period in Xinjiang, China. *International Journal of Climatology*, 31(11), 1679-1693.
- Livneh, B., Bohn, T. J., Pierce, D. W., Munoz-Arriola, F., Nijssen, B., Vose, R., . . . Brekke, L. (2015). A spatially comprehensive, hydrometeorological data set for Mexico, the US, and Southern Canada 1950–2013. *Scientific data*, 2(1), 1-12.
- Logan, T. J. (1993). Agricultural best management practices for water pollution control: current issues. *Agriculture, Ecosystems & Environment*, 46(1-4), 223-231.
- Lu, C., Zhang, J., Tian, H., Crumpton, W. G., Helmers, M. J., Cai, W.-J., . . . Lohrenz, S. E. (2020). Increased extreme precipitation challenges nitrogen load management to the Gulf of Mexico. *Communications Earth & Environment*, 1(1), 1-10.
- Lu, Y., Jiang, S., Ren, L., Zhang, L., Wang, M., Liu, R., & Wei, L. (2019). Spatial and temporal variability in precipitation concentration over mainland China, 1961–2017. *Water*, 11(5), 881.
- Mahmood, R., Pielke Sr, R. A., Hubbard, K. G., Niyogi, D., Bonan, G., Lawrence, P., . . . Gameda, S. (2010). Impacts of land use/land cover change on climate and future research priorities. *Bulletin of the American Meteorological Society*, 91(1), 37-46.
- Makhtoumi, Y., Li, S., Ibeanusi, V., & Chen, G. (2020). Evaluating water balance variables under land use and climate projections in the upper choctawhatchee River Watershed, in Southeast US. *Water*, 12(8), 2205.
- Maraun, D., Wetterhall, F., Ireson, A., Chandler, R., Kendon, E., Widmann, M., . . . Themeßl, M. (2010). Precipitation downscaling under climate change: Recent developments to bridge the gap between dynamical models and the end user. *Reviews of Geophysics*, 48(3).
- Marhaento, H., Booij, M. J., & Hoekstra, A. Y. (2018). Hydrological response to future land-use change and climate change in a tropical catchment. *Hydrological Sciences Journal*, 63(9), 1368-1385.
- Markonis, Y., Papalexiou, S., Martinkova, M., & Hanel, M. (2019). Assessment of water cycle intensification over land using a multisource global gridded precipitation dataset. *Journal of Geophysical Research: Atmospheres*, 124(21), 11175-11187.

- Martin-Vide, J. (2004). Spatial distribution of a daily precipitation concentration index in peninsular Spain. *International Journal of Climatology: A Journal of the Royal Meteorological Society*, 24(8), 959-971.
- Masih, I., Maskey, S., Uhlenbrook, S., & Smakhtin, V. (2011). Assessing the Impact of Areal Precipitation Input on Streamflow Simulations Using the SWAT Model 1. *JAWRA Journal of the American Water Resources Association*, 47(1), 179-195.
- Massey, J. H., Mark Stiles, C., Epting, J. W., Shane Powers, R., Kelly, D. B., Bowling, T. H., . . . Pennington, D. A. (2017). Long-term measurements of agronomic crop irrigation made in the Mississippi delta portion of the lower Mississippi River Valley. *Irrigation Science*, 35(4), 297-313.
- Masui, T., Matsumoto, K., Hijioka, Y., Kinoshita, T., Nozawa, T., Ishiwatari, S., . . . Kainuma, M. (2011). An emission pathway for stabilization at 6 Wm<sup>-2</sup> radiative forcing. *Climatic change*, 109(1-2), 59.
- McHenry, J. R., Ritchie, J. C., & Schiebe, F. R. (1977). ESTIMATING THE SUSPENDED SEDIMENT LOAD IN RESERVOIRS 1. *JAWRA Journal of the American Water Resources Association*, 13(1), 81-92.
- McKee, P. W., & Hays, P. D. (2002). *The Sparta Aquifer: A Sustainable Water Resource?* (2327-6932). Retrieved from
- McNulty, S., Caldwell, P., Doyle, T. W., Johnsen, K., Liu, Y., Mohan, J., . . . Sun, G. (2013). Forests and climate change in the Southeast USA. In *Climate of the Southeast United States: Variability, change, impacts, and vulnerability* (pp. 165-189). Washington, DC: Island Press: Springer.
- MDEQ, H. C. W. I. T.-. (2009). *HICKAHALA CREEK WATERSHED IMPLEMENTATION PLAN*. Retrieved from [https://www.mdeq.ms.gov/wp-content/uploads/SurfaceWaterBasinMgtNonPointSourceBranch/Watershed\\_Plans/Group\\_II/YZ/Watershed\\_Plans/Hickahala\\_Creek\\_Watershed\\_Plan\\_2009.pdf](https://www.mdeq.ms.gov/wp-content/uploads/SurfaceWaterBasinMgtNonPointSourceBranch/Watershed_Plans/Group_II/YZ/Watershed_Plans/Hickahala_Creek_Watershed_Plan_2009.pdf)
- MDEQ, M. D. o. E. Q. (2003). *Sediment TMDL for the Coldwater River*. Retrieved from MDEQ: [www.deq.state.ms.us](http://www.deq.state.ms.us)
- Meehl, G. A., Arblaster, J. M., & Branstator, G. (2012). Mechanisms contributing to the warming hole and the consequent US east–west differential of heat extremes. *Journal of Climate*, 25(18), 6394-6408.
- Meehl, G. A., Stocker, T. F., Collins, W. D., Friedlingstein, P., Gaye, T., Gregory, J. M., . . . Noda, A. (2007). Global climate projections.
- Meinshausen, M., Smith, S. J., Calvin, K., Daniel, J. S., Kainuma, M., Lamarque, J.-F., . . . Riahi, K. (2011). The RCP greenhouse gas concentrations and their extensions from 1765 to 2300. *Climatic change*, 109(1-2), 213.

- Melles, S., Benoy, G., Booty, B., Leon, L., Vanrobaeys, J., & Wong, I. (2010). Scenarios to Investigate the Effect of Wetland Position in a Watershed on Nutrient Loadings.
- Mondal, S., Mishra, A. K., & Leung, L. R. (2020). Spatiotemporal characteristics and propagation of summer extreme precipitation events over United States: A complex network analysis. *Geophysical Research Letters*, 47(15), e2020GL088185.
- Monteith, J. L. (1965). *Evaporation and environment*. Paper presented at the Symposia of the society for experimental biology.
- Moon, J., Srinivasan, R., & Jacobs, J. (2004). Stream flow estimation using spatially distributed rainfall in the Trinity River basin, Texas. *Transactions of the ASAE*, 47(5), 1445.
- Moriasi, D., Wilson, B. N., Douglas-Mankin, K., Arnold, J., & Gowda, P. (2012). Hydrologic and water quality models: Use, calibration, and validation. *Transactions of the ASABE*, 55(4), 1241-1247.
- Moriasi, D. N., Arnold, J. G., Van Liew, M. W., Bingner, R. L., Harmel, R. D., & Veith, T. L. (2007). Model evaluation guidelines for systematic quantification of accuracy in watershed simulations. *Transactions of the ASABE*, 50(3), 885-900.
- Morris, M. D. (1991). Factorial sampling plans for preliminary computational experiments. *Technometrics*, 33(2), 161-174.
- Moss, R., Babiker, M., Brinkman, S., Calvo, E., Carter, T., Edmonds, J., . . . Hibbard, K. (2008). *Towards New Scenarios for Analysis of Emissions*. Paper presented at the Climate Change, Impacts, and Response Strategies (IPCC Expert Meeting Report, IPCC, Geneva, 2008).
- Moss, R. H., Edmonds, J. A., Hibbard, K. A., Manning, M. R., Rose, S. K., Van Vuuren, D. P., . . . Kram, T. (2010). The next generation of scenarios for climate change research and assessment. *Nature*, 463(7282), 747-756.
- Moustakis, Y., Papalexiou, S. M., Onof, C. J., & Paschalis, A. (2021). Seasonality, intensity, and duration of rainfall extremes change in a warmer climate. *Earth's Future*, 9(3).
- MRLC-Consortium, M.-R. L. C. (2019). Retrieved from <https://www.mrlc.gov/data>
- MRLC-Consortium, M.-R. L. C. (2021). Retrieved from <https://www.mrlc.gov/data>
- MSPB. (2021). Mississippi Soybean Promotion Board. Retrieved from <https://www.mssoy.org/>
- Mueller-Warrant, G., Phillips, C., & Trippe, K. (2019). Use of SWAT to model impact of climate change on sediment yield and agricultural productivity in western Oregon, USA. *Open Journal of Modern Hydrology*, 9(02), 54.

- Murdoch, P. S., Baron, J. S., & Miller, T. L. (2000). POTENTIAL EFFECTS OF CLIMATE CHANGE ON SURFACE-WATER QUALITY IN NORTH AMERICA 1. *JAWRA Journal of the American Water Resources Association*, 36(2), 347-366.
- Myhre, G., Alterskjaer, K., Stjern, C. W., Hodnebrog, Ø., Marelle, L., Samset, B. H., . . . Schulz, M. (2019). Frequency of extreme precipitation increases extensively with event rareness under global warming. *Scientific reports*, 9(1), 1-10.
- N. Nakagaki, M. E. W., S. L. Qi, . (2016). Estimates of subsurface tile drainage extent for 619 the conterminous United States, early 1990s. In (2016 ed.). U.S. Geological Survey data release.
- Nakicenovic, N., Alcamo, J., Grubler, A., Riahi, K., Roehrl, R., Rogner, H.-H., & Victor, N. (2000). *Special report on emissions scenarios (SRES), a special report of Working Group III of the intergovernmental panel on climate change*: Cambridge University Press.
- Nash, J. E., & Sutcliffe, J. V. (1970). River flow forecasting through conceptual models part I— A discussion of principles. *Journal of Hydrology*, 10(3), 282-290.
- Nearing, M. A. (2013). Soil erosion and conservation. *Environmental modelling: Finding simplicity in complexity*, 365-378.
- Neitsch, S. L., Arnold, J. G., Kiniry, J. R., & Williams, J. R. (2011). *Soil and water assessment tool theoretical documentation version 2009*. Retrieved from
- NRC, N. R. C., & CRC, C. R. C. (2005). *Radiative Forcing of Climate Change: Expanding the Concept and Addressing Uncertainties*: National Academies Press.
- O'Neil, P., Shepard, T., & Cook, M. (2006). Habitat and biological assessment of the Terrapin Creek watershed and development of the index of biotic integrity for the Coosa and Tallapoosa River systems. *Open-File Report*, 601.
- Oliver, J. E. (1980). Monthly precipitation distribution: a comparative index. *The Professional Geographer*, 32(3), 300-309.
- Osei, M. A., Amekudzi, L. K., Wemegah, D. D., Preko, K., Gyawu, E. S., & Obiri-Danso, K. (2019). The impact of climate and land-use changes on the hydrological processes of Owabi catchment from SWAT analysis. *Journal of Hydrology: Regional Studies*, 25, 100620.
- Ouyang, F., Zhu, Y., Fu, G., Lü, H., Zhang, A., Yu, Z., & Chen, X. (2015). Impacts of climate change under CMIP5 RCP scenarios on streamflow in the Huangnizhuang catchment. *Stochastic environmental research and risk assessment*, 29(7), 1781-1795.
- Pachauri, R. K., Allen, M. R., Barros, V. R., Broome, J., Cramer, W., Christ, R., . . . Dasgupta, P. (2014). *Climate change 2014: synthesis report. Contribution of Working Groups I, II and*

*III to the fifth assessment report of the Intergovernmental Panel on Climate Change:*  
Ipcc.

- Pai, N., Saraswat, D., & Daniels, M. (2011). Identifying priority subwatersheds in the Illinois River drainage area in Arkansas watershed using a distributed modeling approach. *Transactions of the ASABE*, 54(6), 2181-2196.
- Panagos, P., Borrelli, P., Poesen, J., Ballabio, C., Lugato, E., Meusburger, K., . . . Alewell, C. (2015). The new assessment of soil loss by water erosion in Europe. *Environmental science & policy*, 54, 438-447.
- Pandey, B. K., Khare, D., Kawasaki, A., & Mishra, P. K. (2019). Climate change impact assessment on blue and green water by coupling of representative CMIP5 climate models with physical based hydrological model. *Water resources management*, 33(1), 141-158.
- Pandey, S., Kumar, P., Zlatic, M., Nautiyal, R., & Panwar, V. P. (2021). Recent advances in assessment of soil erosion vulnerability in a watershed. *International Soil and Water Conservation Research*, 9(3), 305-318.
- Papalexiou, S. M., & Montanari, A. (2019). Global and regional increase of precipitation extremes under global warming. *Water Resources Research*, 55(6), 4901-4914.
- Parajuli, P., Jayakody, P., Sassenrath, G., & Ouyang, Y. (2016). Assessing the impacts of climate change and tillage practices on stream flow, crop and sediment yields from the Mississippi River Basin. *Agricultural Water Management*, 168, 112-124.
- Park, J., Ale, S., Teague, W., & Dowhower, S. (2017). Simulating hydrologic responses to alternate grazing management practices at the ranch and watershed scales. *Journal of Soil and Water Conservation*, 72(2), 102-121.
- Peleg, N., Blumensaat, F., Molnar, P., Fatichi, S., & Burlando, P. (2017). Partitioning the impacts of spatial and climatological rainfall variability in urban drainage modeling. *Hydrology and Earth System Sciences*, 21(3), 1559-1572.
- Peleg, N., Skinner, C., Ramirez, J. A., & Molnar, P. (2021). Rainfall spatial-heterogeneity accelerates landscape evolution processes. *Geomorphology*, 390, 107863.
- Pendergrass, A. G., & Hartmann, D. L. (2014). Changes in the distribution of rain frequency and intensity in response to global warming. *Journal of Climate*, 27(22), 8372-8383.
- Pfahl, S., O'Gorman, P. A., & Fischer, E. M. (2017). Understanding the regional pattern of projected future changes in extreme precipitation. *Nature Climate Change*, 7(6), 423-427.
- Pierce, D., & Cayan, D. (2016). Downscaling humidity with localized constructed analogs (LOCA) over the conterminous united states. *Climate dynamics*, 47(1-2), 411-431.

- Pierce, D. W., Cayan, D. R., Maurer, E. P., Abatzoglou, J. T., & Hegewisch, K. C. (2015). Improved bias correction techniques for hydrological simulations of climate change. *Journal of Hydrometeorology*, 16(6), 2421-2442.
- Pierce, D. W., Cayan, D. R., & Thrasher, B. L. (2014). Statistical downscaling using localized constructed analogs (LOCA). *Journal of Hydrometeorology*, 15(6), 2558-2585.
- Pignotti, G., Rathjens, H., Cibin, R., Chaubey, I., & Crawford, M. (2017). Comparative analysis of HRU and grid-based SWAT models. *Water*, 9(4), 272.
- Pimentel, D. (2006). Soil erosion: a food and environmental threat. *Environment, development and sustainability*, 8(1), 119-137.
- Pimentel, D., & Burgess, M. (2013). Soil erosion threatens food production. *Agriculture*, 3(3), 443-463.
- Poloczanska, E., Mintenbeck, K., Portner, H. O., Roberts, D., & Levin, L. A. (2018). *The IPCC Special Report on the Ocean and Cryosphere in a Changing Climate*. Paper presented at the 2018 Ocean Sciences Meeting.
- Prabhanjan, A., Rao, E., & Eldho, T. (2015). Application of SWAT model and geospatial techniques for sediment-yield modeling in ungauged watersheds. *Journal of Hydrologic Engineering*, 20(6), C6014005.
- Price, K. (2011). Effects of watershed topography, soils, land use, and climate on baseflow hydrology in humid regions: A review. *Progress in physical geography*, 35(4), 465-492.
- Price, K., Purucker, S., & Kraemer, S. (2011). Multi-scale comparison of stage IV NEXRAD (MPE) and gauge precipitation data for watershed modeling.
- Price, K., Purucker, S. T., Kraemer, S. R., Babendreier, J. E., & Knightes, C. D. (2014). Comparison of radar and gauge precipitation data in watershed models across varying spatial and temporal scales. *Hydrological Processes*, 28(9), 3505-3520.
- Pruski, F. F., & Nearing, M. A. (2002). Runoff and soil-loss responses to changes in precipitation: A computer simulation study. *Journal of Soil and Water Conservation*, 57(1), 7-16.
- Pulley, S., & Collins, A. (2020). Sediment loss in response to scheduled pasture ploughing and reseeding: The importance of soil moisture content in controlling risk. *Soil and Tillage Research*, 204, 104746.
- Qiu, J., Shen, Z., Chen, L., & Hou, X. (2019). Quantifying effects of conservation practices on non-point source pollution in the Miyun Reservoir Watershed, China. *Environmental monitoring and assessment*, 191(9), 582.

- Rabalais, N. N., Turner, R. E., Wiseman, J., William J, & Dortch, Q. (1998). Consequences of the 1993 Mississippi River flood in the Gulf of Mexico. *Regulated Rivers: Research & Management: An International Journal Devoted to River Research and Management*, 14(2), 161-177.
- Rahman, M. M., Thompson, J. R., & Flower, R. J. (2016). An enhanced SWAT wetland module to quantify hydraulic interactions between riparian depressional wetlands, rivers and aquifers. *Environmental Modelling & Software*, 84, 263-289.
- Razad, A. A., Shamsuddini, S., Setu, A., & Sidek, L. M. (2021). Future impacts of climate change on sediment influx rate in hydropower reservoir using SWAT. Paper presented at the IOP Conference Series: Earth and Environmental Science.
- Reynolds, L. V., Shafrroth, P. B., & Poff, N. L. (2015). Modeled intermittency risk for small streams in the Upper Colorado River Basin under climate change. *Journal of Hydrology*, 523, 768-780.
- Riahi, K., Grübler, A., & Nakicenovic, N. (2007). Scenarios of long-term socio-economic and environmental development under climate stabilization. *Technological Forecasting and Social Change*, 74(7), 887-935.
- Riahi, K., Rao, S., Krey, V., Cho, C., Chirkov, V., Fischer, G., . . . Rafaj, P. (2011). RCP 8.5—A scenario of comparatively high greenhouse gas emissions. *Climatic change*, 109(1-2), 33.
- Riahi, K., Van Vuuren, D. P., Kriegler, E., Edmonds, J., O'neill, B. C., Fujimori, S., . . . Fricko, O. (2017). The shared socioeconomic pathways and their energy, land use, and greenhouse gas emissions implications: an overview. *Global Environmental Change*, 42, 153-168.
- Ribaudo, M., Horan, R. D., & Smith, M. E. (1999). *Economics of water quality protection from nonpoint sources: theory and practice*. Retrieved from
- Ritchie, J. C., McHenry, J. R., & Schiebe, F. R. (1978). The vertical distribution of suspended sediments in reservoirs. *Journal (Water Pollution Control Federation)*, 734-738.
- Ritchie, J. T. (1972). Model for predicting evaporation from a row crop with incomplete cover. *Water Resources Research*, 8(5), 1204-1213.
- Rose, S., & Peters, N. E. (2001). Effects of urbanization on streamflow in the Atlanta area (Georgia, USA): a comparative hydrological approach. *Hydrological Processes*, 15(8), 1441-1457.
- Roth, V., & Lemann, T. (2016). Comparing CFSR and conventional weather data for discharge and soil loss modelling with SWAT in small catchments in the Ethiopian Highlands. *Hydrology and Earth System Sciences*, 20(2), 921-934.

- Ruan, H., Zou, S., Cong, Z., Wang, Y., Yin, Z., Lu, Z., . . . Xu, B. (2016). Runoff simulation by SWAT model using high-resolution gridded precipitation in the upper Heihe River Basin, Northeastern Tibetan Plateau. *Hydrology and Earth System Sciences Discussions*, 1-23.
- Saha, S., Moorthi, S., Pan, H.-L., Wu, X., Wang, J., Nadiga, S., . . . Behringer, D. (2010). The NCEP climate forecast system reanalysis. *Bulletin of the American Meteorological Society*, 91(8), 1015-1058.
- Saltelli, A., Tarantola, S., Campolongo, F., & Ratto, M. (2004). *Sensitivity analysis in practice: a guide to assessing scientific models* (Vol. 1): Wiley Online Library.
- Sanderson, B. M., Knutti, R., & Caldwell, P. (2015a). Addressing interdependency in a multimodel ensemble by interpolation of model properties. *Journal of Climate*, 28(13), 5150-5170.
- Sanderson, B. M., Knutti, R., & Caldwell, P. (2015b). A representative democracy to reduce interdependency in a multimodel ensemble. *Journal of Climate*, 28(13), 5171-5194.
- Santhi, C., Arnold, J. G., Williams, J. R., Dugas, W. A., Srinivasan, R., & Hauck, L. M. (2001). Validation of the swat model on a large river basin with point and nonpoint sources 1. *JAWRA Journal of the American Water Resources Association*, 37(5), 1169-1188.
- Schiefer, E., Petticrew, E. L., Immell, R., Hassan, M. A., & Sonderegger, D. L. (2013). Land use and climate change impacts on lake sedimentation rates in western Canada. *Anthropocene*, 3, 61-71.
- Schmidt, G. A., Ruedy, R., Hansen, J. E., Aleinov, I., Bell, N., Bauer, M., . . . Cheng, Y. (2006). Present-day atmospheric simulations using GISS ModelE: Comparison to in situ, satellite, and reanalysis data. *Journal of Climate*, 19(2), 153-192.
- Seaber, P. R., Kapinos, F. P., & Knapp, G. L. (1987). Hydrologic unit maps.
- Sexton, A., Sadeghi, A., Zhang, X., Srinivasan, R., & Shirmohammadi, A. (2010). Using NEXRAD and rain gauge precipitation data for hydrologic calibration of SWAT in a northeastern watershed. *Transactions of the ASABE*, 53(5), 1501-1510.
- Sharifi, A., Yen, H., Boomer, K. M., Kalin, L., Li, X., & Weller, D. E. (2017). Using multiple watershed models to assess the water quality impacts of alternate land development scenarios for a small community. *Catena*, 150, 87-99.
- Sheffield, J., Barrett, A. P., Colle, B., Nelun Fernando, D., Fu, R., Geil, K. L., . . . Langenbrunner, B. (2013). North American climate in CMIP5 experiments. Part I: Evaluation of historical simulations of continental and regional climatology. *Journal of Climate*, 26(23), 9209-9245.

- Sheshukov, A. Y., Douglas-Mankin, K. R., Sinnathamby, S., & Daggupati, P. (2016). Pasture BMP effectiveness using an HRU-based subarea approach in SWAT. *Journal of environmental management*, 166, 276-284.
- Simon, A., Kuhnle, R., Knight, S., & Dickerson, W. (2001). ``Reference''and Enhanced Rates of Suspended-Sediment Transport for Use in Developing Clean-Sediment TMDL's: Examples from Mississippi and the Southeastern United States. In *Wetlands Engineering & River Restoration 2001* (pp. 1-12).
- Sleeter, B. M., Loveland, T., Wickham, J., Domke, G., Herold, N., Wood, N., . . . Sleeter, B. (2018). Land Cover and Land-Use Change. In D. R. Reidmiller, C. W. Avery, D. R. Easterling, K. E. Kunkel, K. L. M. Lewis, T. K. Maycock, & B. C. Stewart (Eds.), *Impacts, Risks, and Adaptation in the United States: Fourth National Climate Assessment* (Vol. Volume II, pp. 202–231). U.S. Global Change Research Program, Washington, DC, USA.
- Smith, S. J., & Wigley, T. (2006). Multi-gas forcing stabilization with Minicam. *The Energy Journal*(Special Issue# 3).
- Sobel, A. H., Camargo, S. J., Hall, T. M., Lee, C.-Y., Tippett, M. K., & Wing, A. A. (2016). Human influence on tropical cyclone intensity. *Science*, 353(6296), 242-246.
- Sohl, T. L., Sayler, K. L., Bouchard, M. A., Reker, R. R., Friesz, A. M., Bennett, S. L., . . . Soulard, C. (2014). Spatially explicit modeling of 1992–2100 land cover and forest stand age for the conterminous United States. *Ecological Applications*, 24(5), 1015-1036.
- Sohl, T. L., Wimberly, M. C., Radeloff, V. C., Theobald, D. M., & Sleeter, B. M. (2016). Divergent projections of future land use in the United States arising from different models and scenarios. *Ecological Modelling*, 337, 281-297.
- SoilSurvey. (2019a). National Value Added Look Up (value) Table Database for the Gridded Soil Survey Geographic (gSSURGO) Database for the United States of America and the Territories, Commonwealths, and Island Nations served by the USDA-NRCS. Retrieved from <https://gdg.sc.egov.usda.gov/>
- SoilSurvey. (2019b). Natural Resources Conservation Service, United States Department of Agriculture. Retrieved from <http://websoilsurvey.nrcs.usda.gov/>
- SoilSurvey. (2021a). National Value Added Look Up (value) Table Database for the Gridded National Soil Survey Geographic (gNATSGO) Database for the United States of America and the Territories, Commonwealths, and Island Nations served by the USDA-NRCS. Retrieved from <https://gdg.sc.egov.usda.gov/>
- SoilSurvey. (2021b). Natural Resources Conservation Service, United States Department of Agriculture. Retrieved from <http://websoilsurvey.nrcs.usda.gov/>

- Srivastava, A., Deb, P., & Kumari, N. (2020). Multi-model approach to assess the dynamics of hydrologic components in a tropical ecosystem. *Water Resources Management*, 34(1), 327-341.
- Stone, M. C., Hotchkiss, R. H., & Stone, A. B. (2005). Climate change impacts on Missouri River Basin water yields: the influence of temporal scales. In *Impacts of Global Climate Change* (pp. 1-10).
- Sudheer, K., Lakshmi, G., & Chaubey, I. (2011). Application of a pseudo simulator to evaluate the sensitivity of parameters in complex watershed models. *Environmental Modelling & Software*, 26(2), 135-143.
- Sun, A. Y., Xia, Y., Caldwell, T. G., & Hao, Z. (2018). Patterns of precipitation and soil moisture extremes in Texas, US: A complex network analysis. *Advances in water resources*, 112, 203-213.
- Sun, G. (2013). Impacts of climate change and variability on water resources in the Southeast USA. In *Climate of the Southeast United States* (pp. 210-236): Springer.
- Sunde, M. G., He, H. S., Hubbart, J. A., & Urban, M. A. (2017). Integrating downscaled CMIP5 data with a physically based hydrologic model to estimate potential climate change impacts on streamflow processes in a mixed-use watershed. *Hydrological Processes*, 31(9), 1790-1803.
- Sunde, M. G., He, H. S., Hubbart, J. A., & Urban, M. A. (2018). An integrated modeling approach for estimating hydrologic responses to future urbanization and climate changes in a mixed-use midwestern watershed. *Journal of environmental management*, 220, 149-162.
- Tamm, O., Maasikamäe, S., Padari, A., & Tamm, T. (2018). Modelling the effects of land use and climate change on the water resources in the eastern Baltic Sea region using the SWAT model. *Catena*, 167, 78-89.
- Tan, M. L., Gassman, P. W., Liang, J., & Haywood, J. M. (2021). A review of alternative climate products for SWAT modelling: Sources, assessment and future directions. *Science of the total environment*, 795, 148915.
- Taylor, K. E., Balaji, V., Hankin, S., Juckes, M., Lawrence, B., & Pascoe, S. (2011). *CMIP5 data reference syntax (DRS) and controlled vocabularies*. Paper presented at the PCMDI.
- Taylor, K. E., Stouffer, R. J., & Meehl, G. A. (2012). An overview of CMIP5 and the experiment design. *Bulletin of the American Meteorological Society*, 93(4), 485-498.
- Teutschbein, C., & Seibert, J. (2010). Regional climate models for hydrological impact studies at the catchment scale: a review of recent modeling strategies. *Geography Compass*, 4(7), 834-860.

- Theobald, D. M. (2005). Landscape patterns of exurban growth in the USA from 1980 to 2020. *Ecology and society*, 10(1).
- Thomson, A. M., Calvin, K. V., Smith, S. J., Kyle, G. P., Volke, A., Patel, P., . . . Clarke, L. E. (2011). RCP4. 5: a pathway for stabilization of radiative forcing by 2100. *Climatic change*, 109(1-2), 77.
- Tobin, K. J., & Bennett, M. E. (2009). Using SWAT to Model Streamflow in Two River Basins With Ground and Satellite Precipitation Data 1. *JAWRA Journal of the American Water Resources Association*, 45(1), 253-271.
- Trail, M., Tsimpidi, A., Liu, P., Tsigaridis, K., Hu, Y., Nenes, A., . . . Russell, A. (2013). Potential impact of land use change on future regional climate in the Southeastern US: reforestation and crop land conversion. *Journal of Geophysical Research: Atmospheres*, 118(20), 11,577-511,588.
- Tuo, Y., Duan, Z., Disse, M., & Chiogna, G. (2016). Evaluation of precipitation input for SWAT modeling in Alpine catchment: A case study in the Adige river basin (Italy). *Science of the total environment*, 573, 66-82.
- U.S. Geological Survey. (2017). 1/3rd arc-second Digital Elevation Models (DEMs) - USGS National Map 3DEP Downloadable Data Collection: U.S. Geological Survey.
- USDA-ERS. (2019). *Fertilizer Use and Price*. Retrieved from: <https://www.ers.usda.gov/data-products/fertilizer-use-and-price.aspx>
- USDA-NASS. (2007). Agricultural Statistics USDA NASS 2007. Retrieved from [https://www.nass.usda.gov/Statistics\\_by\\_State/Mississippi/Publications/Crop\\_Releases/index.php](https://www.nass.usda.gov/Statistics_by_State/Mississippi/Publications/Crop_Releases/index.php)
- USDA-NASS. (2009). *2007 Census of Agriculture* Retrieved from [https://agcensus.library.cornell.edu/census\\_parts/2007-mississippi/](https://agcensus.library.cornell.edu/census_parts/2007-mississippi/)
- USDA-NCRS. (1999). *Mississippi Planting Guide*. Retrieved from USDA-NCRS: [https://www.ncrs.usda.gov/Internet/FSE\\_DOCUMENTS/nrcs142p2\\_017068.pdf](https://www.ncrs.usda.gov/Internet/FSE_DOCUMENTS/nrcs142p2_017068.pdf)
- USWeatherService. (2019). U.S. Climate Data. Retrieved from [www.usclimatedata.com/](http://www.usclimatedata.com/)
- Valayamkunnath, P., Barlage, M., Chen, F., Gochis, D. J., & Franz, K. J. (2020). Mapping of 30-meter resolution tile-drained croplands using a geospatial modeling approach. *Scientific data*, 7(1), 1-10.
- Van Vuuren, D. P., Den Elzen, M. G., Lucas, P. L., Eickhout, B., Strengers, B. J., Van Ruijen, B., . . . Van Houdt, R. (2007). Stabilizing greenhouse gas concentrations at low levels: an assessment of reduction strategies and costs. *Climatic change*, 81(2), 119-159.

- Van Vuuren, D. P., Edmonds, J., Kainuma, M., Riahi, K., Thomson, A., Hibbard, K., . . . Lamarque, J.-F. (2011). The representative concentration pathways: an overview. *Climatic change*, 109(1-2), 5.
- Van Vuuren, D. P., Stehfest, E., den Elzen, M. G., Kram, T., van Vliet, J., Deetman, S., . . . Beltran, A. M. (2011). RCP2. 6: exploring the possibility to keep global mean temperature increase below 2 C. *Climatic change*, 109(1-2), 95.
- Vázquez, M., Nieto, R., Liberato, M. L., & Gimeno, L. (2020). Atmospheric moisture sources associated with extreme precipitation during the peak precipitation month. *Weather and Climate Extremes*, 30, 100289.
- Veettil, A. V., & Mishra, A. K. (2016). Water security assessment using blue and green water footprint concepts. *Journal of Hydrology*, 542, 589-602.
- Vélez, A., Martin-Vide, J., Royé, D., & Santaella, O. (2019). Spatial analysis of daily precipitation concentration in Puerto Rico. *Theoretical and Applied Climatology*, 136(3), 1347-1355.
- Verma, S., Bhattacharai, R., Bosch, N. S., Cooke, R. C., Kalita, P. K., & Markus, M. (2015). Climate change impacts on flow, sediment and nutrient export in a Great Lakes watershed using SWAT. *CLEAN–Soil, Air, Water*, 43(11), 1464-1474.
- Verstraeten, W. W., Veroustraete, F., & Feyen, J. (2008). Assessment of evapotranspiration and soil moisture content across different scales of observation. *Sensors*, 8(1), 70-117.
- Vigiak, O., Malagó, A., Bouraoui, F., Vanmaercke, M., & Poesen, J. (2015). Adapting SWAT hillslope erosion model to predict sediment concentrations and yields in large Basins. *Science of the total environment*, 538, 855-875.
- Villamizar, S. R., Pineda, S. M., & Carrillo, G. A. (2019). The Effects of Land Use and Climate Change on the Water Yield of a Watershed in Colombia. *Water*, 11(2), 285.
- Villarini, G., Serinaldi, F., Smith, J. A., & Krajewski, W. F. (2009). On the stationarity of annual flood peaks in the continental United States during the 20th century. *Water Resources Research*, 45(8).
- Villarini, G., & Smith, J. A. (2010). Flood peak distributions for the eastern United States. *Water Resources Research*, 46(6).
- Vose, R., Easterling, D. R., Kunkel, K., & Wehner, M. (2017). *Temperature changes in the United States*. Retrieved from
- Waldschläger, K., Brückner, M. Z., Almroth, B. C., Hackney, C. R., Adyel, T. M., Alimi, S. O., . . . Gray, A. (2022). Learning from natural sediments to tackle microplastics challenges: A multidisciplinary perspective. *Earth-Science Reviews*, 104021.

- Walsh, J., Wuebbles, D., Hayhoe, K., Kossin, J., Kunkel, K., Stephens, G., . . . Willis, J. (2014a). Ch. 2: Our Changing Climate. *Climate Change Impacts in the United States*. Retrieved from
- Walsh, J., Wuebbles, D., Hayhoe, K., Kossin, J., Kunkel, K., Stephens, G., . . . Willis, J. (2014b). Ch. 2: Our Changing Climate. Climate Change Impacts in the United States: The Third National Climate Assessment, JM Melillo, Terese (TC) Richmond, and GW Yohe, Eds., US Global Change Research Program, 19-67. doi: 10.7930/J0KW5CXT. In.
- Wang, L., Zheng, F., Liu, G., Zhang, X. J., Wilson, G. V., Shi, H., & Liu, X. (2021). Seasonal changes of soil erosion and its spatial distribution on a long gentle hillslope in the Chinese Mollisol region. *International Soil and Water Conservation Research*, 9(3), 394-404.
- Wang, Q., Qi, J., Qiu, H., Li, J., Cole, J., Waldhoff, S., & Zhang, X. (2021). Pronounced Increases in Future Soil Erosion and Sediment Deposition as Influenced by Freeze–Thaw Cycles in the Upper Mississippi River Basin. *Environmental Science & Technology*, 55(14), 9905-9915.
- Wang, R., Kalin, L., Kuang, W., & Tian, H. (2014). Individual and combined effects of land use/cover and climate change on Wolf Bay watershed streamflow in southern Alabama. *Hydrological Processes*, 28(22), 5530-5546.
- Wasko, C., & Nathan, R. (2019). Influence of changes in rainfall and soil moisture on trends in flooding. *Journal of Hydrology*, 575, 432-441.
- Wasko, C., Nathan, R., Stein, L., & O'Shea, D. (2021). Evidence of shorter more extreme rainfalls and increased flood variability under climate change. *Journal of Hydrology*, 603, 126994.
- Wear, D. N. (2011). Forecasts of county-level land uses under three future scenarios: a technical document supporting the Forest Service 2010 RPA Assessment. *Gen. Tech. Rep. SRS-141. Asheville, NC: US Department of Agriculture Forest Service, Southern Research Station. 41 p.*, 141, 1-41.
- Wei, L., Zhang, B., & Wang, M. (2007). Effects of antecedent soil moisture on runoff and soil erosion in alley cropping systems. *Agricultural Water Management*, 94(1-3), 54-62.
- Westra, S., Fowler, H. J., Evans, J. P., Alexander, L. V., Berg, P., Johnson, F., . . . Roberts, N. (2014). Future changes to the intensity and frequency of short-duration extreme rainfall. *Reviews of Geophysics*, 52(3), 522-555.
- Wheeler, D., & Shaw, G. (1994). *Statistical techniques in geographical analysis*. New York: Halsted press.
- Wilby, R. L., Hay, L. E., Gutowski Jr, W. J., Arritt, R. W., Takle, E. S., Pan, Z., . . . Clark, M. P. (2000). Hydrological responses to dynamically and statistically downscaled climate model output. *Geophysical Research Letters*, 27(8), 1199-1202.

- Williams, J., & Berndt, H. (1977). Sediment yield prediction based on watershed hydrology. *Transactions of the ASAE*, 20(6), 1100-1104.
- Williams, J. R. (1969). Flood routing with variable travel time or variable storage coefficients. *Transactions of the ASAE*, 12(1), 100-0103.
- Winchell, M., Srinivasan, R., Di Luzio, M., & Arnold, J. (2013). ArcSWAT Interface for SWAT2012. User's Guide. 464 pp. *Temple, TX: Blackland Research and Extension Center, Texas AgriLife Research, College Station*.
- Wischmeier, W. H., & Smith, D. D. (1965). Predicting rainfall-erosion losses from cropland east of the Rocky Mountains.
- Wischmeier, W. H., & Smith, D. D. (1978). *Predicting rainfall erosion losses: a guide to conservation planning*: Department of Agriculture, Science and Education Administration.
- Wise, M., Calvin, K., Thomson, A., Clarke, L., Bond-Lamberty, B., Sands, R., . . . Edmonds, J. (2009). Implications of limiting CO<sub>2</sub> concentrations for land use and energy. *Science*, 324(5931), 1183-1186.
- Xie, H., Nkonya, E., & Wielgosz, B. (2011). Assessing the risks of soil erosion and small reservoir siltation in a tropical river basin in Mali using the SWAT model under limited data condition. *Applied Engineering in Agriculture*, 27(6), 895-904.
- Xu, Z., Pang, J., Liu, C., & Li, J. (2009). Assessment of runoff and sediment yield in the Miyun Reservoir catchment by using SWAT model. *Hydrological Processes: An International Journal*, 23(25), 3619-3630.
- Xu, Z., Zhang, S., & Yang, X. (2021). Water and sediment yield response to extreme rainfall events in a complex large river basin: A case study of the Yellow River Basin, China. *Journal of Hydrology*, 597, 126183.
- Yang, L., Jin, S., Danielson, P., Homer, C., Gass, L., Bender, S. M., . . . Fry, J. (2018). A new generation of the United States National Land Cover Database: Requirements, research priorities, design, and implementation strategies. *ISPRS journal of photogrammetry and remote sensing*, 146, 108-123.
- Yang, Z., Zhang, Q., & Hao, X. (2016). Evapotranspiration trend and its relationship with precipitation over the loess plateau during the last three decades. *Advances in Meteorology*, 2016.
- Yasarer, L. M., Bingner, R. L., Garbrecht, J., Locke, M., Lizotte, R., Momm, H., & Busteed, P. (2017). Climate Change Impacts on Runoff, Sediment, and Nutrient Loads in an Agricultural Watershed in the Lower Mississippi River Basin. *Applied Engineering in Agriculture*, 33(3), 379.

- Yasarer, L. M., Taylor, J. M., Rigby, J. R., & Locke, M. A. (2020). Trends in land use, irrigation, and streamflow alteration in the Mississippi River Alluvial Plain. *Frontiers in Environmental Science*, 8, 66.
- Zeiger, S., & Hubbart, J. (2017). An assessment of mean areal precipitation methods on simulated stream flow: a SWAT model performance assessment. *Water*, 9(7), 459.
- Zhang, J., Howard, K., Langston, C., Kaney, B., Qi, Y., Tang, L., . . . Martinaitis, S. (2016). Multi-Radar Multi-Sensor (MRMS) quantitative precipitation estimation: Initial operating capabilities. *Bulletin of the American Meteorological Society*, 97(4), 621-638.
- Zhang, Q., Xu, C.-y., Gemmer, M., Chen, Y. D., & Liu, C. (2009). Changing properties of precipitation concentration in the Pearl River basin, China. *Stochastic environmental research and risk assessment*, 23(3), 377-385.
- Zhang, X. C., & Nearing, M. A. (2005). Impact of climate change on soil erosion, runoff, and wheat productivity in central Oklahoma. *Catena*, 61(2-3), 185-195.
- Zhang, Y., Reed, S., & Kitzmiller, D. (2011). Effects of retrospective gauge-based readjustment of multisensor precipitation estimates on hydrologic simulations. *Journal of Hydrometeorology*, 12(3), 429-443.
- Zhou, J., Fu, B., Gao, G., Lü, Y., Liu, Y., Lü, N., & Wang, S. (2016). Effects of precipitation and restoration vegetation on soil erosion in a semi-arid environment in the Loess Plateau, China. *Catena*, 137, 1-11.
- Zhu, Z., Wright, D. B., & Yu, G. (2018). The impact of rainfall space-time structure in flood frequency analysis. *Water Resources Research*, 54(11), 8983-8998.
- Zink, M., Kumar, R., Cuntz, M., & Samaniego, L. (2017). A high-resolution dataset of water fluxes and states for Germany accounting for parametric uncertainty. *Hydrology and Earth System Sciences*, 21(3), 1769-1790.
- Zubieta, R., Saavedra, M., Silva, Y., & Giráldez, L. (2017). Spatial analysis and temporal trends of daily precipitation concentration in the Mantaro River basin: central Andes of Peru. *Stochastic environmental research and risk assessment*, 31(6), 1305-1318.

## **BIOGRAPHICAL SKETCH**

Yashar Makhtoumi was born in Gonbad-e Kavus, Iran. After completing his schoolwork at Baghiat Allah High school- NODET (National Organization for Development of Exceptional Talents), Yashar entered University of Shams in Gonbad-e Kavus and received a Bachelor of Science with a major in Civil Engineering in July 2014. In February 2017, he received a Master of Science from Amirkabir University of Technology in Tehran with a major in Water Resources and Hydraulic Structures Engineering. Since August 2018, he was employed as Research Assistant at Florida State University in Tallahassee, Florida. In November 2022, he graduated with a Ph.D. degree in Civil Engineering.